UNIVERSITY OF OKLAHOMA

GRADUATE COLLEGE

MECHANISTIC INPUT PARAMETERS AND MODEL CALIBRATION FOR DESIGN AND PERFORMANCE EVALUATION OF FLEXIBLE PAVEMENTS IN OKLAHOMA

A DISSERTATION

SUBMITTED TO THE GRADUATE FACULTY

in partial fulfillment of the requirements for the

Degree of

DOCTOR OF PHILOSOPHY

By

NUR HOSSAIN
Norman, Oklahoma
2017

MECHANISTIC INPUT PARAMETERS AND MODEL CALIBRATION FOR DESIGN AND PERFORMANCE EVALUATION OF FLEXIBLE PAVEMENTS IN OKLAHOMA

A DISSERTATION APPROVED FOR THE
SCHOOL OF CIVIL ENGINEERING AND ENVIRONMENTAL SCIENCE

BY

Dr. Musharraf Zaman, Chair

Dr. Gerald A. Miller

Dr. Kianoosh Hatami

Dr. Jeffery Volz

Dr. Ahmad Ghassemi

DEDICATION

“To my Family”

ACKNOWLEDGEMENTS

First, I would like to thank the Almighty for his countless blessings and giving me ability to complete this dissertation.

I would like to express my sincerest gratitude to my mentor and the chair of my doctoral committee, Dr. Musharraf Zaman. Without his continuous guidance, constant support and tremendous inspirations, my Ph.D. would not have been completed. Dr. Zaman has very high work ethics that transmits to his students very early in their career which I believe is the essence for his students' success. I started working in the Civil/Geotechnical consulting industry in Oklahoma since graduating with my Master's Degree in 2010. It was Dr. Zaman who inspired me to pursue my Ph.D. sometime in 2012 and made me believe that it is entirely plausible to get a Ph.D. degree even while working as a full-time employee in the industry. Because of his belief in me, I made the decision to start my PhD in the spring of 2014 and progressed with this dissertation gradually. When I look back, I feel very good knowing that I took the best decision of my life by working with Dr. Zaman. I will always be indebted to him for his encouragement, guidance, help and continuous support. May Almighty give him even greater rewards throughout his life.

I would like to thank Dr. Dharamveer Singh, for his guidance, collaboration and research ideas throughout this journey. Dharamveer acted as my go-to person for discussing ideas and trouble-shooting in their execution. Since receiving his Ph.D. from OU, he has been working as an Assistant Professor at the Indian Institute of Technology in Mumbai, India. By the grace of technology, we could bridge the gap caused by the

geographical distance and the time-zone, of course. On an average, Dharamveer and I had telephone and skype conversation for at least once bi-weekly. I am truly grateful for his support. More than a coworker, I have found a lifelong friend and brother in him. May Almighty bless you and your family.

I would like to thank Dr. Gerald Miller for serving on my doctoral committee. My first graduate class at OU was Dr. Miller's "Advanced Soil Mechanics." I also attended Dr. Miller's "Structural Design of Pavement" class. I learned a lot from Dr. Miller and was always impressed by his practical experience and theoretical knowledge during his lectures.

I want to thank Dr. Kianoosh Hatami for serving in my doctoral committee. I learned a lot from his "Introduction to Geosynthetics" course. I also want to thank Dr. Ahmad Ghassemi for serving on my committee. I attended his "Introduction to Rock Mechanics" course and learned a lot from that course. I would also like to thank Dr. Jeffery Volz for serving in my committee and sharing his thoughts with me.

I would like to acknowledge the help and guidance from Dr. David Timm from Auburn University. Not only Dr. Timm guided me through the forensic study and subsequent analyses of data from the test section, but also he was involved in the "Field Performance Monitoring and Modeling of Instrumented Pavement on I-35 In McClain County" project. Dr. Timm is well known within the international pavement community and has been a tremendous help throughout this study.

I am grateful to many colleagues who supported me in laboratory testing, collection of field data, analyses of collected and other research-related tasks. I would

specifically like to acknowledge Mr. S.M. Rassel Shazzad, Mr. Md. Ridwan Alam, Dr. Rouzbeh Ghachi, Dr. Manik Barman, and Dr. Debaroti Ghosh. All of these people have been a source of friendship as well as good advice and collaboration.

I would like to express my sincere appreciation to the Oklahoma Department of Transportation (ODOT), Southern Plains Transportation Center (SPTC), and Federal Highway Administration (FHWA) for providing financial support for this study. Specifically, I would like to acknowledge the support from Josh Randell, John Bowman, David Streb, Bryan Hurst, Kenneth Hobson and Chris Westland, all from ODOT, for their direct and indirect assistance with this project. Bryan Cooper from ODOT deserves special thanks for his considerable contributions during the construction and instrumentation phase of this project. He also played a key role in arranging quarterly field testing. I would like to thank Haskell Lemon Construction Company for providing materials and field testing support for this project.

Finally, I would like to express my boundless love and gratitude to my mother, Mrs. Begum Nurun Nahar; my wife, Mrs. Tania Munmun; my father, Mr. Rezaul Hossain; and my son Arish Yousuf Hossain, for their inspiration, sacrifice, patience and support. I would like to stress the inspiration from my mother who had a dream that one day her son will become a Doctor of Philosophy. I express my heartiest gratitude to my beautiful wife for her endless sacrifice, patience and encouragement throughout these years to pursue my mother's dream. Without her unconditional support, I am pretty sure I would not have achieved this success.

Table of Contents

List of Tables

List of Figures

ABSTRACT

The Mechanistic-Empirical Pavement Design Guide (MEPDG) – a product of research and experience involving more than 20 years of traffic, climate and materials data from different regions in the U.S. – has elevated pavement designs to a new level. The MEPDG has three different input categories: (1) traffic, (2) climate and (3) materials. It also has three different levels of input data: Level 1 (highest accuracy), Level 2 (medium accuracy) and Level 3 (default values/lowest accuracy). Lack of materials, climate, and traffic data and absence of locally calibrated distress models have been a major problem in the implementation of MEPDG by the state Departments of Transportation. This study was undertaken to enhance implementation of MEPDG in Oklahoma through collection of site specific materials and traffic data and local calibration of rut models.

A 1,000 ft. long instrumented test section was constructed on Interstate-35 near Purcell, Oklahoma. The test section consisted of five layers: two Hot Mix Asphalt (HMA), one aggregate base, one stabilized subgrade, and natural subgrade. MEPDG input parameters for traffic, climate and materials were developed from this test section's data. The site included a weigh-in-motion (WIM) station and lateral positioning sensors to obtain input parameters for traffic. In addition, laboratory tests, namely Dynamic Modulus, Resilient Modulus, Dynamic Shear Rheometer and other pertinent tests were conducted using materials obtained from this test section. Rutting, fatigue cracking, and International Roughness Index (IRI) were measured at the test section for six years at three months interval. Minimal cracking and significant rutting were observed at the test section. The highest recorded rut value was 0.868 in. Cores were extracted from the

cracked pavement locations, which revealed that the cracks were located primarily in the surface layer.

Differences in traffic input parameters between Level 3 (default) and Level 1 (site specific) were identified and discussed in this study. In addition, sensitivity and contribution of these input parameters to pavement designs are discussed. Since, developing Level 1 traffic inputs requires significant time and resources, the parametric study was focused on identifying the most sensitive traffic input parameters for pavement design. The Axle Load Spectra was found to be the most sensitive traffic input parameter, followed by Vehicle Class Distribution factors and Monthly Adjustment factors.

Significant errors (more than 30%) were observed when rut was predicted using Level 3 inputs. Although the average error was reduced to approximately 10% by using the Level 1 inputs, differences still existed, which necessitated the development of local calibration factors. Two approaches were used for this purpose: total rut and layer-wise rut. The calibration process using the total rut approach reduced the average error to less than 5%. The optimized calibration coefficients were found to be: β_{r1} = 2, β_{r2}= 1, β_{r3}= 0.93 for asphalt layers; β_{GB}= 1 for aggregate base layer, and β_{SG}= 0.5 for natural subgrade layer.

At the end of field performance monitoring, forensic investigation was conducted to investigate the contribution of different pavement layers to rut. It was observed that the rut was contributed mostly by the HMA layers, more specifically by the surface layer. Since, negligible rut was found in the aggregate base and subgrade layers, the rut model coefficients were recalibrated using layer-wise approach. The optimized calibration

coefficients were: β_{r1} = 1.25, β_{r2} = 1, β_{r3} = 1.05 for HMA; β_{GB} = 0.05 for aggregate base, and β_{SG} = 0.05 for natural subgrade layers.

The database for Level 1 pavement design as well as the local calibration coefficients of the MEPDG rut models developed in this study are expected to enhance implementation of the MEPDG in Oklahoma. Also, the results from this study are expected to assist pavement designers in addressing rut problems in future design.

CHAPTER

1

Introduction

1.1 Background and Needs

The AASHTO 1993 empirical design method is based on limited data obtained from the AASHO road test in the 1960s (Muthadi and Kim, 2008). The AASHO road test utilized identical axle loads and configurations to develop empirical design equations, instead of using mixed traffic loads or traffic load spectra, as observed in an in-service pavement. Instead of using the axle load spectra concept, the AASHTO 1993 Guide uses Equivalent Single Axle Load (ESALs) to define traffic levels. Previous studies show that pavement materials respond differently to traffic pattern, frequency and loading (AASHTO, 2008). Also traffic loading in different seasons of the year differently influences the response of the pavement structure. Design traffic volumes, particularly level of heavy truck traffic has increased about 10 to 20 times since the design levels used in the 1960's. For example, the original Interstate pavements were designed for 5 to 15 million trucks, whereas today the same pavements are designed for 50 to 200 million trucks and longer design lives (e.g., 30-40 years versus 20 years) (FHWA, 2015; AASHTO, 2008). Because the AASHO road test was conducted at one specific geographic location, it is impossible to address the effects of different climatic conditions on pavement performance based on those data. Also, all test sections at the AASHO road test site involved only one type of subgrade soil. Nationally, pavement designs must consider different types of soil to ensure desired performance. Additional limitations

include insufficient environmental data and pavement layer configuration. Therefore, the existing 1993 AASHTO design guide cannot be used reliably for designing pavements for the level of traffic and varying climatic and material conditions experienced currently and expected in future. Consequently, Oklahoma Department of Transportation (ODOT) is increasingly moving from the AASHTO's 1993 empirical design method to Mechanistic-Empirical based pavement designs, which takes into account of vehicular traffic, climate and material properties such as stress-strain behavior in a realistic manner.

In the Mechanistic-Empirical design, the word "Mechanistic" refers to the application of the principles of engineering mechanics, which leads to a rational design process (AASHTO, 2008, Hossain, 2010). Performance of roadway pavements can be adequately understood from its response including stresses, strains and deflections under moving traffic loads and empirically relating them to actual field performance. Mechanistic analyses and design approaches are more robust and applicable to a much wider range of environmental, material and traffic conditions (Timm et al., 2004).

The Mechanistic-Empirical Pavement Design Guide (MEPDG) is a product of research and experience involving more than 20 years of data from different regions, climate, and materials in the U.S. (AASHTO, 2008; NCHRP, 2004; Thompson, 1996).

Consequently, the MEPDG is believed to better predict pavement performance through better utilization of local materials, traffic conditions and regional climate (Tarefder and Rodriguez-Ruiz, 2013; Souliman et al., 2010; Flintsch et al., 2008). It is believed that the use of MEPDG has resulted in significant improvements in pavement design nationally including savings in materials and construction costs and enhanced performance. In the MEPDG, the designer not only has the ability to design a pavement

using the local traffic, climate, subgrade, and construction conditions, but also can evaluate adequacy of the method through prediction of key distresses and smoothness. Thus, the designer is fully involved in the design process and has the flexibility to consider different design features or scenarios and materials for the prevailing site conditions. This approach makes it possible to optimize the design and to more fully insure that specific distress types are addressed (AASHTO, 2008).

However, realizing the full benefits of pavement design using the MEPDG can be a challenging task. The MEPDG has three different input categories: (1) traffic, (2) climate and (3) materials. It also has three different levels of input data: Level 1, Level 2 and Level 3. Level 1 inputs provide the highest level of accuracy and, therefore, would have the lowest level of uncertainty or error. Level 1 inputs, however, require site-specific data based on field and/or laboratory tests. Level 2 inputs provide an intermediate level of accuracy. Level 2 inputs are typically user-selected. These inputs could be selected from an agency database or obtained from a limited testing program, or estimated using correlations. Level 3 inputs provide the lowest level of accuracy.

Developing the Level 1 input parameters, specifically, the traffic input parameters require significant efforts and resources (Hossain et al., 2016; Hall et al., 2011; Hoegh et al., 2010; and Mehta et al., 2008). For example, a Level 1 design requires site-specific traffic data for the particular pavement (e.g., traffic count, speed, lateral wander, vehicle class, axle configuration, axle load, tire pressure, etc.) from a Weigh-in-Motion (WIM) station, reflecting the composition of actual traffic at the site. Not only has a WIM site required periodic maintenance, data collected from the WIM site need to be checked for quality to ensure accuracy. In addition, WIM data need to be processed for traffic input

parameters such as growth rate, vehicle class distribution factors, hourly distribution factors, monthly adjustment factors, and axle load spectra.

In this study, an instrumented test section on Interstate-35 near Purcell, Oklahoma was used to collect traffic data and determine Level 1 input parameters. The average annual daily truck traffic at this site consisted of approximately 8,200 AADTT (Average Annual Daily Truck Traffic) (Solanki et al., 2013). Since developing the Level 1 traffic input parameters is time-consuming and costly, it is important to know which traffic inputs are most sensitive and critical for design purposes. It is also important to know the frequency of the dominant classes of vehicles to develop these input parameters. Sensitivity analyses could be used to identify the most sensitive input parameters for reliable designs.

Not only the input parameters have different levels, but also have different settings for calibration factors of the distress (fatigue, rut, low temperature cracks) prediction models. Usually performance of the MEPDG distress models are evaluated by comparing field measured values with the predicted values by these models. The distress models incorporated in the MEPDG are nationally calibrated which may or may not work for a selected region or for a specific site (Priest, 2005). The nationally calibrated models have shown mixed performance for different states. Some states have reported that these models do not require calibration for their states while other states have indicated needs for calibration (Tarefdar and Rodriguez-Ruiz, 2013; Walubita et al., 2013). The purpose of incorporating local calibration of model parameters in the MEPDG is to address differences in construction practices, traffic and environmental conditions, maintenance policies and practices, and material specifications across the United States (Tarefdar and

Rodriguez-Ruiz, 2013; FHWA, 2010; Mehta et al., 2008). Although laboratory data are frequently used in local calibration of performance models, use of field data and comparison with field performance add credibility to such calibration. The present study uses both laboratory and field data for local calibration of rut models in the MEPDG.

Local calibration of distress models in the MEPDG can have significant impact on the structural design of pavements. Without the knowledge of realistic inputs and calibration coefficients, a majority of highway pavements may be either over-designed or under-designed. The resulting variation in pavement construction costs could be substantial. For example, based on the ODOT Weighted Average Item Price Report (ODOT Price History from July 1, 2015 to December 31, 2015), it costs approximately $100,000 to construct 1 in. thick asphalt layer per lane mile of typical interstate pavements in Oklahoma. Typical thicknesses of asphalt layers in interstate pavements in Oklahoma range from 9 to 12 inches (Hossain et al., 2014). According to a majority of DOTs in the U.S., without accurate input data and calibration coefficients, pavements are typically overdesigned by approximately 25% (Hall et al., 2011). Therefore, for asphalt layers alone, approximately $225,000 to $300,000 could be saved per lane mile of interstate pavements from better knowledge of calibration coefficients.

Based on the above discussions, one might ask the following questions:

1) Is it important to develop Level 1 input parameters for successful implementation of the MEPDG?
2) Which input parameters (i.e., traffic, material, and climate) is most sensitive considering distresses in flexible pavements?

3) Is calibration of the MEPDG distress models required? How calibration factors of a distress model change with different levels of input parameters?

4) How different layers in a flexible pavement contribute to distresses?

To answer the aforementioned questions, in a related study (Solanki et al., 2013), a 1,000 ft. long test section was constructed on the (outer) southbound lane of Interstate-35 near Purcell, Oklahoma and was instrumented for traffic and field data collection. The materials used in constructing the pavement were collected from the test section and laboratory tests were conducted to develop Level 1 input parameters. Also, quarterly field measurements were performed at the test section to collect the pavement performance data namely rut, crack mapping and International Roughness Index (IRI). At the end of the project, a forensic investigation was performed by trenching to determine the contribution of different pavement layers to rut.

1.2 Objectives

The specific objectives of this study are to:

(a) Develop Level 1 material, traffic, and climate input parameters for design of pavements using the MEPDG and to compare these parameters with the Level 3 default input parameters;

(b) Conduct sensitivity analyses of the traffic input parameters on rut models in the MEPDG;

(c) Calibrate the rut models in the MEPDG using Level 1 input parameters and compare these calibration factors with those obtained from the calibration of the same models using Level 3 input parameters; and

(d) Evaluate contribution of different pavement structural layers to the observed rut by forensic investigation of the test section.

1.3 Organization of this Dissertation

This dissertation is composed of a total of eight chapters. Chapter 1, entitled "*Introduction*," identifies the background and research needs. This chapter also presents the objectives of this dissertation.

Following this chapter, Chapter 2, entitled "*Review of Literature,*" presents an overview of the input parameters in the MEPDG related to traffic, materials, and climate input parameters. This chapter also discusses the rut prediction models in the MEPDG. A thorough literature review is presented in this chapter to identify the major findings of previous studies in this field. In addition, critical gaps in the existing literature and the expected contributions of this dissertation are discussed in this chapter.

Chapter 3, entitled "*Field Test Facility and Data Collection,*" discusses the construction and instrumentation of test section on Interstate-35 near Purcell, Oklahoma. This instrumented test section was used to collect continuous traffic data and to monitor in-service pavement performance and response under actual environmental conditions. Continuous traffic data were collected from the test section for approximately four years (from June, 2008 through May, 2012). Three types of pavement performance data namely, rut, fatigue cracking and International Roughness Index (IRI) were collected from the test section for approximately six years (from August, 2008 through October, 2014). This chapter provides details of performance monitoring and changes in pavement conditions throughout the study period.

Chapter 4, entitled "*Development of MEPDG Input Parameters,*" describes the development of site specific traffic, materials and climate input parameters employed in this study. Several traffic input parameters, namely Vehicle Class Distribution Factors, Monthly Adjustment Factors, Hourly Distribution Factors, Axle Load Spectra, and Lateral Traffic Wander were developed from the collected traffic data. This chapter also describes the tests conducted on materials collected from the test section, the test procedures and the test results.

Chapter 5, entitled "*Sensitivity of Level 1 Input Parameters on Pavement Performance,*" provides an overview of the need for developing Level 1 traffic and materials input parameters. Sensitivity of different input levels is also discussed. A comparison between default (Level 3) and site specific (Level 1) inputs and their influence on pavement performance prediction are also presented in this chapter. Additionally, this chapter discusses the most sensitive traffic input parameters and desired frequency for developing the traffic input parameters for better performance prediction.

Chapter 6, entitled "*Local Calibration of the MEPDG Rut Models,*" discusses the MEPDG rut models and the need for calibration of these models for Oklahoma conditions. This chapter also discusses the methodology developed for the calibration of rut models. The local calibration was performed by comparing the measured rut with the MEPDG predicted rut over time. These analyses were first done for the default (Level 3) calibration parameters and then adjusted using Level 1 input parameters. Sensitivity of some calibration factors over others are also discussed in this chapter.

Chapter 7, entitled "*Contribution of Different Structural Layers to Rutting,*" provides a comparison of the pavement surface profiles observed at the test section with

the profiles observed in previous major studies. A forensic investigation was performed at the end of the project to determine the contribution of different structural layers to overall rut. Local calibration of the MEPD rut models was performed again based on the layer-wise rut data obtained from the forensic study.

Finally, the overall summary and conclusions of this dissertation as well as the recommendations for future studies are presented in Chapter 8.

CHAPTER

2

Review of Literature

2.1 Introduction

This chapter provides an overview of MEPDG input parameters and rut models in the MEPDG. A literature review was performed to identify the major findings of the previous studies in this field. This chapter also discusses the critical gaps in the existing literature and contributions of the current study.

2.2 MEPDG Input Parameters

MEPDG requires three basic inputs for pavement design: traffic, climate and materials. Each of these basic inputs is further divided into multiple input parameters. The following sections briefly discuss these input parameters.

2.2.1 Traffic

Traffic data is one of the most important inputs required for the structural design of pavements. It involves the estimated load and frequency of traffic the pavement will carry throughout its service life. Typical traffic data required for design are listed below (AASHTO, 2004):

- Base year truck-traffic volume;
- Vehicle operational speed;
- Truck-traffic directional and lane distribution factors;

- Vehicle (truck) class distributions;
- Axle load distribution factors;
- Axle and wheel base configurations;
- Tire characteristics and inflation pressure;
- Truck lateral distribution factors; and
- Truck growth factors.

The above inputs can be grouped into four basic types of traffic data as listed below:

- Traffic volume – base year information;
- Traffic volume adjustment factors:
    - Monthly adjustment factors;
    - Vehicle class distribution factors;
    - Hourly truck distribution factors; and
    - Traffic growth factors.
- Axle load distribution factors;
- General traffic inputs:
    - Mean wheel location;
    - Traffic wander standard deviation;
    - Design lane width;
    - Number of axles/truck;
    - Axle configuration; and
    - Wheel base.

2.2.1.1 Traffic Volume - Base Year Information

The first year of traffic input is defined as the base year for design purposes. The following information is required for the base year traffic:

a) *Two-way annual average daily truck traffic (AADTT):* Two-way AADTT is the total volume of truck traffic (FHWA vehicle classes 4 through 13) in a roadway segment in both directions over a 24-hour period.

b) *Number of lanes in the design direction:* Number of lanes in the design direction represents the total number of lanes in one direction.

c) *Percent trucks in design direction:* Percent trucks in the design direction is also known as the directional distribution factor (DDF). This represents any differences in the overall truck volume in two directions.

d) *Percent trucks in design lane:* Percent trucks in the design lane, also called lane distribution factor (LDF), represents the truck traffic distribution between the lanes in one direction. Typically, the following values of LDFs are used (AASHTO, 2004):

   - Single-lane roadways in one direction: LDF = 1.0,
   - Two-lane roadways in one direction: LDF = 0.9,
   - Three-lane roadways in one direction: LDF = 0.6,
   - Four-lane roadways in one direction: LDF = 0.45.

e) *Vehicle (truck) operational speed:* This is the vehicular operational speed of trucks expressed in mile/hour.

2.2.1.2 Traffic Volume Adjustment Factors

a) Monthly Adjustment Factor

The monthly adjustment factor (MAF) represents the proportion of annual truck traffic for a given class of vehicle that occurs in a specific month. Hence, the monthly distribution factors for a specific month is equal to the monthly truck traffic for a given class for the month divided by the total truck traffic for that truck class for the entire year. The MEPDG assumes a constant MAF for the entire design period for all types of vehicles. Usually vehicle classes of 4 through 13 are used to develop MAF.

$$MAF_i = \frac{AMDTT_i}{\sum_{i=1}^{12} AMDTT_i} \times 12 \quad (2.1)$$

where:

MAF_i = Monthly adjustment factor for month i; and

$AMDTT_i$ = Average monthly daily truck traffic factor for month i.

b) Hourly Distribution Factor

The hourly distribution factor (HDF) represents the percentage of average annual daily truck traffic (AADTT) within each hour of the day. There can be Level 1, Level 2 or Level 3 inputs for the hourly distribution factors. The following steps are involved in generating HDF:

Step 1: First, the total number of trucks within each hour of traffic data in the sample is determined.

Step 2: Then, the number of trucks for each 24 hours period in the sample is averaged.

Step 3: The 24 hourly averages from Step 2 are counted together to have one number.

Step 4: Finally, each 24 hour average from Step 2 is divided by the total from Step 3 and multiplied by 100 to obtain the HDF.

c) *Vehicle Class Distribution Factor*

Vehicle class distribution (VCD) factor is determined from the data collected from the vehicle classification counting programs such as Automatic Vehicle Count (AVC), Weigh-In-Motion (WIM) and vehicle counts. Normalized VCD represents the percentage of each truck class (Class 4 through Class 13) through the AADTT for the base year. A default VCD is provided in the MEPDG software. The design guide lists 17 Truck Traffic Classification (TTC) groups based on the roadway function class and the traffic stream expected on a given roadway. The designer can use the default set of TTC or can use the Level 1 VCD developed from the actual traffic data for a given project. The latter option gives the designer the most accurate vehicle class distribution for a particular design application.

d) *Traffic Growth Factor*

Traffic growth factors provide the growth of traffic over design period for a particular site. MEPDG allows three different traffic growth functions for computing growth or decay of truck traffic over time. The three growth functions considered in the MEPDG are: no growth, linear growth, and compound growth.

2.1.1.3 Axle Load Distribution Factors

The axle load distribution factors, commonly referred to as axle load spectra (ALS), represent the percentage of total axle applications within each load interval for a specific axle type and vehicle class. This input is a major step forward in pavement deign using MEPDG from the traditional 1993 AASHTO design guide, where Equivalent Single Axle Load (ESAL) is used for pavement design. The following load intervals and loading ranges are used in the MEPDG for different axle types:

- Single Axles: 3 kips to 40 kips, at 1 kip interval;
- Tandem Axles: 6 kips to 80 kips, at 2 kips interval; and
- Tridem and Quad Axles: 12 kips to 102 kips at 3 kips interval.

The normalized axle load spectra can only be determined from WIM data. Therefore, the level of inputs depends on the data source (site specific, regional or national). For design purpose, axle load spectra are normalized on an annual basis.

2.2.1.4 General Traffic Inputs

The inputs in this category generally define the axle load configurations and loading details used for determining pavement response.

a) *Mean Wheel Location*

Mean wheel location is the distance from the outer edge of the wheel to the pavement marking. A designer can use site specific values through direct measurements (Level 1), or a regional/statewide average value (Level 2), or the national average value (Level 3). The default (Level 3) mean wheel location value in the MEPDG is 18 in.

b) *Traffic Wander Standard Deviation*

This is the standard deviation of the lateral traffic wander. A site specific value can be determined or the default value can be used.

c) *Design Lane Width*

This parameter refers to the actual traffic lane width. The default value of this input is 12 ft.

d) *Number of Axle/Truck*

This input represents the average number of axles for each truck class (Class 4 to Class 13) for each axle type (single, tandem, tridem and quad). A designer can use the values determined through analysis of site-specific data (Level 1), or regional/statewide traffic data (Level 2), or default values based on analyses of national databases (Level 3).

e) *Axle Configuration*

Under this input, a series of data including tire pressure and axle configurations are provided. Analyses of pavements using the MEPDG are sensitive to both wheel locations and interactions between wheels for a given axle. Typically, these data are obtained directly from the truck manufacturers.

2.2.2 Climate

One of the major advances in pavement design using the MEPDG approach over the 1993 AASHTO approach is consideration of site specific data. Numerous weather stations are installed in various places throughout the U.S. A designer can use the actual climatic data from these weather stations. Alternatively, a user is allowed to call up to six nearby weather stations' data and thereby generate a virtual weather station based on the

GPS coordinates of the site. Also, a user can use site specific climate data obtained from the installed weather station(s).

2.2.3 Materials

The present study is focused on flexible pavements. Therefore, the input parameters for materials only consider Hot Mix Asphalt (HMA), aggregate base, stabilized subgrade and natural subgrade. The following sections briefly describe the required material inputs for different layers:

2.2.3.1 Asphalt Layers

a) *Asphalt Surface Shortwave Absorptivity:*

This dimensionless parameter defines the fraction of available solar energy absorbed by the pavement surface. The default value of this parameter is 0.85.

b) Thickness:

This input represents the thickness of the HMA layer in inches.

c) Unit Weights:

These inputs represent the unit weights of HMA layers and are typically obtained from the HMA Mix Design Sheet.

d) Effective Binder Content:

Effective binder content is the total asphalt binder content of the HMA less the portion of asphalt binder lost by absorption into the aggregate.

e) Air Voids:

This input represents the design air voids of the asphalt layer.

f) *Poisson's Ratio:*

Poisson's ratio of the HMA layers can be obtained from laboratory tests or a typical value can be used as input. A typical value of the Poisson's ratio of HMA layers is 0.35.

g) *Dynamic Modulus:*

As a viscoelastic materials, asphalt mixes and asphalt binders are highly sensitive to temperature and loading rate. For such materials, dynamic modulus is obtained from the stress-strain relationship under a continuous sinusoidal loading (Huang, 2004, Singh, 2011).

h) *Complex Shear Modulus and Phase Angle:*

Complex shear modulus is the ratio of maximum shear stress to maximum strain. It is a measure of the total resistance to deformation when the asphalt binder is subjected to shear loading. The MEPDG requires the complex shear modulus (G*) and phase angle (δ) data of the asphalt binder over a range of temperature.

i) *Creep Compliance:*

Creep compliance is defined as time-dependent strain per unit stress. Creep is the tendency of a solid material to move slowly or deform permanently under the influence of stress. It occurs as a result of long-term exposure to high levels of stress that are still below the yield strength of the asphalt materials (Huang, 2004).

2.2.3.2 Aggregate Base, Stabilized Subgrade, and Natural Subgrade Layers

a) *Layer Thicknesses:*

These inputs represent the thicknesses of the aggregate base, stabilized subgrade and natural subgrade layers in inches.

b) *Poisson's Ratios:*

These inputs represent the Poisson's ratios of the aggregate base, stabilized subgrade and natural subgrade layers.

c) *Coefficient of Lateral Earth Pressure (k_0)*

Coefficient of lateral earth pressure is the ratio of the lateral earth pressure to the vertical earth pressure.

d) *Resilient Modulus:*

Resilient modulus is a measure of stiffness of unbound materials and subgrade. Generally, it is described as the ratio of applied deviatoric stress to recoverable or "resilient" strain.

e) *Gradation and other Engineering Properties:*

These inputs represent an array of engineering properties such as gradation, Atterberg limits, maximum dry unit weight, saturated hydraulic conductivity, and specific gravity.

2.4 Literature Review

Many researchers (e.g., Cunagin et al., 2013; Haider et al., 2011, Hajek et al., 2011) have expressed concerns in using Level 3 values for design of pavements. For example, Lu et al. (2006) and Tam et al. (2003) have used the data collected from the LTPP section to develop input parameters for the MEPDG. Because the material input

parameters such as dynamic modulus are not available for the LTPP section, they had to be estimated at Level 3 using the Witczak equation (AASHTO, 2004). The Witczak equation has been found to under-predict or over-predict dynamic modulus of asphalt mixes (Singh et al., 2011), indicating needs for determining calibration factors. Although Level 1 inputs are desired for improved accuracy, Singh et al. (2011) suggested for comparative studies between the Level 1 and Level 3 inputs to assess the significance of Level 1 input parameters for a particular state/region. A comparative study can also show the differences in performance prediction when using Level 1 inputs vs. using Level 3 inputs. Such comparisons can help state agencies to better utilize their resources.

Over the past decade, a number of states (e.g., Michigan, New York, Louisiana, Virginia, Washington and Arkansas) have attempted to develop Level 1 input parameters from their respective databases. Most of these states were successful in developing Level 1 and Level 2 input parameters for traffic only. It was observed that developing Level 1 inputs for materials is generally challenging, partly because of the lack of test data (for example, dynamic modulus data of asphalt mixes). An overview of pertinent previous studies is given below.

Haider et al. (2011) developed the following Level 1 (site specific) and Level 2 (statewide average) input parameters for traffic from sites in Michigan: MAF, VCD, HDF, and ALS. It was reported that Level 3 inputs were not suitable for Michigan, therefore, Level 1 traffic data were recommended. The MEPDG default and statewide averages for HDF exhibited under and over predictions of up to 11 years of pavement life. It was also found that traffic characteristics are unique to a state depending on the local industry, land use, and truck configurations. Based on the sensitivity analyses, it

was concluded that for certain traffic inputs Level 3 data can be acceptable, however, they should be used with caution.

Romanoschi et al. (2011) developed Level 1 input parameters using data from 23 sites in New York for the following traffic inputs: MAF, VCD, HDF, ALS, growth rate and axle groups per vehicle. These data were collected over a five-year period, from 2004 to 2009. It was found that only the VCDs had values close to those recommended by the MEPDG model only for roads classified as Rural–Principal Arterial–Interstates. The HDF values were found to be site specific. It was suggested that using state averages for the HDF should be avoided in the pavement design process. It was also reported that the MDFs varied significantly in New York.

Ishak et al. (2010) developed the following Level 1 traffic inputs from the WIM and vehicle classification sites in Louisiana: VCD by roadway functional class, VCD for Truck Traffic Classification (TTC) groups, HDF, growth rate, and axle groups per vehicle. It was recommended that when developing ALS, the TTC grouping method be used for grouping the WIM sites, instead of the roadway functional classification only. A significant variation in VCD was observed for the same roadway functional classification, and therefore, grouping by roadway functional class only was not recommended. Ishak et al. (2010) also recommended development of strategic plan for installing permanent WIM sites and use axle load data from existing weight enforcement sites to supplement data collected by portable WIM sites.

Smith and Diefenderfer (2010) developed Level 1 traffic input parameters using data from 8 representative WIM sites across Virginia. It was found that the predicted time to failure for the total rut was significantly different when the Level 1 ALS data were

used compared with the default ALS. It was also observed that Level 1 data for the four traffic inputs considered (ALS, MAF, VCD, and number of axles per truck) did not have any statistically significant effect on the MEPDG-predicted pavement distress, considering uncertainty of the pavement distress models.

Li et al. (2009) developed Level 1 traffic input parameters using data from 12 WIM sites across Washington. It was found that one group of ALS can present the vast majority of Washington's axle load characteristics when the MEPDG is used. For typical pavement designs, the MEPDG was found to be only moderately sensitive to the alternative ALS data developed from the WIM data collected from the WIM stations in Washington. It was further concluded that Washington not only needs to develop Level 1 traffic and material inputs but also need to calibrate the MEPDG.

Tran and Hall (2007) developed Level 1 ALS data from 10 WIM stations in Arkansas. Default values were used for the following inputs: MAF, VCD, and HDF. It was found that statewide ALS data were different from the default values in the MEPDG. The difference in predicted pavement life was found to be more than 25%. It was recommended that efforts be made to develop Level 1 ALS data for future design purposes.

In conjunction with developing site-specific traffic input parameters, a number of states (Colorado, New Mexico, Arkansas, Texas, North Carolina, Minnesota, and Washington) have conducted research on the local calibration of the rut models in MEPDG. These rut models have a total of 5 coefficients for local calibration. They are: β_{r1}, β_{r2} , β_{r3} for asphalt layers, β_{GB} for granular base layer, and β_{SG} for subgrade layer. Two different approaches have been used for the calibration: (1) total rut

accumulated in a pavement section; (2) layer-wise rut in a pavement section. Details on the local calibration efforts are discussed in Chapter 6. In this chapter, a brief overview of the local calibration coefficients developed by researchers from various states is presented in Table 2.1.

2.5 Critical Gaps in Existing Literature

From the aforementioned literature review, it is evident that researchers from several states have been successful in developing some of the traffic input parameters at Level 1. However, Level 1 inputs for materials have not been developed yet, which is important for an accurate design of pavements using the MEPDG. Even in case of traffic inputs, they have been developed for a specific month or a year at most, not for an extended period of time (say 3 to 4 years). Some researchers have taken initiative in assessing the sensitivity of traffic inputs, however, yearly sensitivity analyses of a majority of these inputs have not yet been performed. Several researchers have also calibrated the MEPDG distress models using the LTPP database. It is known that the LTPP data have some inherent deficiencies. For example, data collection at LTPP sites is not frequent enough to capture the progression of distresses (rut, fatigue, thermal cracking). Also, most LTPP sites do not have Level 1 materials data (for example, dynamic modulus of asphalt mixes). Close monitoring of pavement distresses is needed for accurate and efficient calibration of coefficients for distress models in the MEPDG. These efforts need to be complemented by forensic studies to evaluate performance of different pavement layers. To this end, some of these gaps are addressed in the present study to ensure successful implementation of MEPDG-based pavement designs in Oklahoma.

2.6 Scope

In this study, Level 1 traffic and material input parameters are developed from an instrumented test section in Oklahoma. The developed Level 1 input parameters are compared with the default values to determine the differences between the Level 1 and Level 3 inputs.

Sensitivity of the traffic inputs are analyzed in this study. Since developing Level 1 traffic inputs requires significant time and resources, an understanding of the most sensitive parameters is beneficial to design of pavements rationally. An understanding of input parameters related to traffic will allow transportation agencies to utilize their resources efficiently in collecting these parameters. Oklahoma Department of Transportation (ODOT) has not been able to use the MEPDG effectively, partly because of the lack of data and partly because of the uncalibrated distress models in the MEPDG (Randell, 2016).

Data obtained from the forensic investigation conducted at the test section provide an insight of the level of contribution of different pavement layers to rut. The findings of the forensic investigation are expected to be helpful in adjusting thicknesses and/or materials in designing pavements of similar attributes.

2.7 Summary

A detailed review of existing literature was conducted in this study to identify critical gaps and potential areas of improvement for successful implementation of MEPDG for pavement design. The key findings from this literature review study are discussed in this chapter, which include an overview of input parameters and rut models in the MEPDG. Overall, it is evident that although researchers have made considerable

efforts to generate Level-1 traffic input parameters for MEPDG, progress to generate Level-1 material input data has been limited. This chapter also provides an overview of the scope of this study.

Table 2.1: Summary of Previous Studies in Local Calibration of Rut Models

Authors	State	Proposed Calibration Coefficients				
		β_{r1}	β_{r2}	β_{r3}	β_{GB}	β_{SG}
Bhattacharya et al., 2016	Colorado	4.3	1	1	0.22	0.37
Tarefder et al. (2013)	New Mexico	1.1	1.1	0.8	0.8	1.2
Hall et al., (2011)	Arkansas	1.2	1	0.8	1	0.5
Banerjee et al. (2009)	Texas	2.39	1	0.856	1	0.5
Li et al. (2009)	Washington	1.05	1.109	1.1	1	0

CHAPTER

3

Field Test Facility and Data Collection

3.1 Introduction

An instrumented pavement section was constructed as part of an earlier study to monitor pavement performance under in-service traffic loading and environmental conditions (Solanki et al., 2013; Hossain et al., 2010). Continuous traffic data were collected for about four years, while performance of the test section was monitored for about six years. An overview of the construction and instrumentation of the test section is given in this chapter. This chapter also discusses the traffic and pavement performance data (rut, fatigue cracking, and roughness) obtained from the test section.

3.2 Location of the Test Section

The instrumented test section was located in the southbound (rightmost) lane of Interstate-35 (I-35) near Purcell, Oklahoma (Figure 3.1). The 1,000 ft. long test section was constructed in May, 2008. The test section was deliberately designed thinner so that it fails in a relatively short period of time, and its in-service performance can be monitored over the entire life. A weigh-in-motion (WIM) station was installed at approximately ¾ mile south of the test section to record traffic data. To monitor performance, the test section was divided into six different stations located at approximately 100 ft. intervals.

The stations were numbered as 144, 235, 319, 540, 738 and 900, as shown in Figure 3.2. These station numbers actually denote their distances (in feet) from the beginning of the test section.

3.3 Layout of the Test Section

The test section consisted of five layers (Figure 3.3). The top Hot Mix Asphalt (HMA) surface course was 2 in. thick and was constructed using a S4 Superpave® mix with a nominal maximum aggregate size (NMAS) of ½ in. The second HMA layer (base course) was 5 in. thick and constructed using a S3 mix having a NMAS of ¾ in. Both HMA mixes were produced using an asphalt binder with a Performance Grade (PG) of 64-22. The second HMA layer contained approximately 25% Reclaimed Asphalt Pavement (RAP). The third layer was an 8 in. thick aggregate base layer having type "A" gradation, as per Oklahoma Department of Transportation (ODOT) specification (ODOT, 2009). The fourth layer consisted of an 8 in. thick subgrade layer stabilized with 12% Class C fly ash. The bottom layer was compacted natural subgrade soil, consisting of lean clay with a liquid limit (LL) of 33 and a plasticity index (PI) of 15. Groundwater table was observed at approximately 10 ft. below the existing grade (Solanki et al., 2013).

3.4 Construction and Instrumentation of the Test Section

To monitor traffic and pavement response due to induced traffic loading and climate, the test section was instrumented with an array of gadgets, namely, asphalt strain gauges, earth pressure cells, temperature probes, lateral positioning censors, and moisture probes (Figure 3.4). A detailed description of the instrumentation can be found in Hossain (2010) and in Solanki et al. (2013). Only the lateral positioning and WIM station sensors are discussed in this dissertation because data obtained from these two sensors were used.

Before construction of the test section, the HMA layers as well as the base layer of the existing pavement were removed. After removing these layers, the construction equipment experienced soft subgrade soils (sandy silty clay) with high moisture contents, in excess of 16% (Solanki et al., 2013). Because the soft subgrade was not considered suitable for construction, it was removed up to a depth of 2 ft. and backfilled with better soils from the northbound lane. After backfilling, the subgrade was graded uniformly using a dozer and then compacted using an Ingersoll Rand sheep-foot roller. The subgrade was further smoothened by using a smooth-drum roller.

The stabilized subgrade layer was constructed on the top of the compacted natural subgrade layer. As mentioned earlier, Class C Fly Ash (CFA) was used as the stabilizing agent. The CFA was hauled from Red Rock, Texas located about 130 miles from the site. The CFA was spread using a motor grader. A pulver mixer was used to mix the soil with the CFA (12%). According to the contractor, mixing of soil with CFA after installation of earth pressure cell and moisture probe could damage these instruments and cables by the teeth of the pulver mixer. Therefore, it was decided to install the EPC and the MP on the top of the natural subgrade layer after mixing the subgrade soil with CFA (Hossain, 2010; Solanki et al., 2013). The compacted soil-CFA mix was allowed to cure for a few days and then one set of EPC and MP was installed on the top of the stabilized subgrade layer. Also, separator fabric was placed on top of the stabilized subgrade.

The aggregates were hauled from the Dolese plant in Davis, Oklahoma. The aggregates were spread using a Caterpillar® D6R dozer on the geotextile separator fabric. A nuclear density gauge was used to measure in-situ density at selected stations located on top of the compacted aggregate base layer. The compacted aggregate base layer was

then coated with emulsion, known as the prime coat. After the application of the prime coat, the aggregate layer was allowed to cure for one day before installing the strain gauges on the top of this layer. With assistance of the National Center for Asphalt Technology (NCAT) personnel, 12 asphalt strain gauges were installed at selected locations on the top of the aggregate base layer (Figure 3.4). Then EPC and MP were installed on the top of the aggregate base layer following the same procedure as before.

The first HMA layer was constructed starting at the north end of the site using a paver manufactured by Caterpillar®. A vibratory roller was used for compaction. The compaction pattern consisted of two passes in heavy vibratory mode and one pass with static mode (no vibration). The compacted density was found to be lower than the desired density. Consequently, the actual air voids were higher than the target air voids. For example, the actual air voids obtained from the extracted field cores for the top HMA layer (S4 mix) and the bottom HMA layer (S3 mix) were 9.1% and 8%, respectively (Solanki et al., 2013). A tack coat was applied before the second lift of S3 was placed. Another layer of tack coat was applied before laying the surface course (S4). After completion of paving, five temperature probes were bundled together and installed in the pavement by drilling through the constructed pavement and dropping the bundle in the hole. A small trench was then cut in the surface layer for placing the probe cables. The trench was filled subsequently with a mixture of epoxy and sand (Solanki et al., 2013).

Installation of lateral position sensors (also known as axle sensors) was performed after installation of temperature probes. First, a concrete saw was used to cut three slots in the pavement. Two of these slots were perpendicular to the direction of traffic, while the third slot was inclined. Each slot was approximately 1.5 in. wide by 1.5 in. deep in

cross-section. Then, a leaf blower was used to dry out the slots and remove debris. After drying, the axle sensors, supplied by International Road Dynamics (IRD), were placed in the slots and a mixture of epoxy and sand was placed to secure the sensors in the pavement (Figure 3.5).

All the sensors were then attached to the Data Acquisition System located in a previously installed box near the test section. After cleaning the surface, the test section was opened to traffic on May 30, 2008 (Solanki et al., 2013).

3.5 Lateral Positioning Sensors

As noted above, a total of three Dynax® axle sensors were installed in a Z-pattern. Each sensor provided a time stamp for the traversing wheel. These time stamps along with the geometry were used for calculating the velocity and lateral offset of a vehicle from the end of the sensing strip of the sensor (Timm and Priest, 2005).

The axle sensing strips of these sensors are approximately 1 in. by 1 in. in cross-section. Two of these parallel sensors were 7.3 ft. long, while the diagonal sensor was 10 ft. long. Under no-load condition, the resistance of each sensor exceeds 10 MΩ while application of pressure reduces the resistance between 0.002 MΩ and 0.05 MΩ. A photographic view of the axle sensors is shown in Figure 3.5.

3.6 WIM Station

Good quality traffic data is essential for cost-effective and rational design of pavements. Characterization of traffic, their loading patterns and frequency play an important role in accurately predicting pavement performance. Currently, the weigh-in-motion (WIM) technology is widely used nationally because of its ability to collect large amounts of traffic data continuously. An existing WIM station, located approximately ¾

mile south of the instrumented section, was used in this study. This specific location was chosen because the two piezoelectric sensors were needed to be embedded in the asphalt pavement on a straight section without any curvature. The WIM sensors were calibrated after installation and then were calibrated on an annual basis. These calibration were performed by ODOT, and involved a vehicle of known weight passing 15 times over each lane and measuring the percent error of the gross vehicle weight. A piezoelectric WIM system is expected to provide gross weight that is within 15% of the actual vehicle weight for 95% of the vehicles in compliance with ASTM 1318-02 (Solanki et al., 2013).

Both the inner and the outer lanes near the WIM station were instrumented with two inductive loops and two piezoelectric sensors, each having a length of 12 ft. (Figures 3.6 and 3.7). The inductive loops detect the presence of a vehicle, whereas the piezoelectric sensors detect and record the number of axles, distance between axles and weight of each vehicle. The continuous traffic data were recorded for approximately four years by a 2 MB onboard memory and an automated electronic counter, called ADR 3000 (PEEK TOPS, 2010). Additionally, the piezoelectric sensor measures the weight of each axle and determines the gross weight of the vehicle by adding all axle loads. The piezoelectric sensor is triggered when a pressure is applied to it and produces an electric charge. Knowing the amount electric charge produced, the weight of a passing tire or a group of axles is determined using the calibration data [see Hossain (2010) and Breidy et al. (2011) for details].

3.7 Traffic Data Collection

The daily traffic data were downloaded from the WIM station to a laptop computer using a dial up Internet connection. For each day, two files were created, each

ending with a different extension (.bin and .pvr). However, both files are needed to generate the traffic data. A user-friendly Windows™ software is available to read the traffic data files recorded by the WIM station. The software used in the present study is called Traffic Operations Processing Software (TOPS version 3.7.1), which was provided by PEEK Traffic, through ODOT. The TOPS program allows multi-file processing, previewing, and editing of reports. It is also capable of generating daily, weekly, and monthly reports (PEEK TOPS, 2010).

In this study, four years (June, 2008 through May, 2012) of continuous traffic data were collected and processed. The analyses presented in this section summarize the traffic data collected over this period. For convenience, this time period is divided into four years, Year 1 covering June 2008 through May 2009, and Year 2 covering June 2009 through May 2010. Year 3 and Year 4 data follow the same nomenclature. It is important to note that the data during this four-year period were not entirely continuous; data from some days were lost due to technical problems with the WIM station. Overall, about 1 to 2% traffic data were lost over this four-year period. Also, only data for vehicles having two or more axles (FHWA Class 4 through Class 13) are considered herein. Motorcycles, cars and SUVs (Class 1 through Class 3) are excluded from the analysis for two reasons: first, these types of vehicles are not detectable by the WIM station, and second, their load impacts on the pavement are insignificant as compared to trucks.

Table 3.1 shows the yearly traffic volume that passed on the instrumented section and the difference in volume between two consecutive years. Year 2 had the lowest traffic volume, with a difference of -1.0% from the previous year. Year 3 and Year 4 showed an increase in traffic volume of about 2.3% and 3.3% from their previous years, respectively.

In total, more than 4.7 million vehicles (Class 4 through Class 13) passed through the section during the four-year period. This translates into Annual Average Daily Truck Traffic (AADTT) of 8,200 trucks per day on the Interstate-35 near the test section. A detailed description on the development of other traffic parameters (e.g., axle load, vehicle class, etc.) is given in Chapter 4.

3.8 Materials Property Data Collection

An array of laboratory and field tests was conducted to collect the materials property data. Specifically, Falling Weight Deflectometer (FWD) tests were conducted quarterly on the test section to obtain the in-situ layer moduli. In addition, asphalt mixes, aggregate base and natural subgrade materials were collected from the site during construction to conduct laboratory tests (namely, dynamic modulus, resilient modulus, dynamic shear rheometer tests, etc.). Details of the laboratory tests conducted and the material properties obtained are addressed in Chapter 4.

3.9 Pavement Performance Data Collection

Three types of pavement performance data, namely rut, crack mapping and International Roughness Index (IRI), were collected from the test section over a period of approximately six years (from August, 2008 through October, 2014). In consultation with the funding agency, it was decided to collect pavement performance data quarterly. This data collection interval was considered logical for two reasons:

a) The test section needs to be temporarily closed and all the intestate traffic needs to be channeled on the faster lane throughout the data collection time. Since, the test section has a heavy traffic volume (ADT of approximately

50,000 with appropriately 8,200 AADTT), it was not feasible to close down the traffic more frequently than every three months.

b) The data collection process required collaboration between the OU research team and ODOT personnel. Several traffic control personnel from ODOT Division Three and personnel from Planning and Research Division were actively involved in the data collection. Data collection cost was yet another factor in selecting the collection interval.

3.9.1 Rut Measurements

Rut measurements were conducted along the transverse direction of traffic flow at six selected locations specified above (Figure 3.2). Road straps were laid down on the pavement surface at these stations during the first distress survey on August 21, 2008. The rut measurements were taken along these straps to ensure that the measurement locations did not change with time. Two different methods were used to conduct rut measurements. The first method used a straight edge-rut gauge combination, while a Face Dipstick® was used in the second method. During the first three distress surveys (on August 21, 2008; December 3, 2008; and January 8, 2009), the straight edge-rut gauge combination method was used (Figure 3.8). Rut data obtained from the straight edge-rut gauge combination exhibited some inconsistencies in the beginning. For example, even with increased cumulative traffic traversing the pavement, the rut depth decreased in some sections, which is counter intuitive. Consequently, more accurate rut measurements were conducted using a Face Dipstick® (Figure 3.9) for the remaining five years (from May, 2009 through October, 2014). Details of the rut measurements and comparisons of

rut data between the straight edge-rut gauge combination and Face Dipstick® can be found in Hossain (2010).

A total of 18 rut measurements were conducted over the six-year period (August, 2008 to October, 2014). The rut progression graphs for all six stations are presented in Figure 3.10, each curve representing the rut progression at a specific station. The first three points on each curve (pertaining to August 21, 2008, December 3, 2008 and January 8, 2009 measurements) represent the highest rut depths measured with the straight edge-rut gauge combination. The rest of the points on each curve (from May 19, 2009 to July 21, 2014) represent the highest rut depths of the two wheel paths measured with the Face Dipstick®.

From the measured values (Figure 3.10), it is evident that the rut depths increased especially during warmer months, as expected (Hossain, 2010). After about four years of service (October, 2012), the maximum rut depth of 0.77 in. was recorded at Station 738. Comparatively, the minimum rut depth of 0.44 in. were observed at Station 900. The corresponding cumulative axles (not Equivalent Single Axle Load (ESAL)) traversing the test section were about 18.7 million. Although the rut values increased with time, most rut was accumulated during the summer months. For example, out of 0.77 in. of rut measured at Station 738, approximately 0.48 in. was accumulated during the summer months. Also, the rate of rut in the first summer months was much higher than in the second, third, and fourth summer months, although the cumulative axles during each summer were similar (approximately 1.2 million). A similar behavior of accumulation of rut in summer months has been reported in previous studies (Finn et al., 1977; Selvaraj, 2007).

It is observed from Figure 3.10 that the rut values generally increased for all the stations, with few exceptions. The increase in rut varied from 0.010 in. to 0.156 in. between the measurement intervals. At the end of the project (after about six years) the highest recorded rut value was 0.868 in., recorded on October 6, 2014 at Station 738.

Field measurements of rut show that all stations have undergone both primary rut and secondary rut. No tertiary rut was observed at any station. Similar type of rut behavior was observed at the AASHO road test (Finn et al., 1977) and NCAT Test Track (Selvaraj, 2007). Finn et al. (1977) and Selvaraj (2007) reported visible increase in rut depths during summer and fall months, but not in winter months. Thus, the observations from the present study are in agreement with those from the AASHO road test and the NCAT studies. Further discussions of field rut measurements can be found in Hossain (2010).

3.9.2 Crack Mapping

Crack mapping was performed for the entire test section during the quarterly field trips. For Stations 144, 319, 540, 738 and 900, crack mapping was performed over a distance of 50 ft. each way (north and south) at each station. To eliminate overlapping of mapping area, crack mapping was performed at 41 ft. north and 34 ft. south of Station 235.

Pavement cracks were observed on the traffic lane of the test section during the field trip in July, 2014, for the first time after approximately 6 years of service life and after approximately 4.3 million Equivalent Single Axle Load (ESAL) of traffic loading. Some of the cracks were longitudinal while the others were transverse. Figure 3.11 shows some of the cracks and their approximate locations. All the cracks were located within approximately 4 ft. from the beginning to approximately 132 ft. of the test section.

In addition, visible longitudinal cracking originating from the construction joint was observed along the pavement edge stripe. Figure 3.12 (a) shows a photographic view of the visible construction joints on February 14, 2011 at a distance of 38 ft. from the north end of the test section. For comparative purpose, additional photographs were taken on February 22nd, 2012, May 2nd, 2012, and August 21st, 2012, as shown in Figures 3.12 (b), (c) and (d), respectively. Photographic views of the construction joint at a distance of 795 ft. from the north end of the test section are presented in Figures 3.13 (a) through (d). It is evident from Figures 3.12 and 3.13 that the longitudinal crack opening increased with time. It is believed that repeated freeze-thaw cycles and precipitation played a key role in the significant growth in these longitudinal cracks.

The pavement surface also showed loss of aggregates (or raveling), as shown in Figures 3.14 and 3.15 at a distance of 318 and 741 ft. from the north end, respectively. Also, Figures 3.16 (a), (b), (c), and (d) show a comparison of pavement surface condition at Station 144 in the form of photographs taken on June 5, 2009, February 14, 2011, May 2, 2012, and August 21, 2012, respectively. It is evident from Figures 3.16 (a) through (d) that the pavement has undergone noticeable deterioration along the edges (between the driving lane and the shoulder). In summary, one can state that the test section showed signs of deterioration in terms of aggregate loss and joint cracking, however, no significant transverse, alligator or longitudinal cracks were observed within its six years of monitoring life. Overall, approximately 1% area of the test section showed some cracking, which can be considered negligible.

3.9.3 International Roughness Index (IRI) Measurements

In this study, the pavement smoothness was measured by a worldwide standard called the International Roughness Index or IRI (AASHTO, 2004). This index measures the pavement smoothness in terms of the number of inches per mile that a laser-mounted in a specialized van moves vertically as it is driven across the road (Solanki et al., 2013). Specifically, IRI is a longitudinal slice of the road showing elevation as it varies with longitudinal distance along a travelled track on the road. The lower the IRI number, the smoother the ride (Nair et al., 2011).

The IRI for the test section was evaluated using the Face Dipstick®. These data were collected at Station 319, spanning 50 ft. north and 50 ft. south and at three different locations, namely inner wheel path, outer wheel path and mid-lane (Figure 3.17). The mid-lane IRI value was evaluated for the test section for comparison purposes. The IRI values obtained from the two wheel paths on a given field trip was averaged to obtain a single IRI value for that trip. The progression of IRI at the test section is presented in graphical form in Figure 3.18. Based on Figure 3.18, the average IRI value of the two wheel paths at the test section started around 70 in./mile and generally increased almost continuously over time. The highest average IRI value was 154 in./mile. In general, the IRI values increased with time, which means that the road surface was getting rougher with time, as expected. Based on the Federal Highway Administration standard (Simpson et al., 2003) and the IRI values (between 95 in./mile and 170 in./mile), the pavement condition at the test section was considered “Fair” after six years of service life.

3.10 Summary

The following is a summary of the items discussed in this chapter:

- A 1,000 ft. long test section was constructed on the southbound (rightmost) lane of Interstate-35 (I-35) near Purcell, Oklahoma. A weigh-in-motion (WIM) station was installed approximately ¾ mile south of the test section to record the traffic data (vehicle type, axle load, axle configuration, etc.).
- The test section consisted of five layers: 2 HMA layers, an aggregate base layer, and a stabilized subgrade layer over natural subgrade. The overall thickness of the pavement was approximately 23 in.
- Traffic data were collected for approximately four years. The average truck traffic (AADTT) was found to be 8,200 trucks per day.
- Three types of pavement performance data: rut, crack mapping and International Roughness Index (IRI) were collected from the test section, at an interval of approximately three months, over a period of approximately six years (from August 2008 through October 2014).
- Rut data were collected mostly using a Face Dipstick®. A total of 18 sets of rut measurements was taken over this period. After six years of project life, the highest recorded rut value on the test section was 0.868 in. at Station 738. In general, it was observed that the rut depths increased especially during the warmer months. All stations exhibited both primary rut and secondary rut. No tertiary rut was observed at any station.
- Pavement cracks were observed on the traffic lane during the field trip in July, 2014, for the first time, after approximately six years of service life and after approximately 4.3 million Equivalent Single Axle Load (ESAL). In addition, visible longitudinal cracks originating from the construction joint were

observed along the pavement edge stripe. The test section exhibited signs of deterioration in terms of aggregate loss and joint cracking, however, no significant transverse, alligator or longitudinal cracking was observed within its six years of monitoring life.

- The IRI of the test section was evaluated using the Face Dipstick®. The highest average IRI value observed was 154 in./mile. In general, the IRI values increased with time, which means that the road surface became rougher with time, as expected.

Table 3.1: Traffic Volume Statistics

Traffic Volume	Lane 1	Lane 2	Total	Difference
Year 1	1,170,870	263,609	1,434,479	--
Year 2	1,156,246	248,544	1,404,791	-1.0%
Year 3	1,187,837	282,139	1,469,976	2.3%
Year 4	1,272,762	296,391	1,569,153	3.3%
Total Years	4,787,715	1,090,683	5,878,398	
Percentage	81.6%	18.4%	100%	

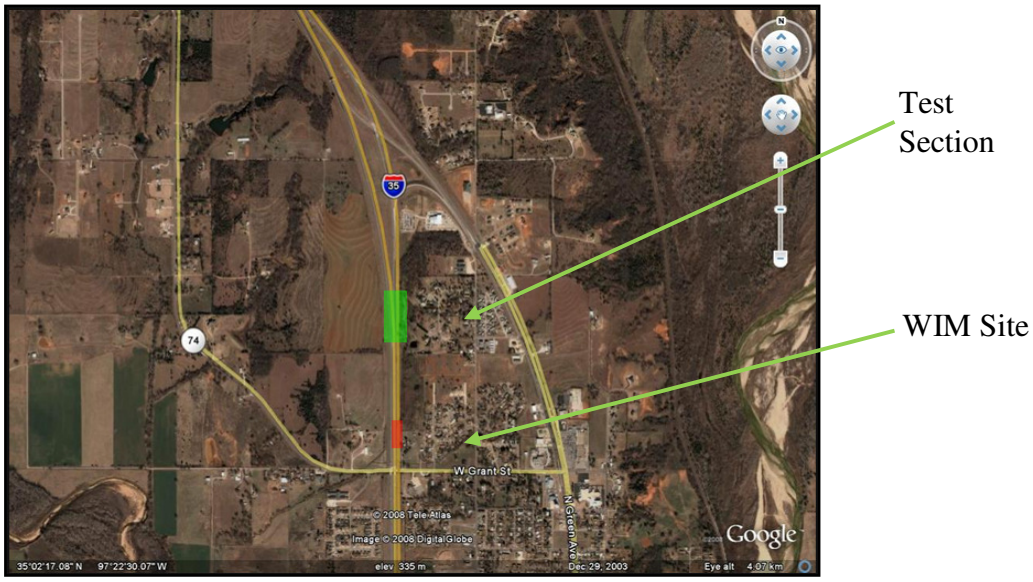

Figure 3.1: Aerial View of the Test Section and the WIM Site (Source: Google Maps) (Solanki et al., 2013)

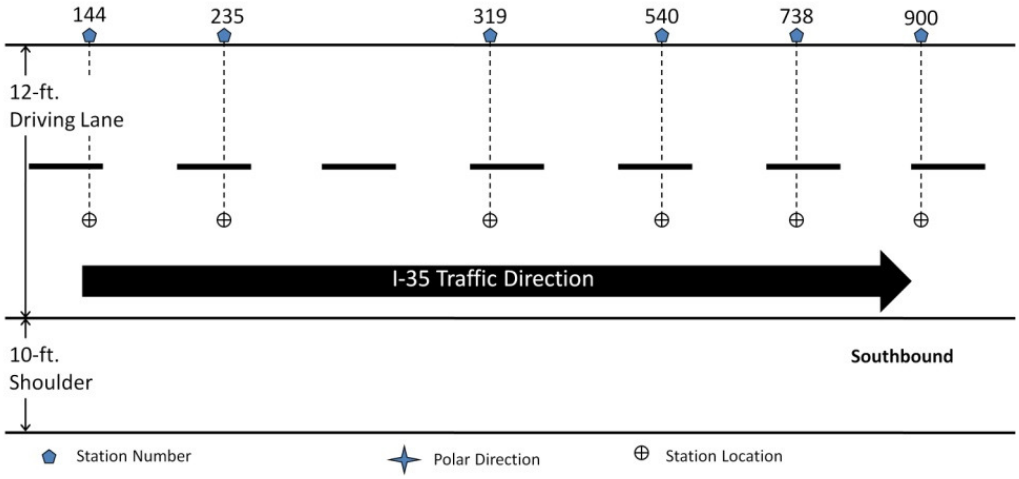

Figure 3.2: Station Locations on the Test Section (Zaman et al., 2009)

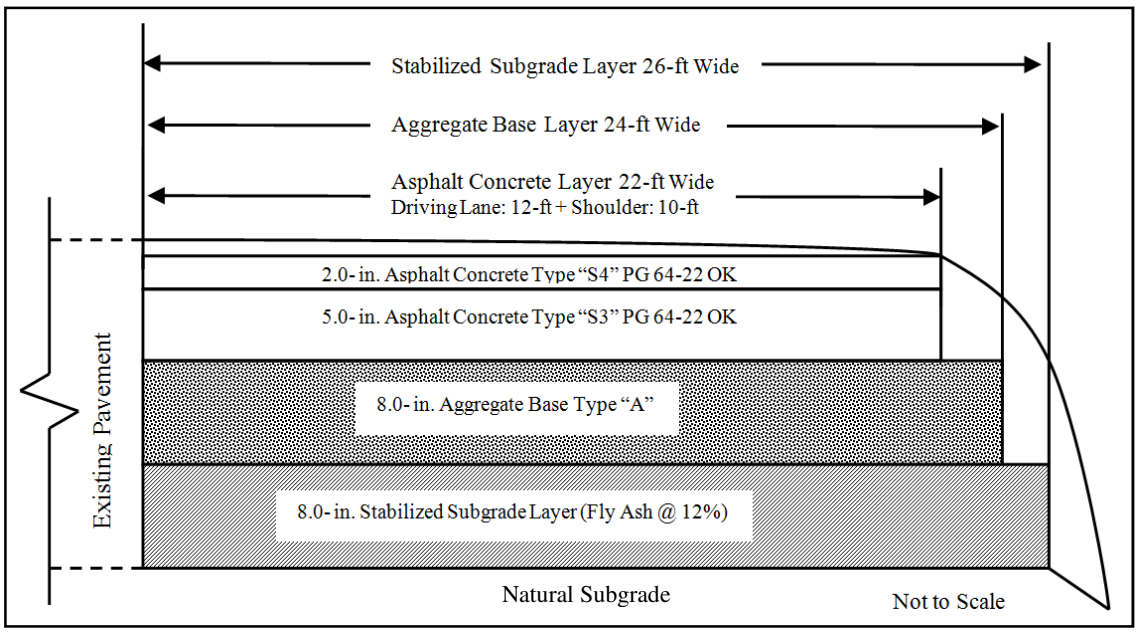

Figure 3.3: Sketch of the Test Section (Solanki et al., 2013, and Hossain et al., 2010)

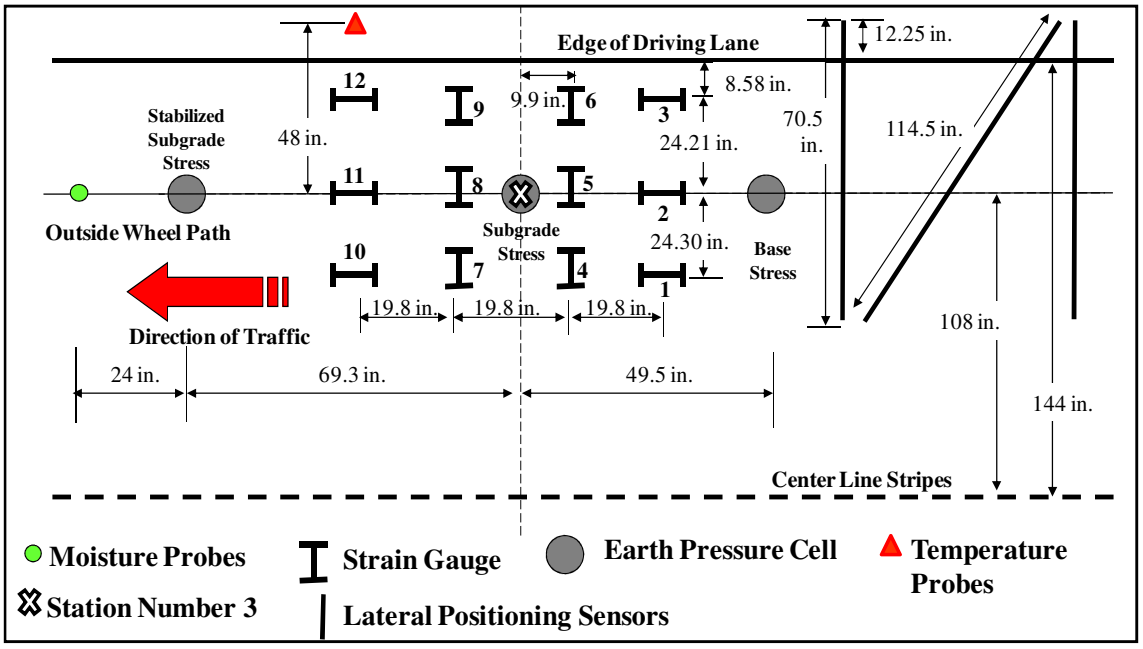

Figure 3.4: Dynamic Data Sensors Layout (Solanki et al., 2013)

Figure 3.5: Dynax® Lateral Positioning Sensors (Solanki et al., 2013)

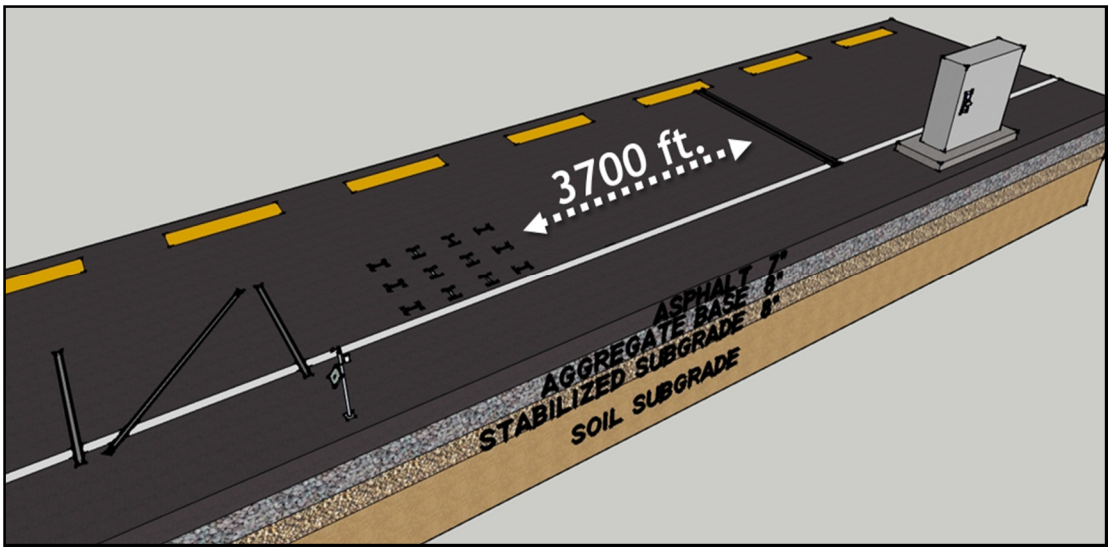

Figure 3.6: WIM Station Location Relative to the Test Section (Breidy et al., 2011)

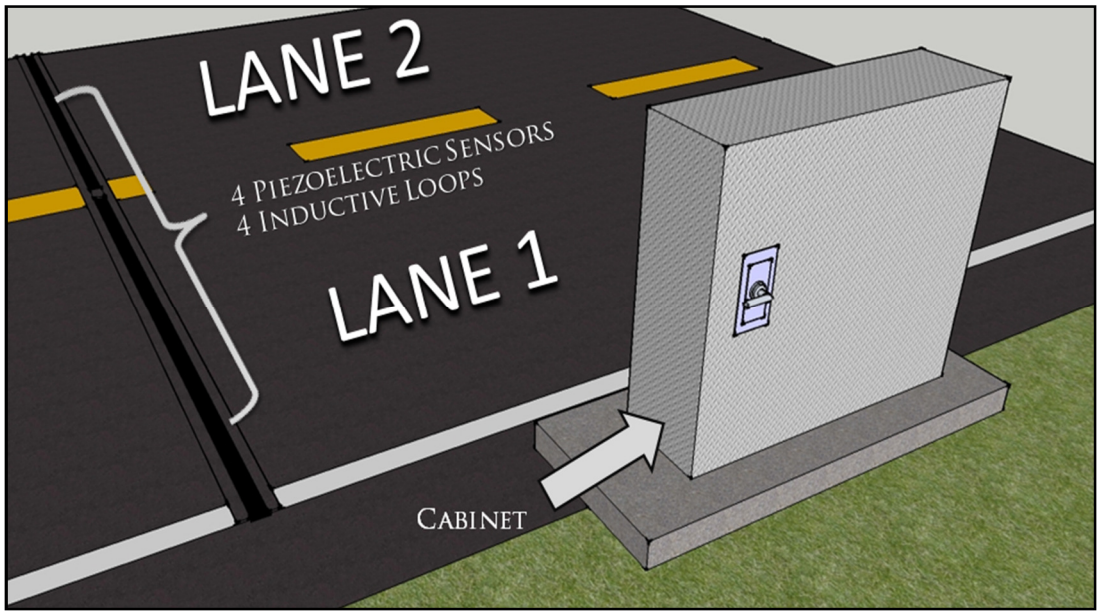

Figure 3.7: WIM Station Sensors (Breidy et al, 2011)

Figure 3.8: Rut Measurements with Straight Edge/Rut Gauge Combination (Hossain et al., 2010)

Figure 3.9: Rut Measurements with Face Dipstick® (Hossain et al., 2010)

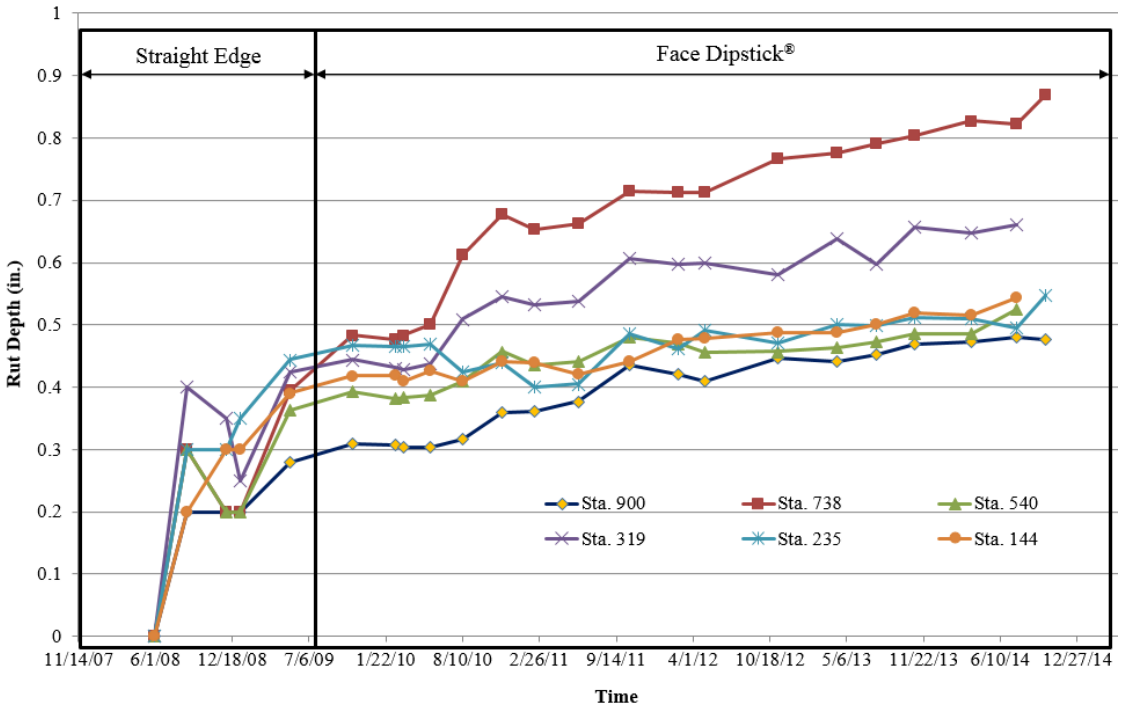

Figure 3.10: Rut Progression on the Test Section (Hossain et al., 2017)

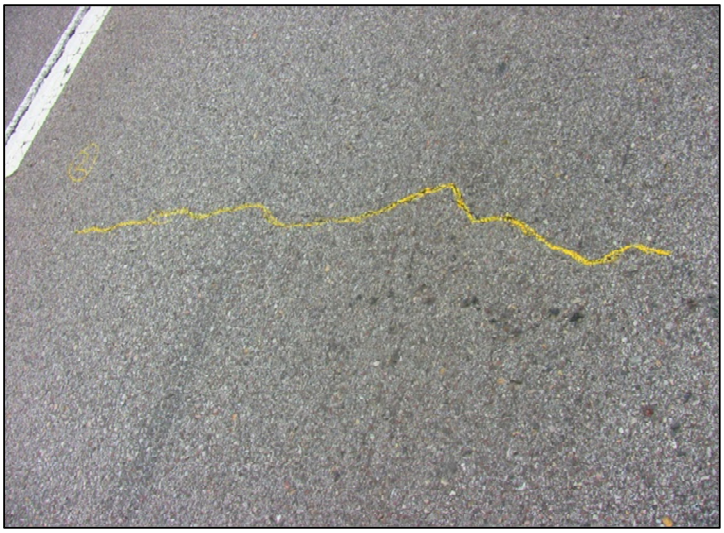

(a) Transverse Crack at 4 ft. from Start

(b) Longitudinal cracks from 24 ft. to 32 ft.

Figure 3.11: Crack Mapping on the Test Section (Hossain et al., 2017)

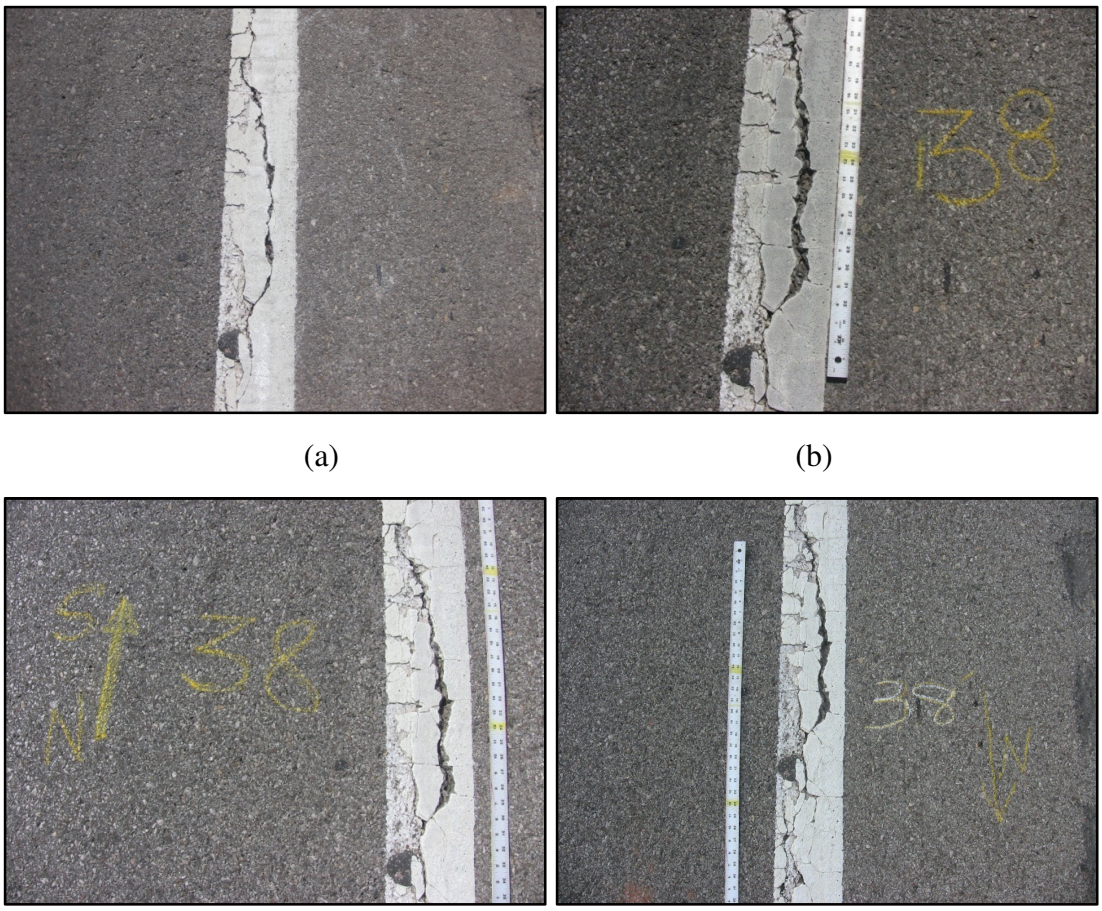

(a) (b)

(c) (d)

Figure 3.12: Photographic View of Construction Joint at a Distance of 38 ft. from North End of the Test Section on (a) February 14, 2011, (b) February 22, 2012, (c) May 02, 2012, and (d) August 21, 2012 (Solanki et al., 2013)

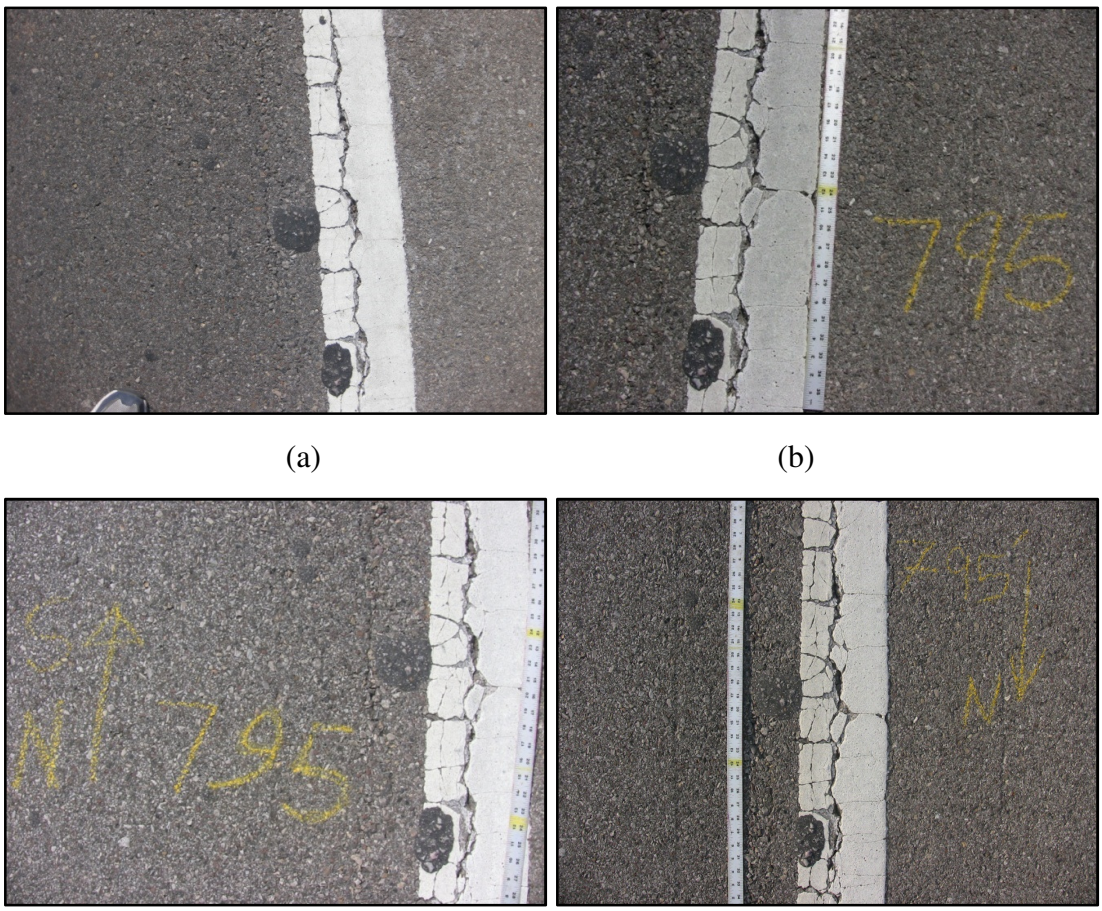

(a) (b)

(c) (d)

Figure 3.13: Photographic View of Construction Joint at a Distance of 795 ft. from North End of the Test Section on (a) February 14, 2011, (b) February 22, 2012, (c) May 02, 2012, and (d) August 21, 2012

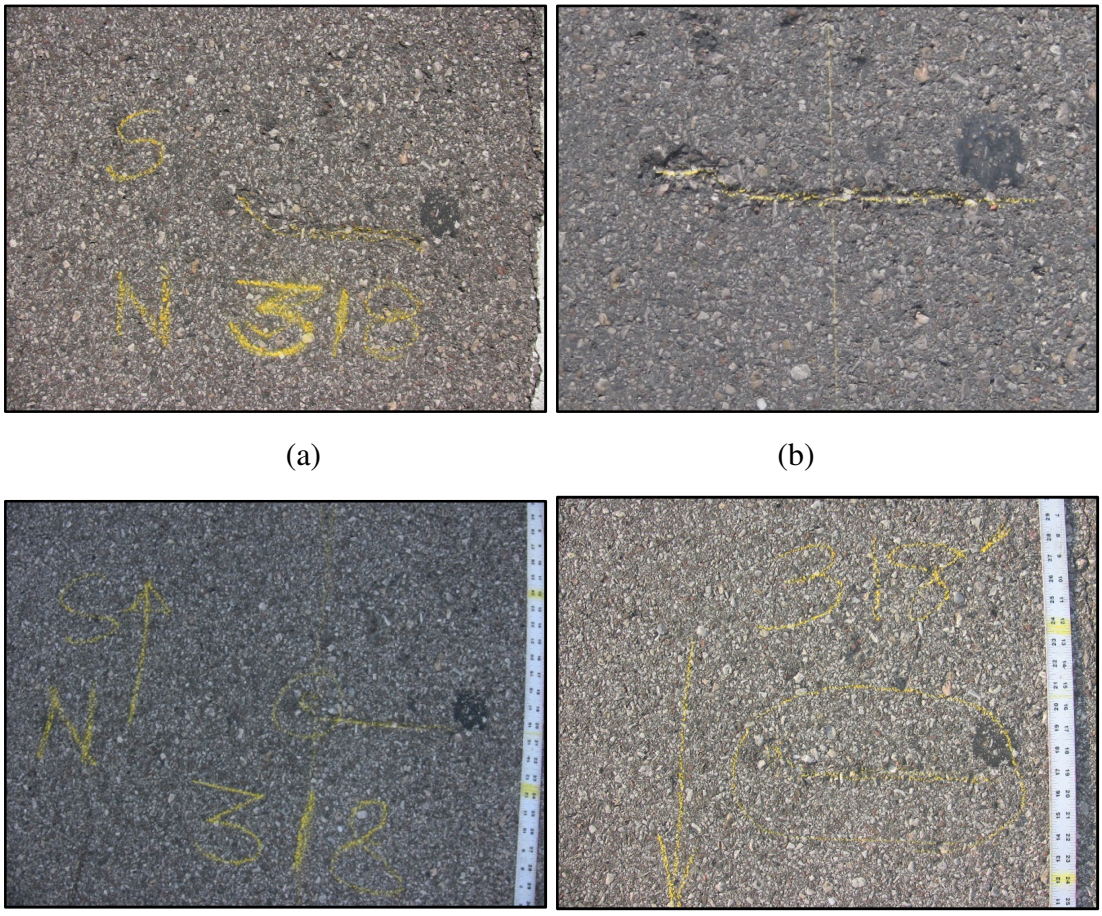

(a) (b)

(c) (d)

Figure 3.14: Photographic View of Loss of Aggregates from Pavement at a Distance of 318 ft. from North End of the Test Section on (a) February 14, 2011, (b) February 22, 2012, (c) May 02, 2012, and (d) August 21, 2012 (Solanki et al., 2013)

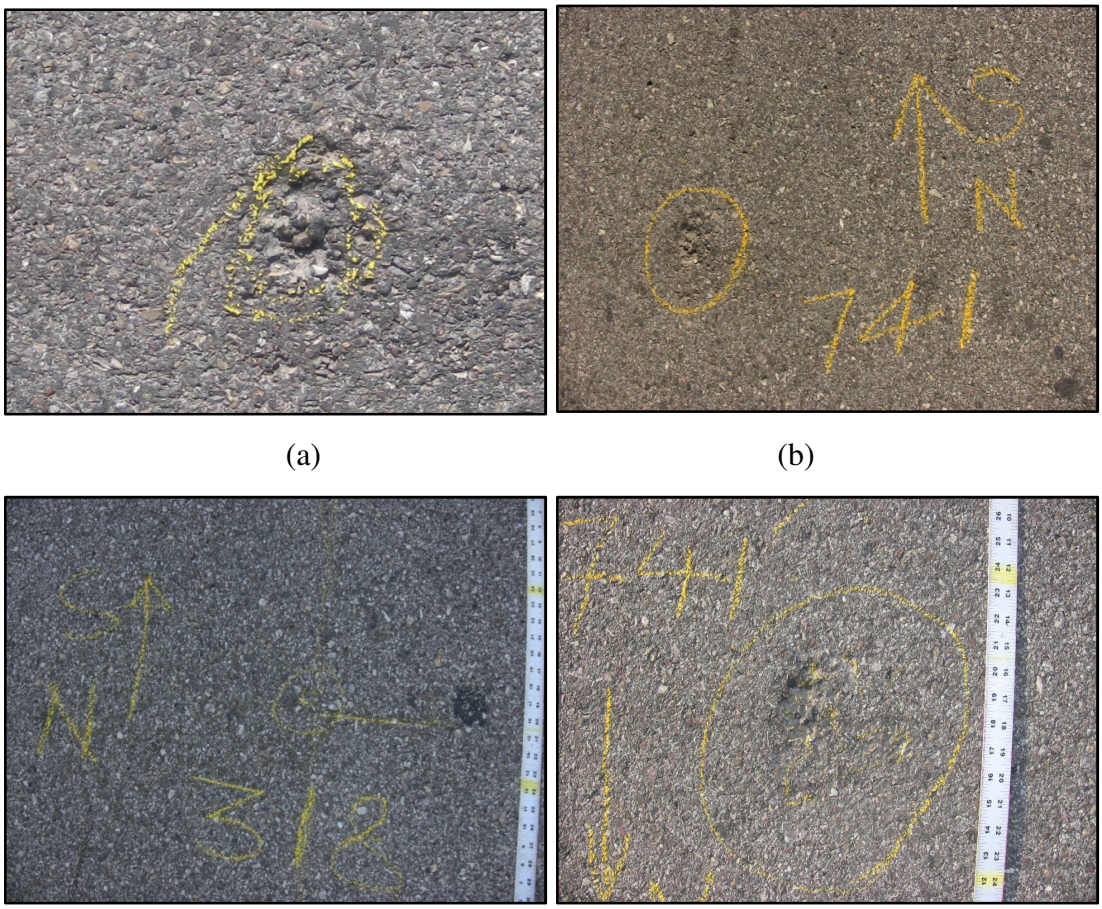

(a) (b)

(c) (d)

Figure 3.15: Photographic View of Loss of Aggregates from Pavement at a Distance of 741 ft. from North End of the Test Section on (a) February 14, 2011, (b) February 22, 2012, (c) May 02, 2012, and (d) August 21, 2012

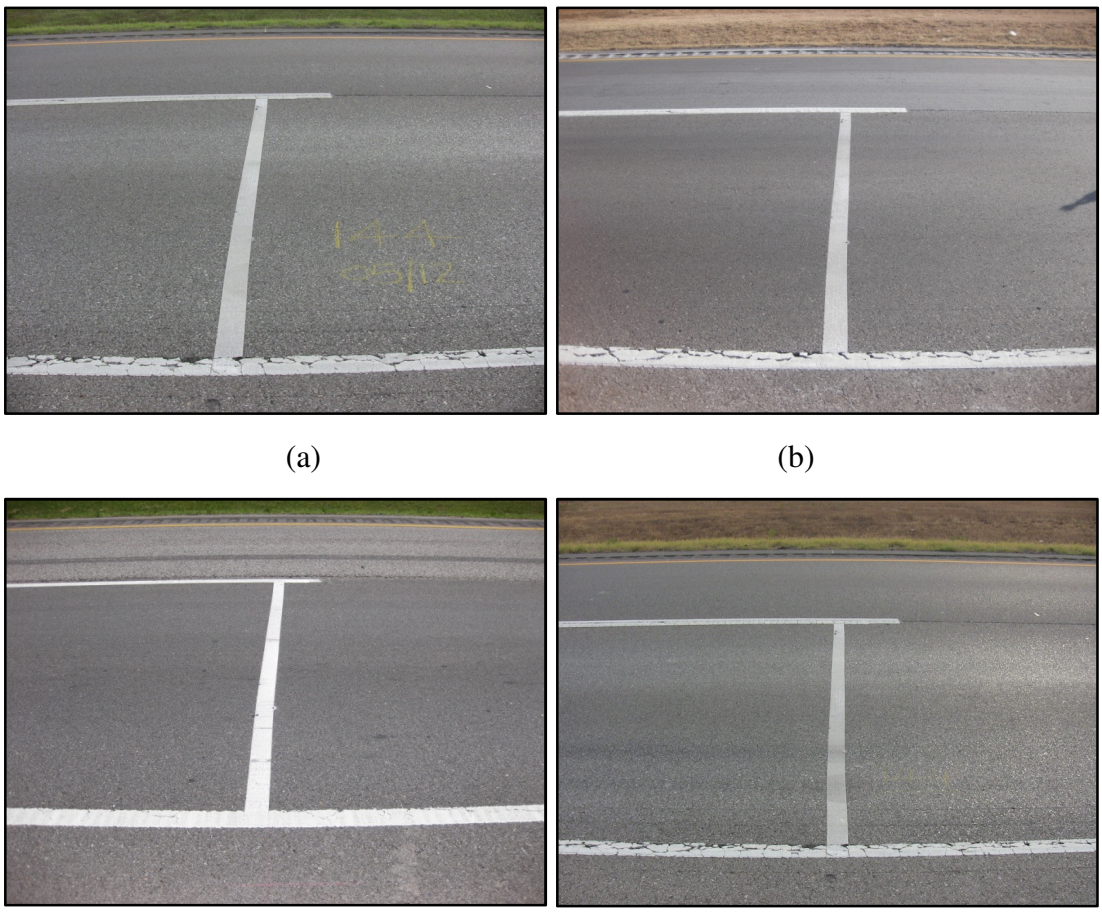

(a) (b)

(c) (d)

Figure 3.16: Photographic View of Pavement Surface at Station No. 144 taken on (a) June 05, 2009, (b) February 14, 2011, (c) May 02, 2012, and (d) August 21, 2012 (Solanki et al., 2013)

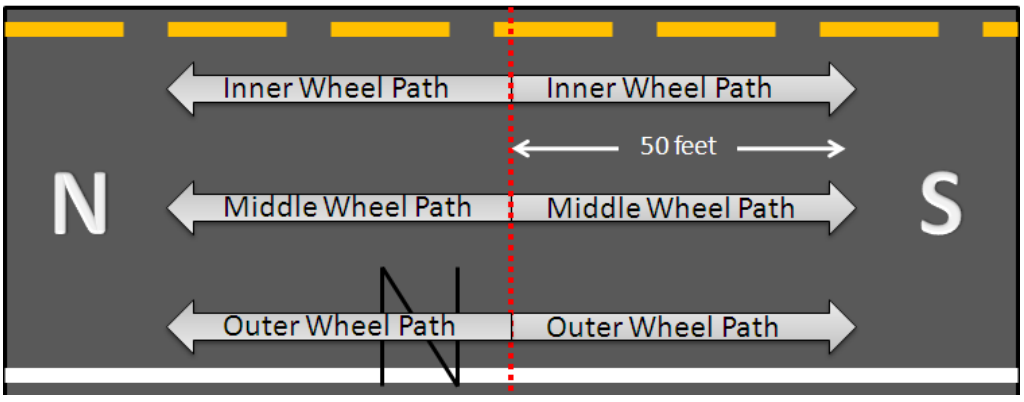

Figure 3.17: Sketch of IRI Locations on the Test Section (Breidy et al, 2011)

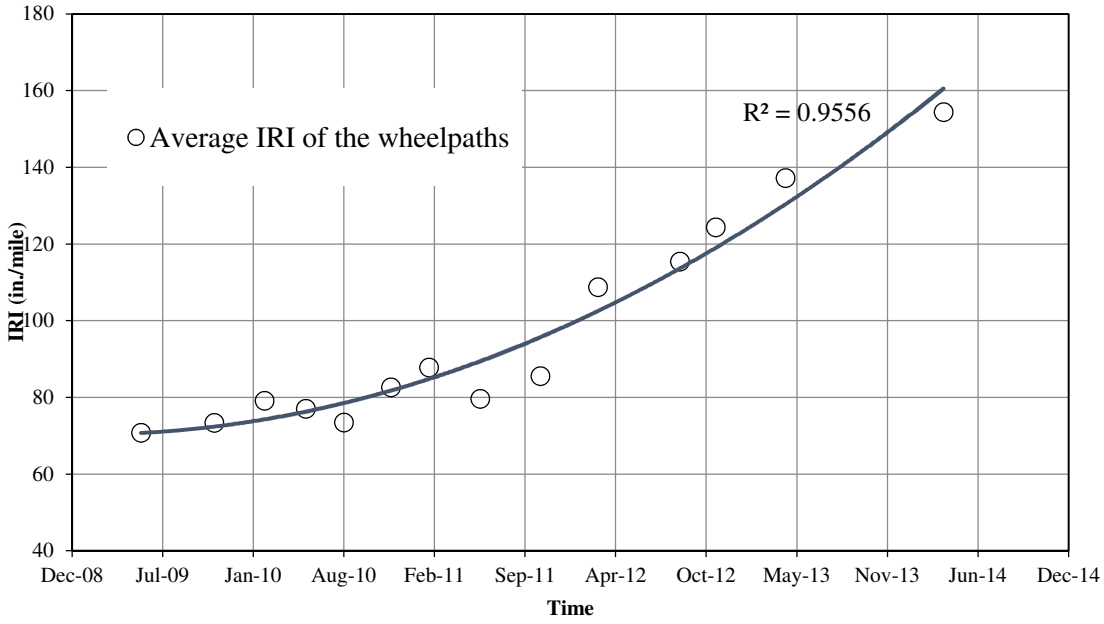

Figure 3.18: Average IRI Values for the Test Section (Hossain et al., 2017)

CHAPTER

4

Development of MEPDG Input Parameters

4.1 Introduction

Development of site specific traffic, material and climate input parameters at Level 1 is the initial step in designing a pavement using the AASTOWare software (AASHTO, 2004). This chapter describes the procedure used in this study to develop the traffic input parameters from the WIM site. Features of the developed inputs are also discussed. Moreover, this chapter discusses the tests conducted on materials collected from the test section, the test procedure and the test results. The developed traffic and materials data were used as Level 1 inputs in this study.

4.2 Development of Traffic Input Parameters

As described in Chapter 3, the WIM site was instrumented with inductive loops and piezoelectric sensors to capture axle configuration, weight, distance between axles, and other pertinent data for each vehicle passing through the test section. A commercial software, TOPS, developed by PEEK Traffic Corporation (PEEK TOPS, 2010), was used to reduce the traffic data collected by the WIM station and then saved as a Microsoft Excel file. Because of the massive volume of these data, they were loaded from Microsoft Excel to a MySQL database for faster processing. The column field of the MySQL database mostly comprises of date, time, vehicle class, and number of axles along with their consecutive distances (i.e., distance between two consecutive axles) and individual

weights. A program was written in SQL (Structured Query Language) to extract and process the data from this stored database. This program was also used to assess the quality of data and eliminate outliers.

As noted earlier, the Level 1 traffic data were developed from four years' (from June 2008 to May 2012) of WIM data collected from the instrumented site on Interstate-35, discussed in Section 3.6. As mentioned previously, Year 1 data represent the data collected from June 2008 through May 2009. Likewise, Year 2 data refer to the data collected from June 2009 through May 2010. Year 3 and Year 4 data follow the same nomenclature.

From the axle definition mentioned in the FHWA vehicle classification manual, the total number of single, tandem, tridem and quad axles was counted from the WIM data and then axles per volume (total number of vehicles) was determined by dividing the total axle count by the total volume of traffic. The SQL program also provided (month wise) axle weights for each axle group and for each FHWA vehicle classification. These output data were then transferred to Microsoft Excel and histograms were generated for different axle groups, on a monthly basis.

4.2.1 Vehicle Class Distribution (VCD) Factor

Vehicle Class Distribution Factors were developed using FHWA's vehicle classification guidelines. In the FHWA guidelines, all vehicles travelling on the U.S. highways are divided in to a total of 13 classes. Figure 4.1 shows a visual description of these vehicle classes. Table 4.1 also shows the category scheme of the classification table (Texas Department of Transportation, 2012). Vehicle class distribution (VCD) factors were developed using four years of traffic data noted above. The developed VCD

considered truck traffic only (FHWA vehicle Class 4 through Class 13). Figure 4.2 shows the vehicle class distribution factors developed. Table 4.2 also shows the percentage of each vehicle class in the respective years, along with the minimum, maximum and standard deviation for the respective vehicle classes for all four years. From the VCD distribution in Figure 4.2, it was observed that the highest percentage of vehicles at this site consisted of Class 9 vehicles (approximately 60%) followed by Class 5 vehicles (approximately 15%) (Hossain et al., 2015). It was also observed from Table 4.2 that Class 9 vehicles had the highest standard deviation (2.9%) whereas Class 7 vehicles had the lowest standard deviation (0.01%). Since, Class 9 vehicles (typical 18-wheeler semi-trailer trucks) are the most prominent trucks in the interstate system, the standard deviation (2.9%) for this vehicle class was considered reasonable. This observation is consistent with previous studies (see e.g., Tran and Hall, 2007). It should be noted that MEPDG lists 17 Truck Traffic Classification (TTC) groups based on the roadway functional class and the traffic stream. From the Level 1 traffic data developed in this study, the VCD data matched closely with the MEPDG truck traffic classification (TTC) for Group 2 (Hossain et al., 2016).

4.2.2 Monthly Adjustment Factor (MAF)

The monthly adjustment factor (MAF) represents the proportion of annual truck traffic for a given class of a vehicle that occurs in a specific month. Thus, the monthly distribution factors for a specific month is equal to the monthly truck traffic for a given class for the month divided by the total truck traffic for that class of truck for the entire year. Tables 4.3 through 4.6 present the MAFs for four years obtained from the collected traffic data. It can be observed from these tables that the MAFs varied from 0.25 to 2.47

during these four years. Based on the standard deviation values reported in these tables, in general, Class 6 vehicles had the maximum variation in MAF values whereas Class 5 and Class 9 had the minimum variation in MAF values.

4.2.3 Hourly Distribution Factor (HDF)

The Hourly Distribution Factor (HDF) represents the percentage of Average Annual Daily Truck Traffic (AADTT) within each hour of the day. Tables 4.7 through 4.10 present the developed HDFs for the four-year period. It was observed that the maximum HDF values varied between 5.93 and 6.03, whereas the minimum HDF values varied between 1.87 and 1.96. Comparatively, the standard deviations varied between 1.33 and 1.40. In general, around 10 a.m. the test section experienced the most traffic, whereas around 1 a.m. the test section experienced the least traffic on a given day.

4.2.4 Axle Load Spectra (ALS)

The axle load distribution factors represent the percentage of total axle applications within each load interval for a specific axle type and vehicle class (Class 4 to Class 13). As noted previously, definitions of load intervals for different axle types were used:

- Single Axles: 3 kips to 40 kips at 1 kip interval,
- Tandem Axles: 6 kips to 80 kips at 2 kips interval,
- Tridem and Quad Axles: 12 kips to 102 kips at 3 kips interval.

Axle load spectra for four axle types (single, tandem, tridem and quad) for all vehicles were developed using the collected WIM data. Tables 4.11 through 4.26 represent the axle load spectra for different axle types. Class 5 and Class 11 did not have

tandem axles, so the axle load spectra for these vehicle classes were unavailable. Therefore, these spectra were shown as 0.00 in Tables 4.12, 4.16, 4.20 and 4.24. Similarly, only Class 7, Class 10 and Class 13 had tridem axles as shown in Tables 4.13, 4.17, 4.21 and 4.25, whereas only Class 10 vehicles had quad axles, as shown in Tables 4.14, 4.18, 4.22 and 4.26.

It was observed that Class 9 vehicles are predominant (approximately 60%) among all vehicle classes. Therefore, the axle load distribution for Class 9 vehicles was further analyzed. Figures 4.3 and 4.4 show the axle load spectra for the single and tandem axles of Class 9 vehicles, respectively. It is observed from Figure 4.3 that for single axles the distribution peaks around 11 kips axle loads, which is the expected range for Class 9 single axles (Tran and Hall, 2007). It can be observed from Figure 4.4 that there are two distinct peaks for the tandem axle distribution: one between 10 and 16 kips and the other between 28 and 36 kips.

4.2.5 Lateral Traffic Wander

Wheel wander or the lateral distribution of wheel loads is a natural phenomenon observed on public roadways (Timm and Priest, 2005). It is defined as the calculated distance between the center of the right wheel of a vehicle's axle and the inside of the edge stripe of the road. Figure 4.5 is an illustration of two calculated distances for a steering and a tandem axle of a Class 9 vehicle. A wheel wander histogram is generated by selecting distances for hundreds of passing axles calculated from the LPS. Assuming a constant speed, the axle sensors calculate the distance by first recording the time stamp when the axle hits each of the three (z-shaped) axle sensors, and then by using the geometry shown in Figure 3.3.

The wheel wander histogram shown in Figure 4.6 was generated using 3,872 data points corresponding to 3,872 truck axles (steering and tandem) collected from 37 field trips between May 30, 2008 and April 14, 2009. By examining the histogram, it is evident that most axles traveled between the right and the center array of strain gauges, with a mean, μ, distance of 15.5 in. (represented by dashed black line) and a standard deviation, σ, of 10.2 in. These data are found to follow an approximately normal distribution, which is consistent with other wheel wander studies (Timm and Priest, 2005).

4.3 Development of Material Input Parameters

As noted previously, laboratory tests were conducted on the materials collected from the test section during construction to develop pertinent input parameters. The test procedures and results are discussed in this section.

4.3.1 Asphalt Layers

A summary of the mix properties for the collected loose asphalt mixes is shown in Table 4.27. It is evident that the S3 mix, which is a coarser mix, had a nominal maximum aggregate size (NMAS) of ¾ in. as compared to a NMAS of ½ in. for the S4 mix. A PG 64-22 binder was used for both mixes. The design binder contents for the S3 and S4 mixes were 4.1% and 4.6%, respectively. The S3 mix contained approximately 25% reclaimed asphalt pavement (RAP), but the S4 mix did not have any RAP.

4.3.1.1 Asphalt Mix

About 1,000 lbs of S4 and S3 bulk mixes were collected from the test section to perform laboratory tests, namely volumetric, dynamic modulus, rut, and fatigue. Dynamic Modulus values of asphalt mixes are used as Level 1 input in the MEPDG. Therefore, only Dynamic Modulus tests are discussed here.

Dynamic modulus tests were conducted on both S4 and S3 mixes in the laboratory in accordance with the AASHTO TP62 test method (AASHTO, 2007). To determine the target air voids for samples, a total of six pavement cores were obtained from the test section and their air voids were determined in the laboratory (Hossain et al., 2013). The average air voids and standard deviation for the top layer (S4 mix) were 9.1% and 0.63%, respectively. For the bottom layer (S3 mix), the corresponding values were 8% and 0.42%, respectively. Therefore, the target air voids for laboratory samples was selected as 9±0.5% and 8±0.5% for the S4 and the S3 layers, respectively. To prepare cylindrical samples, loose mixes were preheated in an oven for two hours at a temperature of 300°F. The compaction temperatures for the mixes were obtained from the mix design sheet. Specimens were compacted using a Superpave Gyratory Compactor (SGC). The SGC machine was operated in height mode so as to stop automatically when the desired height is reached. For each mix, three replicates samples were compacted.

Dynamic modulus tests were performed using a mechanical testing system (MTS) equipped with a servo-hydraulic testing system (MTS System Corporation, 2011). The test specimen was placed in an environmental chamber and allowed to reach equilibrium to the specified testing temperature ±0.5°F. The specimen temperature was monitored using a dummy specimen with a thermocouple mounted at the center. Two linear variable differential transducers (LVDTs) were mounted on the specimen at 4 in. gauge length. Two friction reducing end treatment (teflon papers) were placed between the specimen and loading platens. A sinusoidal axial compressive load was applied to the specimen in a cyclic manner, without any impact. The test was conducted on each specimen at four different temperatures: 40, 70, 104 and 131°F, starting from the lowest temperature and

moving to the highest temperature. For each temperature level, the test was conducted at different loading frequencies from the highest to the lowest: 25, 10, 5, 1, 0.5, and 0.1 Hz. Prior to testing, the specimen was conditioned by applying 200 cycles of load at a frequency of 25 Hz. The load magnitude was adjusted based on the material stiffness, temperature, and frequency to keep the strain level within 50-150 micro-strains (Tran and Hall, 2006). The data was recorded for the last 5 cycles of each loading sequence. Dynamic modulus values were calculated for combinations of temperatures and frequencies. The coefficient of variation (COV) for the dynamic modulus values was found to be less than 15%, which satisfied the limits given in AASHTO TP62 (AASHTO, 2007).

The master curves were constructed using the principle of time-temperature superposition and approach suggested by Bonaquist et al. (2005). The amount of shifting at each temperature required to form the master curve describes the temperature dependency of the material. First, a standard reference temperature is selected (i.e., 70°F), and then data at various temperatures are shifted with respect to time until the curves merge into a single smooth function. Figure 4.7 shows the master curves for both mixes. It can be seen that the bottom layer (S3 mix) has a higher dynamic modulus compared to the top layer (S4 mix) for different combinations of temperature and frequency. These master curves are required to estimate the dynamic modulus values for both the mixes for a wide range of temperature encountered in the field. Table 4.28 shows the dynamic modulus values for the S3 and S4 mixes at different temperature and frequencies. These values were used as he MEPDG inputs in this study.

4.3.1.2 Asphalt Binder

Dynamic Shear Rheometer (DSR) tests were performed on the asphalt binder (PG 64-22) following the ASTM D7175 test methods (ASTM, 2008) to obtain the complex shear modulus (G*) and the phase angle (δ). A small sample of asphalt binder (approximately 0.04 in. thick and 1 in. in diameter) was sandwiched between two plates of the DSR machine. The test specimen was kept at near constant temperature by heating and cooling the environmental chamber. The top plate oscillated at 1.59 Hz in a sinusoidal waveform while the equipment measured the maximum applied stress, the resulting maximum strain and the time lag between them. The DSR software then automatically calculated the complex modulus (G*) and phase angle (δ).

DSR tests were conducted under three different temperatures: 142, 147 and 152°F, for a loading rate of 1.59 Hz. Table 4.29 presents the binder test data used as inputs in this study. The other volumetric properties of the asphalt layers were obtained from the mix design sheets (Hossain, 2010). The mix design sheets for the S3 and S4 mixes are presented in Figures 4.8 and 4.9, respectively.

4.3.2 Aggregate Base Layer

The aggregate base used in this study was supplied by the Dolese Co. from its quarry located in Davis, Oklahoma (Solanki et al., 2013). Bulk aggregate samples were collected from the test site from five different locations during construction. Bulk samples were shoveled into plastic buckets, sealed to avoid any contamination, and hauled to the laboratory for testing. Before the start of any testing, moisture was removed from the bulk aggregates by oven-drying the aggregates for 24 hours in a pan at 237°F.

The gradation curve of the aggregate samples was determined in accordance with the ASTM C136 test method (ASTM, 2001). Figure 4.10 shows the average gradation curve (based on six replicates). The upper and lower limits of Type A aggregate base specified by the Oklahoma Department of Transportation are superimposed on this curve for comparison (ODOT, 2009). From Figure 4.10 it is observed that the maximum aggregate size (MAS) of the aggregate base layer is 1.5 in. The percent passing No. 200 sieve is approximately 4.3% (determined in accordance with the ASTM C-117 test method), which is on the lower end of the gradation curves for a Type 'A' aggregate base.

Before any further testing, the dried aggregates were sieved using a Gilson shaker in accordance with the sieve sizes recommended for Type 'A' gradation (ODOT, 2009). All particles larger than No. 200 (0.075 mm) were washed to remove any fines attached to their surfaces. This process eliminated the use of excess fines in the specimen gradations. The washed aggregates were once again oven-dried for 24 hours and then stored in sealed buckets for testing. These dried aggregates were mixed in the laboratory according to the required weight for preparing specimens.

Moisture-density relationship for the aggregate base was established in accordance with the ASTM D 698 (Method C) test method (ASTM, 2012). Specimens were compacted in a 6 in. mold, using an automatic mechanical compactor, in three equal layers with 56 blows per layer. The moisture-density curve for aggregate base is shown in Figure 4.11. The Optimum Moisture Content (OMC) and Maximum Dry Density (MDD) for the aggregate base was approximately 4.5% and 127.4 pcf, respectively.

Resilient modulus (M_r) tests were performed on two replicate specimens compacted at OMC in accordance with the AASHTO T 307 test method. After aggregates

were uniformly blended, the equivalent amount of water for OMC was added and mixed until uniformity. Then, the mixture was compacted in a cylindrical split steel mold, having a diameter of 6 in. and a height of 12 in, according to the method described by Shah (2007). This employs compaction of a specimen to a dry density approximately 98% of MDD in ten equal layers by applying 44 blows per layer (Solanki et al., 2013). Figures 4.12 and 4.13 show the photographic view of compacted specimen and setup used for M_r testing for aggregate base, respectively. The M_r values at different bulk stress ($\theta = \sigma_d + 3\sigma_3$; where θ = bulk stress, σ_d = deviatoric stress, and σ_3 = confining stress) are presented in Figure 4.14. It is evident that the M_r value of specimen varied from approximately 14,000 to 50,000 psi. Therefore, an average M_r value of 30,000 psi was used for aggregate base materials in this study.

4.3.3 Stabilized Subgrade Layer

The subgrade layer was stabilized with 12% class C fly ash (CFA), provided by Lafarge Corporation, Red Rock, Oklahoma (Solanki et al., 2013). The CFA used in this study had a combined silica, alumina, and ferric oxide (SAF) content of approximately 62%. The average calcium oxide (CaO) content was approximately 24%.

The collected soil was then air dried in the laboratory and processed by passing through a #4 sieve (Solanki et al., 2013). Then the subgrade soil was mixed manually with 12% CFA for determining the moisture-density relationship of soil-CFA mixture. The procedure consists of adding 12% CFA to the processed subgrade soil, based on the dry weight of the soil and conducting Proctor test in accordance with the ASTM D 698 test method. Specimens were compacted manually in a 4 in. diameter mold, using 5.5 lb hammer falling from 12 inches, in three equal layers with 25 blows per layer. The

moisture-density curve for the soil-CFA mix is shown in Figure 4.15. It is observed from Figure 4.15 that the MDD and OMC of the soil-CFA mix are approximately 111.3 pcf and 14%, respectively.

A total of four specimens: two at OMC and two at OMC+2% were prepared for M_r tests. The soil and CFA were mixed manually for uniformity. After the blending process, a desired amount of water was added to the soil, manually mixed for uniformity and pre-wetted for at least 16 hours in air sealed 2 gallon Ziploc® plastic bags. This mix was then compacted in five layers in a mold with a diameter of 4 in. and a height of 8 in. to reach a dry density of between 95%-100% of the MDD. After compaction, specimens were cured at a temperature of $73^o \pm 1.7^o$ F and a relative humidity of approximately 96%. After compaction, samples were tested for Mr in accordance with the AASHTO T 307-99 test method. The M_r test consisted of applying a cyclic haversine-shaped load with a duration of 0.1 seconds and rest period of 0.9 seconds. For each sequence, the applied load and the vertical displacement for the last five cycles were measured and used to determine the M_r values. The load was measured by using an internally mounted load cell, having a capacity of 500 lbf. The resilient displacements were measured using two linear variable differential transformers (LVDTs) fixed to opposite sides of and equidistant from the piston rod outside the test chamber. The LVDTs had a maximum stroke length of 1 in. A MTS Micro Controller system and Multi-Purpose Test Ware software were used in running these tests, as shown in Figure 4.16.

Both specimens were tested at a total of five different curing periods: 2, 8, 16, 23, and 30 days. A summary of average M_r result is presented in Table 4.30 and 4.31 for specimens compacted at OMC and OMC+2%, respectively. One way to observe the

resilient modulus is to evaluate the changes in M_r values at a specific deviatoric stress and confining pressure (Solanki et al., 2013; Drumm et al., 1997). A deviatoric stress-based model commonly used by ODOT was chosen in this study for this purpose.

$$M_r = k_1 \, x \, \sigma_d^{k2} \quad (4.1)$$

In this model, the Mr is expressed as a function of deviatoric stress (σ_d). Table 4.30 and 4.31 present the aforementioned model parameters (k_1 and k_2). The M_r values were calculated at a σ_d of 6 psi and a confining pressure (σ_3) of 4 psi, as suggested by ODOT (Dean, 2008). It can be observed from tables 4.30 and 4.31 that the M_r values are increasing with increased curing time for both the OMC and OMC+2 cases.

4.3.4 Natural Subgrade Layer

To conduct tests on natural subgrade materials, approximately 100 lbs of soil was collected from a location close to the center of the proposed instrumentation array. The collected soil was then air dried in the laboratory and processed by passing through a #4 sieve (Solanki et al., 2013). The maximum dry density (MDD) and optimum moisture content (OMC) were determined by conducting standard Proctor tests in accordance with the ASTM D 698 test method (ASTM, 2012). Specimens were compacted manually in a 4 in. diameter mold, using 5.5 lb hammer falling from 12 inches, in three equal layers with 25 blows per layer. The moisture-density curve for the subgrade soil is shown in Figure 4.17. From this figure, the MDD and OMC are found to be approximately 110.4 pcf and 14.5%, respectively.

Although the AASTOWare software is not calibrated for the M_r of stabilized subgrade layers, M_r of natural subgrade is an essential material input required in the

AASTOWare® (AASHTO, 2004). A total of four specimens were compacted for the M_r tests, two at OMC and the other two at 2% wetter than the OMC (OMC+2%). A desired amount of water was added to the soil, manually mixed for uniformity and pre-wetted for at least 16 hours in air sealed 2 gallon Ziploc® plastic bags. This mix was compacted in five layers in a mold with a diameter of 4 in. and a height of 8 in. to reach a dry density of between 95%-100% of the MDD. After compaction, samples were tested for M_r in accordance with the AASHTO T 307-99 test method. Table 4.32 shows the average resilient modulus values at different deviatoric stress and confining pressures. It is clear from Table 4.32 that subgrade soil samples compacted at OMC and OMC+2% provide a pavement design M_r values of 17,008 and 12,327 psi, respectively (Solanki et al., 2013).

4.4 Development of Climate Input Parameters

Inclusion of climatic data for any particular geographic region and the performance prediction of a pavement based on that specific climate is one of the major advances in pavement design using the AASHTOWare® over the 1993 AASHTO approach. A weather station installed near the test section for this purpose. However, the weather station stopped working after a couple of months. Therefore, a virtual weather station was created using the AASHTOWare® software to generate the climatic data for the test section. The latitude and longitude of the test section were N35.045343° and W97.378348°, respectively. Based on these GPS coordinates, a virtual weather station was created using nearby seven weather stations. Climate data were then generated from this virtual weather station. Figure 4.18 shows the location of those seven weather stations: two from Oklahoma City area, one weather station each from Guthrie, Lawton,

Stillwater, Hobart and McAlester area (Hossain et al., 2015). Table 4.33 shows the coordinates of those stations along with their approximate distances from the test section.

Depth of groundwater is one of the climatic input parameters in the AASHTOWare®. From the subsurface exploration conducted during construction of the section, the groundwater depth was found to be approximately 10 ft. below existing grade, which was used as input in this study.

4.5 Summary

The following conclusions can be drawn from this chapter:

- Level 1 traffic inputs were developed using approximately four years of data collected from the test section. Required traffic inputs including VCD, MAF, HDF, ALS, lateral traffic wander etc. were developed. A WIM site was used to collect the traffic data and several software, namely, TOPS, MySQL, Microsoft Excel etc. were used to analyze the collected traffic data and generate Level 1 traffic inputs for the study.
- It was observed that the highest percentage of vehicle at this site is of Class 9 vehicles (approximately 60%) followed by Class 5 vehicles (approximately 15%).
- The MAFs varied from 0.25 to 2.47 in these four years, with Class 6 vehicles having the maximum variation in MAF values in the test section.
- Based on the HDFs, at around 10 a.m. the test section experienced the most traffic whereas at around 1 a.m. the test section experienced the least traffic on any given day.

- From the lateral traffic wander data, it was found that the most axles traveled between the right and the center array of strain gauges, with a mean distance of 15.5 in. and a standard deviation of 10.2 in.
- An array of tests were conducted on the materials collected from the test section during construction to develop the Level 1 material input parameters for this study. These tests included Dynamic modulus tests on asphalt mixes, DSR tests on asphalt binder, volumetric tests of asphalt, and resilient modulus tests on aggregate base, stabilized subgrade and natural subgrade materials.
- The M_r value for aggregate base varied from approximately 14,000 to 50,000 psi with an average of 30,000 psi. The M_r values obtained for the natural subgrade materials compacted at OMC and OMC+2% provide a pavement design M_r values of 17,008 and 12,327 psi, respectively.
- Climate input parameters were developed by generating a virtual weather station using the AASHTOWare® from nearby seven weather stations.

Table 4.1: FHWA Vehicle Classification Category Scheme

Vehicle Class	General Description	Definition	Additional Identifiers
1	Motorcycles	2 axles, 2 or 3 wheels.	Also motor scooters, mopeds, and 3-wheel motorcycles.
2	Passenger cars	2 axles.	Short-bed pickup (5-6'), no extended cab; SUVs; minivan; sedan.
3	Pickups, panels, vans	2-axle, 4-tire single units. Can have 1- or 2-axle trailers.	Long-bed pickup (8'), no extended cab; short-bed and long-bed pickups with extended cab or 4 doors; conversion van; full-size work van; limousine - regular; short-bed dually.
4	Buses	2- or 3-axle, full length.	School; transit; private; commercial. Does not include compact school buses.
5	Single-unit trucks	2-axle, 6-tire, (dual rear tires), single-unit trucks.	Approx. 21' steering to rear axles; 8' bed dually with 4 full doors; dump or sewage truck (with or without 2-axle trailer); compact school bus or 4 full doors; extended limousines.
6	Single-unit trucks	3-axle, single-unit trucks.	Dump truck; single tractor with 3 axles and no trailer; oil field equipment.
7	Single-unit trucks	4 or more axle, single-unit trucks.	4 or more axle trucks on a single frame.
8	Single-trailer trucks	3- or 4-axle, single-trailer trucks.	2-axle truck/tractor pulling single 1-axle trailer; 2-axle pulling single 2-axle trailer; 3-axle pulling single 1-axle trailer.
9	Single-trailer trucks	5-axle, single-trailer trucks.	3-axle truck/tractor pulling single 2-axle trailer (18-wheeler); 2-axle pulling single 3-axle trailer; dump truck pulling 2-axle trailer.
10	Single-trailer trucks	6 or more axle, single-trailer trucks.	3-axle truck/tractor with single 3 or more axle trailer.
11	Multi-trailer trucks	5 or less axle, multi-trailer trucks.	2-axle truck/tractor with 2 trailers, the first trailer with 1 axle, the second trailer with 2 axles.
12	Multi-trailer trucks	6-axle, multi-trailer trucks.	2-3 axle truck/tractor with 2 trailers, the first trailer with 1-2 axles, the second trailer with 2 axles.
13	Multi-trailer trucks	7 or more axle, multi-trailer trucks.	3-axle truck/tractor with 2 or more trailers.

Table 4.2: Vehicle Class Distribution Factors at the Test Section

Year	Vehicle Class									
	4	**5**	**6**	**7**	**8**	**9**	**10**	**11**	**12**	**13**
Year 1	5.74	15.53	6.31	0.15	9.90	58.53	0.59	2.15	1.01	0.07
Year 2	5.38	14.10	6.34	0.13	9.94	60.09	0.61	2.21	1.13	0.05
Year 3	6.10	15.02	7.49	0.15	9.43	58.04	0.60	2.05	1.04	0.06
Year 4	4.08	12.88	3.16	0.13	9.90	65.40	0.90	2.18	1.11	0.19
Min	4.08	12.88	3.16	0.13	9.43	58.04	0.59	2.05	1.01	0.05
Max	6.10	15.53	7.49	0.15	9.94	65.40	0.90	2.21	1.13	0.19
Standard Deviation (%)	0.77	1.01	1.61	0.01	0.21	2.92	0.13	0.06	0.05	0.06

Table 4.3: Monthly Adjustment Factors for Year 1

Month	Vehicle Class									
	4	**5**	**6**	**7**	**8**	**9**	**10**	**11**	**12**	**13**
June	0.98	0.95	0.93	1.18	1.20	1.13	1.17	1.15	1.06	1.06
July	2.19	2.47	0.78	0.95	1.02	0.64	0.80	0.63	0.68	0.71
August	0.87	0.96	0.80	1.27	1.10	1.15	1.12	1.05	1.15	0.91
September	0.87	0.88	0.82	0.88	1.06	1.09	1.05	1.06	1.14	0.95
October	1.05	0.93	1.24	1.16	1.19	1.12	1.16	1.25	1.20	1.16
November	0.63	0.65	0.66	0.92	0.73	0.70	0.61	0.62	0.69	0.52
December	0.73	0.79	0.81	0.93	0.77	0.89	0.83	0.89	1.07	0.81
January	0.91	0.86	1.24	0.72	0.89	1.05	0.99	1.09	0.95	1.25
February	0.89	0.81	1.25	0.83	0.86	1.03	1.09	1.07	0.95	1.11
March	0.96	0.88	1.16	0.98	1.03	1.07	1.10	1.04	0.95	1.03
April	0.96	0.92	1.29	1.04	1.07	1.06	1.07	1.09	1.06	1.28
May	0.96	0.92	1.04	1.15	1.08	1.06	1.01	1.07	1.10	1.20
Min	0.63	0.65	0.66	0.72	0.73	0.64	0.61	0.62	0.68	0.52
Max	2.19	2.47	1.29	1.27	1.20	1.15	1.17	1.25	1.20	1.28
Mean	1.00	1.00	1.00	1.00	1.00	1.00	1.00	1.00	1.00	1.00
Standard Deviation	0.37	0.45	0.22	0.16	0.15	0.16	0.16	0.19	0.16	0.22

Table 4.4: Monthly Adjustment Factors for Year 2

Month	Vehicle Class									
	4	**5**	**6**	**7**	**8**	**9**	**10**	**11**	**12**	**13**
June	0.51	0.55	0.38	0.43	0.58	0.57	0.54	0.49	0.46	0.39
July	0.85	0.87	0.68	0.72	0.92	0.77	0.83	0.67	0.65	0.91
August	1.33	1.28	1.74	1.23	1.22	1.00	1.01	0.90	0.87	1.28
September	1.14	1.14	1.14	1.29	1.15	1.12	1.28	1.18	1.13	1.26
October	1.23	1.16	1.32	1.18	1.29	1.14	1.18	1.18	1.20	1.18
November	1.16	1.08	1.32	1.06	1.11	1.08	1.04	1.08	1.11	1.18
December	1.18	1.10	1.38	1.11	1.01	1.13	1.09	1.23	1.38	1.09
January	0.82	0.86	0.83	1.11	0.78	0.91	0.87	0.89	0.90	1.14
February	0.76	0.80	0.76	0.97	0.67	0.86	0.77	0.87	0.93	0.74
March	1.05	1.04	1.09	1.07	1.04	1.12	1.03	1.20	1.19	1.05
April	1.01	1.03	0.72	1.11	1.08	1.14	1.12	1.15	1.10	1.05
May	0.96	1.09	0.63	0.74	1.14	1.18	1.26	1.15	1.08	0.72
Min	0.51	0.55	0.38	0.43	0.58	0.57	0.54	0.49	0.46	0.39
Max	1.33	1.28	1.74	1.29	1.29	1.18	1.28	1.23	1.38	1.28
Mean	1.00	1.00	1.00	1.00	1.00	1.00	1.00	1.00	1.00	1.00
Standard Deviation	0.22	0.19	0.38	0.24	0.21	0.18	0.21	0.23	0.24	0.25

Table 4.5: Monthly Adjustment Factors for Year 3

Month	Vehicle Class									
	4	5	6	7	8	9	10	11	12	13
June	0.99	0.94	1.00	1.48	1.12	1.08	0.98	1.15	1.06	0.79
July	0.95	0.95	0.91	1.44	1.14	1.03	1.11	1.07	1.04	1.04
August	0.88	0.93	0.68	1.06	1.04	1.17	1.31	1.14	1.09	0.96
September	0.83	0.87	0.51	0.72	1.10	1.16	1.22	1.06	1.05	1.38
October	0.88	0.90	0.57	1.03	1.17	1.14	1.12	1.09	1.06	1.22
November	0.82	0.88	0.53	1.09	1.05	1.07	1.05	1.04	1.07	1.06
December	0.77	0.86	0.57	0.69	0.94	1.05	1.13	1.00	1.16	1.32
January	0.79	0.79	0.96	0.68	0.84	0.95	0.95	0.97	0.96	0.90
February	0.74	0.68	0.90	0.68	0.64	0.84	0.78	0.84	0.90	0.63
March	1.75	1.47	1.84	1.12	0.97	0.90	0.80	0.99	0.97	0.96
April	1.26	1.33	1.68	1.04	0.91	0.68	0.59	0.72	0.71	0.74
May	1.34	1.40	1.85	0.97	1.09	0.93	0.97	0.94	0.92	1.00
Min	0.74	0.68	0.51	0.68	0.64	0.68	0.59	0.72	0.71	0.63
Max	1.75	1.47	1.85	1.48	1.17	1.17	1.31	1.15	1.16	1.38
Mean	1.00	1.00	1.00	1.00	1.00	1.00	1.00	1.00	1.00	1.00
Standard Deviation	0.29	0.24	0.49	0.26	0.15	0.14	0.19	0.12	0.11	0.22

Table 4.6: Monthly Adjustment Factors for Year 4

Month	Vehicle Class									
	4	5	6	7	8	9	10	11	12	13
June	0.99	1.03	0.93	0.99	1.07	1.02	1.13	1.03	1.04	1.13
July	0.99	1.07	0.91	0.91	1.09	1.03	1.13	1.00	1.06	1.20
August	0.82	1.06	0.72	1.68	1.05	1.10	1.24	1.05	1.10	1.81
September	0.86	0.97	0.74	0.55	1.05	1.02	1.29	0.97	0.99	1.27
October	0.83	1.01	0.61	0.79	1.12	1.05	1.09	1.06	1.02	1.80
November	0.76	1.00	0.64	0.58	1.03	0.99	1.07	0.93	0.97	1.63
December	0.73	0.96	0.55	0.66	0.86	0.91	1.01	0.81	0.87	1.44
January	1.18	0.95	1.51	1.03	0.86	0.96	0.76	0.95	0.94	0.35
February	1.12	0.90	1.47	1.11	0.80	0.93	0.68	0.98	1.01	0.25
March	1.24	1.01	1.34	1.28	1.01	0.98	0.82	1.09	1.07	0.33
April	1.22	0.96	1.21	1.23	0.99	0.98	0.89	1.03	0.95	0.32
May	1.27	1.07	1.39	1.19	1.08	1.02	0.87	1.09	0.99	0.48
Min	0.73	0.90	0.55	0.55	0.80	0.91	0.68	0.81	0.87	0.25
Max	1.27	1.07	1.51	1.68	1.12	1.10	1.29	1.09	1.10	1.81
Mean	1.00	1.00	1.00	1.00	1.00	1.00	1.00	1.00	1.00	1.00
Standard Deviation	0.19	0.05	0.35	0.32	0.10	0.05	0.19	0.08	0.06	0.59

Table 4.7: Hourly Distribution Factors for Year 1

Hour	Hourly Distribution Factor	Hour	Hourly Distribution Factor
0	1.93	12	5.83
1	1.94	13	5.74
2	2.27	14	5.60
3	2.83	15	5.33
4	3.13	16	4.92
5	3.49	17	4.76
6	4.15	18	4.34
7	4.96	19	3.91
8	5.65	20	3.63
9	5.96	21	3.10
10	5.96	22	2.57
11	5.87	23	2.14

Table 4.8: Hourly Distribution Factors for Year 2

Hour	Hourly Distribution Factor	Hour	Hourly Distribution Factor
0	2.01	12	5.77
1	1.96	13	5.63
2	1.99	14	5.59
3	2.65	15	5.48
4	3.28	16	5.09
5	3.18	17	4.71
6	3.79	18	4.55
7	4.56	19	4.13
8	5.27	20	3.74
9	5.73	21	3.35
10	5.93	22	3.14
11	5.89	23	2.58

Table 4.9: Hourly Distribution Factors for Year 3

Hour	Hourly Distribution Factor	Hour	Hourly Distribution Factor
0	1.98	12	5.86
1	1.93	13	5.78
2	2.00	14	5.75
3	2.71	15	5.66
4	3.34	16	5.26
5	3.10	17	4.70
6	3.81	18	4.66
7	4.52	19	4.05
8	5.20	20	3.60
9	5.78	21	3.26
10	5.96	22	2.88
11	5.93	23	2.29

Table 4.10: Hourly Distribution Factors for Year 4

Hour	Hourly Distribution Factor	Hour	Hourly Distribution Factor
0	1.88	12	5.90
1	1.87	13	5.72
2	1.97	14	5.63
3	2.68	15	5.53
4	3.35	16	5.16
5	3.26	17	4.62
6	3.88	18	4.66
7	4.56	19	4.04
8	5.30	20	3.69
9	5.79	21	3.32
10	6.03	22	2.90
11	6.00	23	2.28

Table 4.11: Single-Axle Load Spectra for Year 1

Axle Load (lb)	Vehicle Class									
	4	5	6	7	8	9	10	11	12	13
3,000	1.25	7.78	4.63	60.24	10.84	0.49	3.97	0.10	0.10	3.73
4,000	0.75	20.95	0.38	5.98	14.59	0.78	0.80	0.29	0.22	0.84
5,000	1.14	30.60	2.24	1.00	25.46	1.87	0.72	1.36	1.14	2.00
6,000	3.00	15.37	2.90	0.58	14.90	2.09	0.96	4.78	6.03	2.47
7,000	8.21	5.68	1.97	0.56	7.45	1.48	0.99	5.82	10.20	4.92
8,000	11.04	4.04	4.32	0.63	6.14	2.44	2.35	6.11	10.58	6.42
9,000	10.63	3.50	14.42	1.14	6.64	9.64	8.90	11.92	12.36	11.20
10,000	11.93	2.94	23.48	2.59	4.91	26.73	24.41	15.40	15.91	14.99
11,000	13.51	2.05	21.66	3.41	2.58	30.20	27.04	11.53	12.88	12.52
12,000	11.88	1.31	13.28	3.16	1.51	12.72	14.88	9.87	8.34	7.61
13,000	7.66	1.07	6.32	3.12	1.19	3.19	7.05	9.27	7.58	6.67
14,000	5.03	0.90	2.28	2.87	0.96	1.31	3.41	7.99	6.46	5.09
15,000	3.45	0.75	0.91	4.20	0.67	1.20	2.03	5.88	4.24	3.44
16,000	2.58	0.60	0.47	3.60	0.50	1.35	0.96	4.08	2.01	4.46
17,000	2.14	0.48	0.26	1.92	0.38	1.42	0.46	2.58	1.05	3.08
18,000	1.72	0.34	0.16	1.50	0.31	1.26	0.25	1.50	0.49	2.95
19,000	1.23	0.29	0.12	0.97	0.21	0.83	0.21	0.81	0.20	2.21
20,000	0.82	0.24	0.06	0.69	0.16	0.49	0.13	0.40	0.09	1.87
21,000	0.52	0.17	0.04	0.64	0.12	0.23	0.10	0.16	0.04	1.20
22,000	0.31	0.13	0.03	0.39	0.08	0.11	0.09	0.07	0.01	1.23
23,000	0.21	0.11	0.02	0.28	0.06	0.06	0.05	0.03	0.01	0.55
24,000	0.14	0.08	0.00	0.23	0.04	0.03	0.05	0.01	0.02	0.10
25,000	0.12	0.08	0.01	0.25	0.04	0.02	0.05	0.01	0.01	0.10
26,000	0.10	0.07	0.01	0.00	0.03	0.01	0.03	0.00	0.01	0.09
27,000	0.08	0.06	0.01	0.00	0.03	0.01	0.02	0.00	0.00	0.09
28,000	0.07	0.06	0.00	0.04	0.03	0.01	0.00	0.00	0.00	0.00
29,000	0.06	0.05	0.00	0.00	0.02	0.00	0.02	0.00	0.00	0.00
30,000	0.05	0.04	0.00	0.00	0.02	0.00	0.00	0.00	0.00	0.00
31,000	0.05	0.04	0.00	0.00	0.02	0.00	0.02	0.00	0.01	0.00
32,000	0.04	0.03	0.01	0.00	0.01	0.00	0.00	0.00	0.00	0.00
33,000	0.05	0.03	0.00	0.00	0.02	0.00	0.00	0.00	0.00	0.00
34,000	0.04	0.03	0.00	0.00	0.01	0.00	0.02	0.00	0.00	0.00
35,000	0.04	0.03	0.00	0.00	0.01	0.00	0.00	0.00	0.00	0.00
36,000	0.04	0.03	0.00	0.00	0.01	0.00	0.00	0.00	0.00	0.09
37,000	0.03	0.02	0.00	0.00	0.01	0.00	0.00	0.00	0.00	0.00
38,000	0.03	0.02	0.00	0.00	0.01	0.00	0.00	0.00	0.00	0.00
39,000	0.03	0.02	0.00	0.00	0.01	0.00	0.02	0.00	0.00	0.09
40,000	0.03	0.01	0.00	0.00	0.01	0.00	0.02	0.00	0.00	0.00
41,000	0.00	0.00	0.00	0.00	0.00	0.00	0.00	0.00	0.00	0.00

Table 4.12: Tandem-Axle Load Spectra for Year 1

Axle Load (lb)	Vehicle Class									
	4	5	6	7	8	9	10	11	12	13
6,000	0.76	0.00	1.61	95.47	4.18	0.75	0.49	0.00	0.09	1.04
8,000	1.03	0.00	5.55	0.00	8.99	1.81	0.19	0.00	0.08	1.24
10,000	2.75	0.00	7.61	0.00	8.84	4.03	0.55	0.00	0.73	2.53
12,000	3.07	0.00	8.75	0.00	12.56	6.97	2.93	16.67	4.44	2.95
14,000	4.92	0.00	16.20	0.00	17.92	9.78	4.85	0.00	10.15	4.00
16,000	7.66	0.00	16.38	0.00	15.44	7.81	6.22	0.00	16.46	5.97
18,000	7.18	0.00	9.27	0.00	10.97	6.04	10.70	0.00	21.34	8.47
20,000	6.06	0.00	4.41	0.00	7.32	5.21	11.02	0.00	21.60	11.14
22,000	5.63	0.00	2.64	0.00	4.98	4.75	9.99	0.00	15.08	9.41
24,000	6.08	0.00	2.25	0.00	3.41	4.54	8.19	0.00	6.71	12.12
26,000	7.94	0.00	2.05	0.00	2.15	4.89	8.31	0.00	2.08	11.78
28,000	9.37	0.00	2.14	0.76	1.33	6.31	8.30	8.33	0.76	5.11
30,000	8.93	0.00	2.62	1.19	0.72	8.85	7.70	0.00	0.25	3.85
32,000	6.82	0.00	3.73	0.00	0.38	10.47	6.86	0.00	0.07	4.06
34,000	5.50	0.00	4.14	1.39	0.22	9.10	4.90	0.00	0.04	2.07
36,000	4.79	0.00	3.91	0.00	0.17	5.34	3.07	0.00	0.04	3.33
38,000	3.84	0.00	2.97	0.00	0.11	2.20	2.46	0.00	0.03	4.03
40,000	2.77	0.00	1.77	1.19	0.07	0.74	1.29	0.00	0.03	2.38
42,000	1.99	0.00	1.01	0.00	0.03	0.23	0.55	0.00	0.00	0.70
44,000	1.18	0.00	0.56	0.00	0.04	0.09	0.50	0.00	0.00	0.42
46,000	0.78	0.00	0.26	0.00	0.01	0.04	0.43	0.00	0.00	0.45
48,000	0.39	0.00	0.10	0.00	0.03	0.02	0.22	0.00	0.01	0.39
50,000	0.22	0.00	0.04	0.00	0.02	0.01	0.09	0.00	0.00	0.61
52,000	0.12	0.00	0.02	0.00	0.01	0.01	0.03	0.00	0.00	0.46
54,000	0.11	0.00	0.02	0.00	0.01	0.01	0.10	0.00	0.00	0.00
56,000	0.05	0.00	0.01	0.00	0.01	0.00	0.02	0.00	0.00	0.00
58,000	0.02	0.00	0.00	0.00	0.01	0.00	0.02	0.00	0.00	0.00
60,000	0.01	0.00	0.00	0.00	0.01	0.00	0.00	0.00	0.00	0.69
62,000	0.01	0.00	0.00	0.00	0.00	0.00	0.00	0.00	0.00	0.15
64,000	0.01	0.00	0.00	0.00	0.01	0.00	0.02	0.00	0.00	0.00
66,000	0.00	0.00	0.00	0.00	0.00	0.00	0.00	0.00	0.00	0.00
68,000	0.00	0.00	0.00	0.00	0.01	0.00	0.00	0.00	0.00	0.23
70,000	0.01	0.00	0.00	0.00	0.01	0.00	0.00	0.00	0.00	0.00
72,000	0.00	0.00	0.00	0.00	0.01	0.00	0.00	0.00	0.00	0.00
74,000	0.00	0.00	0.00	0.00	0.01	0.00	0.00	0.00	0.00	0.23
76,000	0.00	0.00	0.00	0.00	0.00	0.00	0.00	0.00	0.00	0.00
78,000	0.00	0.00	0.00	0.00	0.00	0.00	0.00	0.00	0.00	0.00
80,000	0.00	0.00	0.00	0.00	0.00	0.00	0.02	0.00	0.00	0.23
82,000	0.00	0.00	0.00	0.00	0.00	0.00	0.00	0.00	0.00	0.00

Table 4.13: Tridem-Axle Load Spectra for Year 1

Axle Load (lb)	Vehicle Class									
	4	5	6	7	8	9	10	11	12	13
12,000	0.00	0.00	0.00	21.98	0.00	0.00	6.75	0.00	0.00	1.19
15,000	0.00	0.00	0.00	1.26	0.00	0.00	11.17	0.00	0.00	1.50
18,000	0.00	0.00	0.00	1.20	0.00	0.00	12.00	0.00	0.00	1.25
21,000	0.00	0.00	0.00	1.08	0.00	0.00	8.92	0.00	0.00	1.56
24,000	0.00	0.00	0.00	1.37	0.00	0.00	7.40	0.00	0.00	1.76
27,000	0.00	0.00	0.00	1.98	0.00	0.00	7.33	0.00	0.00	2.45
30,000	0.00	0.00	0.00	4.01	0.00	0.00	6.79	0.00	0.00	2.53
33,000	0.00	0.00	0.00	5.88	0.00	0.00	7.37	0.00	0.00	2.23
36,000	0.00	0.00	0.00	6.42	0.00	0.00	8.04	0.00	0.00	4.59
39,000	0.00	0.00	0.00	10.63	0.00	0.00	7.61	0.00	0.00	8.05
42,000	0.00	0.00	0.00	13.10	0.00	0.00	5.19	0.00	0.00	11.49
45,000	0.00	0.00	0.00	10.15	0.00	0.00	4.21	0.00	0.00	11.52
48,000	0.00	0.00	0.00	8.49	0.00	0.00	3.16	0.00	0.00	12.15
51,000	0.00	0.00	0.00	4.13	0.00	0.00	1.84	0.00	0.00	10.02
54,000	0.00	0.00	0.00	2.57	0.00	0.00	1.09	0.00	0.00	10.31
57,000	0.00	0.00	0.00	2.40	0.00	0.00	0.62	0.00	0.00	7.73
60,000	0.00	0.00	0.00	1.05	0.00	0.00	0.29	0.00	0.00	4.34
63,000	0.00	0.00	0.00	1.04	0.00	0.00	0.09	0.00	0.00	2.95
66,000	0.00	0.00	0.00	0.54	0.00	0.00	0.03	0.00	0.00	0.67
69,000	0.00	0.00	0.00	0.31	0.00	0.00	0.04	0.00	0.00	1.08
72,000	0.00	0.00	0.00	0.26	0.00	0.00	0.00	0.00	0.00	0.40
75,000	0.00	0.00	0.00	0.09	0.00	0.00	0.00	0.00	0.00	0.12
78,000	0.00	0.00	0.00	0.00	0.00	0.00	0.02	0.00	0.00	0.00
81,000	0.00	0.00	0.00	0.00	0.00	0.00	0.03	0.00	0.00	0.13
84,000	0.00	0.00	0.00	0.08	0.00	0.00	0.02	0.00	0.00	0.00
87,000	0.00	0.00	0.00	0.00	0.00	0.00	0.00	0.00	0.00	0.00
90,000	0.00	0.00	0.00	0.00	0.00	0.00	0.00	0.00	0.00	0.00
93,000	0.00	0.00	0.00	0.00	0.00	0.00	0.00	0.00	0.00	0.00
96,000	0.00	0.00	0.00	0.00	0.00	0.00	0.00	0.00	0.00	0.00
99,000	0.00	0.00	0.00	0.00	0.00	0.00	0.00	0.00	0.00	0.00
102,000	0.00	0.00	0.00	0.00	0.00	0.00	0.00	0.00	0.00	0.00

Table 4.14: Quad-Axle Load Spectra for Year 1

Axle Load (lb)	Vehicle Class									
	4	5	6	7	8	9	10	11	12	13
12,000	0.00	0.00	0.00	0.00	0.00	0.00	4.66	0.00	0.00	0.00
15,000	0.00	0.00	0.00	0.00	0.00	0.00	1.35	0.00	0.00	0.00
18,000	0.00	0.00	0.00	0.00	0.00	0.00	6.48	0.00	0.00	0.00
21,000	0.00	0.00	0.00	0.00	0.00	0.00	12.80	0.00	0.00	0.00
24,000	0.00	0.00	0.00	0.00	0.00	0.00	14.62	0.00	0.00	0.00
27,000	0.00	0.00	0.00	0.00	0.00	0.00	7.28	0.00	0.00	0.00
30,000	0.00	0.00	0.00	0.00	0.00	0.00	6.52	0.00	0.00	0.00
33,000	0.00	0.00	0.00	0.00	0.00	0.00	4.74	0.00	0.00	0.00
36,000	0.00	0.00	0.00	0.00	0.00	0.00	5.22	0.00	0.00	0.00
39,000	0.00	0.00	0.00	0.00	0.00	0.00	8.29	0.00	0.00	0.00
42,000	0.00	0.00	0.00	0.00	0.00	0.00	6.85	0.00	0.00	0.00
45,000	0.00	0.00	0.00	0.00	0.00	0.00	5.12	0.00	0.00	0.00
48,000	0.00	0.00	0.00	0.00	0.00	0.00	4.33	0.00	0.00	0.00
51,000	0.00	0.00	0.00	0.00	0.00	0.00	3.36	0.00	0.00	0.00
54,000	0.00	0.00	0.00	0.00	0.00	0.00	2.64	0.00	0.00	0.00
57,000	0.00	0.00	0.00	0.00	0.00	0.00	1.48	0.00	0.00	0.00
60,000	0.00	0.00	0.00	0.00	0.00	0.00	1.30	0.00	0.00	0.00
63,000	0.00	0.00	0.00	0.00	0.00	0.00	1.74	0.00	0.00	0.00
66,000	0.00	0.00	0.00	0.00	0.00	0.00	0.17	0.00	0.00	0.00
69,000	0.00	0.00	0.00	0.00	0.00	0.00	0.44	0.00	0.00	0.00
72,000	0.00	0.00	0.00	0.00	0.00	0.00	0.38	0.00	0.00	0.00
75,000	0.00	0.00	0.00	0.00	0.00	0.00	0.12	0.00	0.00	0.00
78,000	0.00	0.00	0.00	0.00	0.00	0.00	0.00	0.00	0.00	0.00
81,000	0.00	0.00	0.00	0.00	0.00	0.00	0.12	0.00	0.00	0.00
84,000	0.00	0.00	0.00	0.00	0.00	0.00	0.00	0.00	0.00	0.00
87,000	0.00	0.00	0.00	0.00	0.00	0.00	0.00	0.00	0.00	0.00
90,000	0.00	0.00	0.00	0.00	0.00	0.00	0.00	0.00	0.00	0.00
93,000	0.00	0.00	0.00	0.00	0.00	0.00	0.00	0.00	0.00	0.00
96,000	0.00	0.00	0.00	0.00	0.00	0.00	0.00	0.00	0.00	0.00
99,000	0.00	0.00	0.00	0.00	0.00	0.00	0.00	0.00	0.00	0.00
102,000	0.00	0.00	0.00	0.00	0.00	0.00	0.00	0.00	0.00	0.00

Table 4.15: Single-Axle Load Spectra for Year 2

Axle Load (lb)	Vehicle Class									
	4	5	6	7	8	9	10	11	12	13
3,000	2.03	19.05	5.55	65.33	23.93	0.67	5.06	0.14	0.18	8.64
4,000	0.99	28.38	0.59	2.77	20.46	1.27	0.71	0.60	0.49	0.80
5,000	1.81	22.80	2.33	0.43	19.48	2.20	0.57	2.29	2.61	2.88
6,000	3.89	8.87	3.23	0.48	9.64	1.95	1.17	4.98	7.10	3.28
7,000	8.70	4.36	3.12	0.60	5.65	1.87	1.80	5.26	9.48	2.96
8,000	11.38	3.47	4.80	0.79	4.42	2.94	4.03	6.11	9.45	3.75
9,000	10.83	2.85	11.94	1.74	5.24	9.76	9.71	12.49	12.61	12.97
10,000	11.56	2.43	21.41	2.74	4.19	24.92	22.41	17.63	16.18	11.36
11,000	12.43	1.66	20.47	2.19	2.24	29.70	23.83	12.15	13.29	10.63
12,000	10.59	0.99	13.93	3.00	1.29	13.22	14.63	9.44	8.58	7.82
13,000	7.52	0.79	7.21	3.14	0.93	3.52	7.06	8.54	7.27	5.85
14,000	4.75	0.64	3.11	2.70	0.72	1.52	3.90	6.55	5.59	3.81
15,000	3.19	0.49	1.24	2.74	0.52	1.39	2.18	5.06	3.44	5.37
16,000	2.34	0.42	0.54	2.73	0.37	1.46	1.19	3.45	1.90	4.00
17,000	1.83	0.32	0.33	2.57	0.27	1.38	0.59	2.31	0.99	4.37
18,000	1.45	0.26	0.21	2.44	0.21	1.04	0.44	1.43	0.48	3.61
19,000	0.98	0.18	0.20	1.66	0.14	0.60	0.17	0.81	0.19	2.91
20,000	0.61	0.12	0.11	0.93	0.10	0.30	0.13	0.40	0.09	1.56
21,000	0.35	0.07	0.06	0.42	0.07	0.14	0.13	0.20	0.04	1.55
22,000	0.22	0.04	0.04	0.11	0.04	0.07	0.08	0.09	0.03	0.53
23,000	0.11	0.03	0.02	0.29	0.03	0.04	0.04	0.04	0.00	0.30
24,000	0.10	0.02	0.01	0.07	0.02	0.02	0.01	0.01	0.00	0.28
25,000	0.04	0.01	0.01	0.04	0.01	0.01	0.05	0.01	0.00	0.28
26,000	0.03	0.01	0.00	0.04	0.01	0.00	0.02	0.00	0.01	0.30
27,000	0.03	0.00	0.00	0.00	0.00	0.00	0.05	0.00	0.00	0.11
28,000	0.02	0.00	0.00	0.00	0.00	0.00	0.02	0.00	0.00	0.10
29,000	0.01	0.00	0.00	0.00	0.00	0.00	0.00	0.00	0.00	0.00
30,000	0.01	0.00	0.00	0.00	0.00	0.00	0.00	0.00	0.00	0.00
31,000	0.01	0.00	0.00	0.00	0.00	0.00	0.00	0.00	0.00	0.00
32,000	0.00	0.00	0.00	0.00	0.00	0.00	0.00	0.00	0.00	0.00
33,000	0.00	0.00	0.00	0.00	0.00	0.00	0.00	0.00	0.00	0.00
34,000	0.00	0.00	0.00	0.00	0.00	0.00	0.00	0.00	0.00	0.00
35,000	0.00	0.00	0.00	0.00	0.00	0.00	0.00	0.00	0.00	0.00
36,000	0.00	0.00	0.00	0.00	0.00	0.00	0.01	0.00	0.00	0.00
37,000	0.00	0.00	0.00	0.00	0.00	0.00	0.00	0.00	0.00	0.00
38,000	0.00	0.00	0.00	0.00	0.00	0.00	0.00	0.00	0.00	0.00
39,000	0.00	0.00	0.00	0.00	0.00	0.00	0.01	0.00	0.00	0.00
40,000	0.00	0.00	0.00	0.00	0.00	0.00	0.00	0.00	0.00	0.00
41,000	0.00	0.00	0.00	0.00	0.00	0.00	0.00	0.00	0.00	0.00

Table 4.16: Tandem-Axle Load Spectra for Year 2

Axle Load (lb)	Vehicle Class									
	4	5	6	7	8	9	10	11	12	13
6,000	0.88	0.00	2.25	86.18	9.57	1.10	0.38	4.17	0.14	2.76
8,000	1.41	0.00	6.82	0.00	10.55	2.73	0.33	8.33	0.21	1.84
10,000	2.91	0.00	9.18	0.00	10.83	5.70	1.62	4.17	1.49	1.77
12,000	3.75	0.00	11.37	1.04	15.82	8.52	4.51	0.00	7.27	2.91
14,000	6.45	0.00	16.53	0.00	17.61	9.59	6.41	0.00	10.63	2.72
16,000	9.67	0.00	13.08	0.00	12.08	7.11	6.87	8.33	14.12	6.08
18,000	7.22	0.00	7.29	0.00	7.94	5.58	9.26	8.33	21.44	8.28
20,000	5.95	0.00	3.74	0.00	5.40	4.96	10.46	0.00	21.87	9.83
22,000	5.49	0.00	2.58	0.00	3.73	4.59	10.01	0.00	13.67	13.51
24,000	6.60	0.00	2.40	0.83	2.29	4.48	9.80	0.00	6.11	15.88
26,000	8.59	0.00	2.24	0.00	1.43	5.05	8.50	0.00	2.12	12.07
28,000	8.81	0.00	2.32	0.00	1.07	6.74	8.38	0.00	0.56	6.49
30,000	7.32	0.00	2.91	0.00	0.66	9.50	7.56	0.00	0.23	3.02
32,000	5.52	0.00	3.12	0.00	0.41	10.34	5.26	0.00	0.08	2.83
34,000	4.51	0.00	3.55	1.04	0.22	7.73	3.70	0.00	0.00	1.22
36,000	3.76	0.00	3.36	2.78	0.18	3.95	2.50	0.00	0.03	1.81
38,000	3.17	0.00	2.71	1.39	0.07	1.50	1.67	0.00	0.01	1.21
40,000	2.75	0.00	1.95	5.69	0.05	0.49	1.06	0.00	0.00	1.92
42,000	1.90	0.00	1.16	0.00	0.04	0.17	0.60	0.00	0.00	0.80
44,000	1.27	0.00	0.68	0.00	0.02	0.08	0.49	0.00	0.01	0.53
46,000	0.84	0.00	0.34	1.04	0.02	0.04	0.22	0.00	0.00	1.03
48,000	0.52	0.00	0.16	0.00	0.01	0.02	0.09	0.00	0.00	0.62
50,000	0.30	0.00	0.13	0.00	0.00	0.01	0.09	0.00	0.00	0.00
52,000	0.18	0.00	0.04	0.00	0.00	0.01	0.03	0.00	0.00	0.00
54,000	0.09	0.00	0.05	0.00	0.00	0.00	0.05	0.00	0.00	0.00
56,000	0.05	0.00	0.01	0.00	0.00	0.00	0.05	0.00	0.00	0.51
58,000	0.04	0.00	0.01	0.00	0.00	0.00	0.00	0.00	0.00	0.00
60,000	0.02	0.00	0.00	0.00	0.00	0.00	0.05	0.00	0.00	0.36
62,000	0.01	0.00	0.00	0.00	0.00	0.00	0.02	0.00	0.00	0.00
64,000	0.01	0.00	0.00	0.00	0.00	0.00	0.00	0.00	0.00	0.00
66,000	0.02	0.00	0.00	0.00	0.00	0.00	0.00	0.00	0.00	0.00
68,000	0.00	0.00	0.00	0.00	0.00	0.00	0.00	0.00	0.00	0.00
70,000	0.00	0.00	0.00	0.00	0.00	0.00	0.00	0.00	0.00	0.00
72,000	0.00	0.00	0.00	0.00	0.00	0.00	0.00	0.00	0.00	0.00
74,000	0.00	0.00	0.00	0.00	0.00	0.00	0.00	0.00	0.00	0.00
76,000	0.00	0.00	0.00	0.00	0.00	0.00	0.02	0.00	0.00	0.00
78,000	0.00	0.00	0.00	0.00	0.00	0.00	0.00	0.00	0.00	0.00
80,000	0.00	0.00	0.00	0.00	0.00	0.00	0.00	0.00	0.00	0.00
82,000	0.00	0.00	0.00	0.00	0.00	0.00	0.00	0.00	0.00	0.00

Table 4.17: Tridem-Axle Load Spectra for Year 2

Axle Load (lb)	Vehicle Class									
	4	5	6	7	8	9	10	11	12	13
12,000	0.00	0.00	0.00	13.10	0.00	0.00	10.02	0.00	0.00	2.43
15,000	0.00	0.00	0.00	0.79	0.00	0.00	13.69	0.00	0.00	2.34
18,000	0.00	0.00	0.00	1.60	0.00	0.00	12.40	0.00	0.00	1.17
21,000	0.00	0.00	0.00	2.60	0.00	0.00	9.18	0.00	0.00	3.17
24,000	0.00	0.00	0.00	1.88	0.00	0.00	7.22	0.00	0.00	2.17
27,000	0.00	0.00	0.00	2.40	0.00	0.00	7.33	0.00	0.00	1.44
30,000	0.00	0.00	0.00	3.97	0.00	0.00	8.12	0.00	0.00	3.37
33,000	0.00	0.00	0.00	5.33	0.00	0.00	7.31	0.00	0.00	6.33
36,000	0.00	0.00	0.00	9.53	0.00	0.00	7.13	0.00	0.00	4.82
39,000	0.00	0.00	0.00	15.41	0.00	0.00	5.70	0.00	0.00	9.72
42,000	0.00	0.00	0.00	12.01	0.00	0.00	4.07	0.00	0.00	8.19
45,000	0.00	0.00	0.00	11.03	0.00	0.00	3.12	0.00	0.00	9.84
48,000	0.00	0.00	0.00	8.24	0.00	0.00	1.93	0.00	0.00	9.14
51,000	0.00	0.00	0.00	3.05	0.00	0.00	1.17	0.00	0.00	11.50
54,000	0.00	0.00	0.00	3.25	0.00	0.00	0.70	0.00	0.00	9.10
57,000	0.00	0.00	0.00	1.02	0.00	0.00	0.46	0.00	0.00	7.82
60,000	0.00	0.00	0.00	1.65	0.00	0.00	0.24	0.00	0.00	2.77
63,000	0.00	0.00	0.00	0.89	0.00	0.00	0.13	0.00	0.00	2.12
66,000	0.00	0.00	0.00	0.58	0.00	0.00	0.03	0.00	0.00	1.19
69,000	0.00	0.00	0.00	0.71	0.00	0.00	0.04	0.00	0.00	0.72
72,000	0.00	0.00	0.00	0.59	0.00	0.00	0.02	0.00	0.00	0.39
75,000	0.00	0.00	0.00	0.11	0.00	0.00	0.00	0.00	0.00	0.12
78,000	0.00	0.00	0.00	0.10	0.00	0.00	0.00	0.00	0.00	0.00
81,000	0.00	0.00	0.00	0.00	0.00	0.00	0.00	0.00	0.00	0.00
84,000	0.00	0.00	0.00	0.16	0.00	0.00	0.00	0.00	0.00	0.13
87,000	0.00	0.00	0.00	0.00	0.00	0.00	0.00	0.00	0.00	0.00
90,000	0.00	0.00	0.00	0.00	0.00	0.00	0.00	0.00	0.00	0.00
93,000	0.00	0.00	0.00	0.00	0.00	0.00	0.00	0.00	0.00	0.00
96,000	0.00	0.00	0.00	0.00	0.00	0.00	0.00	0.00	0.00	0.00
99,000	0.00	0.00	0.00	0.00	0.00	0.00	0.00	0.00	0.00	0.00
102,000	0.00	0.00	0.00	0.00	0.00	0.00	0.00	0.00	0.00	0.00

Table 4.18: Quad-Axle Load Spectra for Year 2

Axle Load (lb)	Vehicle Class									
	4	5	6	7	8	9	10	11	12	13
12,000	0.00	0.00	0.00	0.00	0.00	0.00	1.89	0.00	0.00	0.00
15,000	0.00	0.00	0.00	0.00	0.00	0.00	3.27	0.00	0.00	0.00
18,000	0.00	0.00	0.00	0.00	0.00	0.00	15.23	0.00	0.00	0.00
21,000	0.00	0.00	0.00	0.00	0.00	0.00	15.11	0.00	0.00	0.00
24,000	0.00	0.00	0.00	0.00	0.00	0.00	16.49	0.00	0.00	0.00
27,000	0.00	0.00	0.00	0.00	0.00	0.00	9.42	0.00	0.00	0.00
30,000	0.00	0.00	0.00	0.00	0.00	0.00	5.23	0.00	0.00	0.00
33,000	0.00	0.00	0.00	0.00	0.00	0.00	6.06	0.00	0.00	0.00
36,000	0.00	0.00	0.00	0.00	0.00	0.00	5.72	0.00	0.00	0.00
39,000	0.00	0.00	0.00	0.00	0.00	0.00	3.76	0.00	0.00	0.00
42,000	0.00	0.00	0.00	0.00	0.00	0.00	5.94	0.00	0.00	0.00
45,000	0.00	0.00	0.00	0.00	0.00	0.00	1.91	0.00	0.00	0.00
48,000	0.00	0.00	0.00	0.00	0.00	0.00	2.71	0.00	0.00	0.00
51,000	0.00	0.00	0.00	0.00	0.00	0.00	1.54	0.00	0.00	0.00
54,000	0.00	0.00	0.00	0.00	0.00	0.00	1.71	0.00	0.00	0.00
57,000	0.00	0.00	0.00	0.00	0.00	0.00	0.79	0.00	0.00	0.00
60,000	0.00	0.00	0.00	0.00	0.00	0.00	0.88	0.00	0.00	0.00
63,000	0.00	0.00	0.00	0.00	0.00	0.00	0.25	0.00	0.00	0.00
66,000	0.00	0.00	0.00	0.00	0.00	0.00	0.63	0.00	0.00	0.00
69,000	0.00	0.00	0.00	0.00	0.00	0.00	0.35	0.00	0.00	0.00
72,000	0.00	0.00	0.00	0.00	0.00	0.00	0.16	0.00	0.00	0.00
75,000	0.00	0.00	0.00	0.00	0.00	0.00	0.39	0.00	0.00	0.00
78,000	0.00	0.00	0.00	0.00	0.00	0.00	0.16	0.00	0.00	0.00
81,000	0.00	0.00	0.00	0.00	0.00	0.00	0.00	0.00	0.00	0.00
84,000	0.00	0.00	0.00	0.00	0.00	0.00	0.00	0.00	0.00	0.00
87,000	0.00	0.00	0.00	0.00	0.00	0.00	0.00	0.00	0.00	0.00
90,000	0.00	0.00	0.00	0.00	0.00	0.00	0.00	0.00	0.00	0.00
93,000	0.00	0.00	0.00	0.00	0.00	0.00	0.00	0.00	0.00	0.00
96,000	0.00	0.00	0.00	0.00	0.00	0.00	0.00	0.00	0.00	0.00
99,000	0.00	0.00	0.00	0.00	0.00	0.00	0.00	0.00	0.00	0.00
102,000	0.00	0.00	0.00	0.00	0.00	0.00	0.22	0.00	0.00	0.00

Table 4.19: Single-Axle Load Spectra for Year 3

Axle Load (lb)	Vehicle Class									
	4	5	6	7	8	9	10	11	12	13
3,000	3.01	25.15	4.93	57.34	25.76	0.72	5.03	0.12	0.11	5.18
4,000	1.49	29.64	0.69	1.52	20.80	1.58	0.62	0.76	0.72	1.91
5,000	2.80	20.32	2.34	0.38	18.15	2.01	0.59	3.48	4.54	1.95
6,000	5.20	8.46	3.73	0.78	10.10	1.90	1.62	5.83	9.66	3.27
7,000	8.85	3.97	4.52	1.14	6.01	2.66	2.39	5.42	9.47	3.92
8,000	10.82	3.02	5.96	1.86	4.48	3.83	3.99	6.66	8.80	5.89
9,000	10.51	2.36	11.27	2.30	4.56	10.03	9.07	11.72	12.35	11.81
10,000	10.78	1.93	18.37	3.09	3.74	22.42	20.35	17.51	14.91	11.73
11,000	11.58	1.35	19.13	3.36	2.06	27.46	23.38	12.92	12.70	8.38
12,000	10.45	0.87	14.02	4.38	1.11	14.44	14.51	9.02	8.61	8.29
13,000	7.78	0.63	8.08	4.12	0.82	4.59	7.89	7.17	6.69	7.52
14,000	5.18	0.54	3.80	4.16	0.60	2.04	4.71	5.92	5.24	7.51
15,000	3.44	0.41	1.56	3.05	0.47	1.66	2.28	4.63	3.39	5.61
16,000	2.48	0.34	0.70	3.59	0.35	1.52	1.39	3.30	1.65	4.40
17,000	1.76	0.28	0.29	2.21	0.27	1.27	0.74	2.33	0.80	3.10
18,000	1.29	0.21	0.19	2.19	0.20	0.86	0.51	1.52	0.23	1.69
19,000	0.92	0.14	0.15	1.38	0.15	0.48	0.27	0.84	0.10	1.75
20,000	0.57	0.11	0.10	1.36	0.11	0.24	0.24	0.45	0.02	1.75
21,000	0.36	0.07	0.05	0.74	0.08	0.12	0.07	0.21	0.01	1.11
22,000	0.21	0.05	0.04	0.36	0.06	0.07	0.07	0.11	0.00	1.05
23,000	0.15	0.04	0.03	0.27	0.03	0.04	0.10	0.04	0.00	0.62
24,000	0.10	0.03	0.01	0.27	0.02	0.02	0.03	0.02	0.01	0.27
25,000	0.06	0.02	0.01	0.02	0.02	0.01	0.05	0.01	0.00	0.54
26,000	0.04	0.02	0.01	0.08	0.01	0.01	0.00	0.00	0.00	0.21
27,000	0.03	0.01	0.00	0.00	0.01	0.00	0.04	0.00	0.00	0.23
28,000	0.02	0.00	0.00	0.03	0.01	0.00	0.00	0.00	0.00	0.17
29,000	0.01	0.01	0.00	0.00	0.00	0.01	0.01	0.00	0.00	0.08
30,000	0.01	0.00	0.00	0.00	0.00	0.00	0.00	0.00	0.00	0.00
31,000	0.02	0.00	0.00	0.00	0.00	0.00	0.05	0.00	0.00	0.00
32,000	0.01	0.00	0.00	0.00	0.00	0.00	0.00	0.00	0.00	0.08
33,000	0.01	0.00	0.00	0.00	0.00	0.00	0.00	0.00	0.00	0.00
34,000	0.01	0.00	0.00	0.00	0.00	0.00	0.00	0.00	0.00	0.00
35,000	0.00	0.00	0.00	0.00	0.00	0.00	0.00	0.00	0.00	0.00
36,000	0.00	0.00	0.00	0.00	0.00	0.00	0.00	0.00	0.00	0.00
37,000	0.01	0.00	0.00	0.00	0.00	0.00	0.00	0.00	0.00	0.00
38,000	0.00	0.00	0.00	0.00	0.00	0.00	0.00	0.00	0.00	0.00
39,000	0.00	0.00	0.00	0.00	0.00	0.00	0.00	0.00	0.00	0.00
40,000	0.00	0.00	0.00	0.00	0.00	0.00	0.00	0.00	0.00	0.00
41,000	0.00	0.00	0.00	0.00	0.00	0.00	0.00	0.00	0.00	0.00

Table 4.20: Tandem-Axle Load Spectra for Year 3

Axle Load (lb)	Vehicle Class									
	4	5	6	7	8	9	10	11	12	13
6,000	0.86	0.00	2.99	77.90	13.07	1.45	0.26	0.00	0.09	1.13
8,000	1.58	0.00	8.26	0.00	10.87	3.81	0.32	0.00	0.33	0.52
10,000	3.18	0.00	9.40	0.00	12.10	6.90	1.60	8.33	2.53	1.41
12,000	4.23	0.00	12.18	0.00	16.94	9.46	5.17	0.00	9.88	3.67
14,000	7.83	0.00	15.74	0.00	15.71	9.30	6.67	4.17	10.14	4.91
16,000	9.21	0.00	11.12	0.00	10.36	6.53	7.63	0.00	14.94	7.88
18,000	7.45	0.00	5.77	1.19	7.03	5.08	8.80	2.08	22.30	7.86
20,000	5.78	0.00	3.28	0.00	4.76	4.70	9.66	15.97	20.19	11.33
22,000	5.53	0.00	2.18	0.00	3.27	4.36	9.39	8.33	11.81	16.15
24,000	6.72	0.00	1.98	0.00	2.26	4.39	8.91	2.78	5.14	12.39
26,000	7.81	0.00	2.16	1.19	1.47	5.17	8.68	0.00	1.94	7.59
28,000	6.98	0.00	2.44	0.00	0.85	6.99	7.51	0.00	0.60	4.31
30,000	5.69	0.00	2.98	0.00	0.51	9.16	7.07	0.00	0.10	3.72
32,000	4.61	0.00	3.32	2.08	0.35	9.56	5.51	0.00	0.01	2.47
34,000	4.43	0.00	3.67	6.53	0.21	7.07	4.19	0.00	0.00	2.11
36,000	4.22	0.00	3.78	0.00	0.12	3.72	3.07	0.00	0.00	2.36
38,000	3.89	0.00	3.16	9.72	0.04	1.47	2.11	0.00	0.01	2.75
40,000	3.17	0.00	2.38	1.39	0.02	0.52	1.27	0.00	0.00	2.60
42,000	2.50	0.00	1.54	0.00	0.02	0.19	0.94	0.00	0.00	1.66
44,000	1.74	0.00	0.83	0.00	0.01	0.08	0.42	0.00	0.00	0.49
46,000	1.13	0.00	0.41	0.00	0.01	0.03	0.28	0.00	0.00	0.47
48,000	0.67	0.00	0.22	0.00	0.01	0.02	0.25	0.00	0.00	0.67
50,000	0.33	0.00	0.10	0.00	0.00	0.01	0.09	0.00	0.00	0.24
52,000	0.19	0.00	0.05	0.00	0.00	0.01	0.04	0.00	0.00	0.44
54,000	0.10	0.00	0.03	0.00	0.00	0.00	0.07	0.00	0.00	0.00
56,000	0.07	0.00	0.02	0.00	0.00	0.00	0.03	0.00	0.00	0.56
58,000	0.04	0.00	0.01	0.00	0.00	0.00	0.03	0.00	0.00	0.00
60,000	0.03	0.00	0.00	0.00	0.00	0.00	0.00	0.00	0.00	0.15
62,000	0.01	0.00	0.00	0.00	0.00	0.00	0.01	0.00	0.00	0.00
64,000	0.00	0.00	0.00	0.00	0.00	0.00	0.01	0.00	0.00	0.00
66,000	0.00	0.00	0.00	0.00	0.00	0.00	0.00	0.00	0.00	0.00
68,000	0.00	0.00	0.00	0.00	0.00	0.00	0.00	0.00	0.00	0.00
70,000	0.00	0.00	0.00	0.00	0.00	0.00	0.00	0.00	0.00	0.00
72,000	0.00	0.00	0.00	0.00	0.00	0.00	0.00	0.00	0.00	0.15
74,000	0.00	0.00	0.00	0.00	0.00	0.00	0.00	0.00	0.00	0.00
76,000	0.00	0.00	0.00	0.00	0.00	0.00	0.00	0.00	0.00	0.00
78,000	0.00	0.00	0.00	0.00	0.00	0.00	0.00	0.00	0.00	0.00
80,000	0.00	0.00	0.00	0.00	0.00	0.00	0.00	0.00	0.00	0.00
82,000	0.00	0.00	0.00	0.00	0.00	0.00	0.00	0.00	0.00	0.00

Table 4.21: Tridem-Axle Load Spectra for Year 3

Axle Load (lb)	Vehicle Class									
	4	5	6	7	8	9	10	11	12	13
12,000	0.00	0.00	0.00	14.71	0.00	0.00	15.60	0.00	0.00	1.28
15,000	0.00	0.00	0.00	1.17	0.00	0.00	11.98	0.00	0.00	0.94
18,000	0.00	0.00	0.00	1.01	0.00	0.00	9.99	0.00	0.00	1.69
21,000	0.00	0.00	0.00	1.09	0.00	0.00	9.58	0.00	0.00	1.03
24,000	0.00	0.00	0.00	1.50	0.00	0.00	7.95	0.00	0.00	2.77
27,000	0.00	0.00	0.00	2.23	0.00	0.00	7.29	0.00	0.00	2.82
30,000	0.00	0.00	0.00	3.35	0.00	0.00	7.22	0.00	0.00	5.44
33,000	0.00	0.00	0.00	7.42	0.00	0.00	8.00	0.00	0.00	4.61
36,000	0.00	0.00	0.00	9.72	0.00	0.00	6.14	0.00	0.00	6.23
39,000	0.00	0.00	0.00	12.65	0.00	0.00	4.74	0.00	0.00	8.91
42,000	0.00	0.00	0.00	11.53	0.00	0.00	3.64	0.00	0.00	8.04
45,000	0.00	0.00	0.00	10.21	0.00	0.00	3.28	0.00	0.00	10.37
48,000	0.00	0.00	0.00	6.43	0.00	0.00	1.81	0.00	0.00	9.41
51,000	0.00	0.00	0.00	5.20	0.00	0.00	1.35	0.00	0.00	9.06
54,000	0.00	0.00	0.00	4.00	0.00	0.00	0.54	0.00	0.00	8.21
57,000	0.00	0.00	0.00	2.79	0.00	0.00	0.42	0.00	0.00	5.33
60,000	0.00	0.00	0.00	2.21	0.00	0.00	0.18	0.00	0.00	6.49
63,000	0.00	0.00	0.00	1.07	0.00	0.00	0.12	0.00	0.00	1.87
66,000	0.00	0.00	0.00	0.74	0.00	0.00	0.06	0.00	0.00	1.52
69,000	0.00	0.00	0.00	0.24	0.00	0.00	0.03	0.00	0.00	1.69
72,000	0.00	0.00	0.00	0.38	0.00	0.00	0.08	0.00	0.00	0.48
75,000	0.00	0.00	0.00	0.13	0.00	0.00	0.00	0.00	0.00	0.77
78,000	0.00	0.00	0.00	0.20	0.00	0.00	0.00	0.00	0.00	0.84
81,000	0.00	0.00	0.00	0.00	0.00	0.00	0.00	0.00	0.00	0.19
84,000	0.00	0.00	0.00	0.00	0.00	0.00	0.00	0.00	0.00	0.00
87,000	0.00	0.00	0.00	0.00	0.00	0.00	0.00	0.00	0.00	0.00
90,000	0.00	0.00	0.00	0.00	0.00	0.00	0.00	0.00	0.00	0.00
93,000	0.00	0.00	0.00	0.00	0.00	0.00	0.00	0.00	0.00	0.00
96,000	0.00	0.00	0.00	0.00	0.00	0.00	0.00	0.00	0.00	0.00
99,000	0.00	0.00	0.00	0.00	0.00	0.00	0.00	0.00	0.00	0.00
102,000	0.00	0.00	0.00	0.00	0.00	0.00	0.00	0.00	0.00	0.00

Table 4.22: Quad-Axle Load Spectra for Year 3

Axle Load (lb)	Vehicle Class									
	4	5	6	7	8	9	10	11	12	13
12,000	0.00	0.00	0.00	0.00	0.00	0.00	7.12	0.00	0.00	0.00
15,000	0.00	0.00	0.00	0.00	0.00	0.00	4.09	0.00	0.00	0.00
18,000	0.00	0.00	0.00	0.00	0.00	0.00	14.19	0.00	0.00	0.00
21,000	0.00	0.00	0.00	0.00	0.00	0.00	17.78	0.00	0.00	0.00
24,000	0.00	0.00	0.00	0.00	0.00	0.00	17.48	0.00	0.00	0.00
27,000	0.00	0.00	0.00	0.00	0.00	0.00	10.42	0.00	0.00	0.00
30,000	0.00	0.00	0.00	0.00	0.00	0.00	5.88	0.00	0.00	0.00
33,000	0.00	0.00	0.00	0.00	0.00	0.00	4.25	0.00	0.00	0.00
36,000	0.00	0.00	0.00	0.00	0.00	0.00	3.58	0.00	0.00	0.00
39,000	0.00	0.00	0.00	0.00	0.00	0.00	2.90	0.00	0.00	0.00
42,000	0.00	0.00	0.00	0.00	0.00	0.00	2.03	0.00	0.00	0.00
45,000	0.00	0.00	0.00	0.00	0.00	0.00	2.22	0.00	0.00	0.00
48,000	0.00	0.00	0.00	0.00	0.00	0.00	1.76	0.00	0.00	0.00
51,000	0.00	0.00	0.00	0.00	0.00	0.00	1.94	0.00	0.00	0.00
54,000	0.00	0.00	0.00	0.00	0.00	0.00	1.12	0.00	0.00	0.00
57,000	0.00	0.00	0.00	0.00	0.00	0.00	1.43	0.00	0.00	0.00
60,000	0.00	0.00	0.00	0.00	0.00	0.00	0.51	0.00	0.00	0.00
63,000	0.00	0.00	0.00	0.00	0.00	0.00	0.58	0.00	0.00	0.00
66,000	0.00	0.00	0.00	0.00	0.00	0.00	0.36	0.00	0.00	0.00
69,000	0.00	0.00	0.00	0.00	0.00	0.00	0.20	0.00	0.00	0.00
72,000	0.00	0.00	0.00	0.00	0.00	0.00	0.00	0.00	0.00	0.00
75,000	0.00	0.00	0.00	0.00	0.00	0.00	0.16	0.00	0.00	0.00
78,000	0.00	0.00	0.00	0.00	0.00	0.00	0.00	0.00	0.00	0.00
81,000	0.00	0.00	0.00	0.00	0.00	0.00	0.00	0.00	0.00	0.00
84,000	0.00	0.00	0.00	0.00	0.00	0.00	0.00	0.00	0.00	0.00
87,000	0.00	0.00	0.00	0.00	0.00	0.00	0.00	0.00	0.00	0.00
90,000	0.00	0.00	0.00	0.00	0.00	0.00	0.00	0.00	0.00	0.00
93,000	0.00	0.00	0.00	0.00	0.00	0.00	0.00	0.00	0.00	0.00
96,000	0.00	0.00	0.00	0.00	0.00	0.00	0.00	0.00	0.00	0.00
99,000	0.00	0.00	0.00	0.00	0.00	0.00	0.00	0.00	0.00	0.00
102,000	0.00	0.00	0.00	0.00	0.00	0.00	0.00	0.00	0.00	0.00

Table 4.23: Single-Axle Load Spectra for Year 4

Axle Load (lb)	Vehicle Class									
	4	5	6	7	8	9	10	11	12	13
3,000	1.37	22.97	3.58	53.21	26.82	1.04	6.04	0.15	0.24	6.71
4,000	0.83	30.95	0.48	1.35	20.72	2.25	1.01	0.84	0.82	1.77
5,000	2.08	21.77	1.72	0.62	17.48	2.73	0.95	3.30	4.40	2.70
6,000	4.80	8.23	2.98	0.47	9.30	2.35	1.71	6.14	9.05	4.11
7,000	10.08	4.00	3.52	0.91	5.85	2.95	3.00	5.84	9.30	5.36
8,000	13.18	3.09	5.33	0.97	4.51	4.02	5.08	6.59	8.69	7.17
9,000	12.41	2.36	11.74	2.36	4.66	9.60	9.49	11.45	12.05	10.78
10,000	11.69	1.87	21.48	4.88	4.17	20.99	18.69	16.93	15.02	13.43
11,000	10.34	1.20	20.81	4.95	2.18	26.43	21.36	12.71	12.03	11.79
12,000	9.23	0.83	13.47	5.69	1.13	15.20	14.45	8.82	8.32	9.13
13,000	7.07	0.64	6.69	5.49	0.78	4.89	7.91	7.07	6.81	6.76
14,000	5.13	0.49	3.52	4.17	0.60	1.99	4.41	5.93	5.78	5.55
15,000	3.58	0.38	1.89	3.40	0.45	1.52	2.43	4.70	3.98	4.28
16,000	2.68	0.32	0.98	2.85	0.35	1.39	1.23	3.50	2.11	3.19
17,000	1.93	0.25	0.56	2.10	0.28	1.14	0.95	2.46	0.91	2.20
18,000	1.36	0.20	0.42	1.75	0.21	0.75	0.53	1.65	0.35	1.19
19,000	0.83	0.15	0.21	1.38	0.17	0.41	0.27	0.96	0.09	1.30
20,000	0.49	0.11	0.19	1.21	0.11	0.19	0.23	0.49	0.03	1.05
21,000	0.32	0.08	0.16	0.80	0.08	0.09	0.11	0.25	0.01	0.62
22,000	0.19	0.04	0.08	0.38	0.05	0.04	0.05	0.11	0.00	0.43
23,000	0.12	0.03	0.10	0.43	0.04	0.02	0.01	0.05	0.00	0.36
24,000	0.09	0.02	0.02	0.33	0.03	0.01	0.03	0.02	0.00	0.07
25,000	0.05	0.01	0.02	0.11	0.02	0.01	0.01	0.01	0.00	0.02
26,000	0.03	0.01	0.01	0.08	0.01	0.00	0.01	0.00	0.00	0.01
27,000	0.03	0.00	0.00	0.09	0.01	0.00	0.01	0.00	0.00	0.00
28,000	0.02	0.00	0.00	0.00	0.00	0.00	0.01	0.00	0.00	0.00
29,000	0.01	0.00	0.00	0.03	0.00	0.00	0.00	0.00	0.00	0.00
30,000	0.01	0.00	0.00	0.00	0.00	0.00	0.01	0.00	0.00	0.01
31,000	0.00	0.00	0.00	0.00	0.00	0.00	0.00	0.00	0.00	0.00
32,000	0.01	0.00	0.00	0.00	0.00	0.00	0.01	0.00	0.00	0.00
33,000	0.00	0.00	0.00	0.00	0.00	0.00	0.00	0.00	0.00	0.00
34,000	0.00	0.00	0.00	0.00	0.00	0.00	0.00	0.00	0.00	0.00
35,000	0.00	0.00	0.00	0.00	0.00	0.00	0.00	0.00	0.00	0.00
36,000	0.00	0.00	0.00	0.00	0.00	0.00	0.00	0.00	0.00	0.00
37,000	0.00	0.00	0.00	0.00	0.00	0.00	0.00	0.00	0.00	0.00
38,000	0.00	0.00	0.00	0.00	0.00	0.00	0.00	0.00	0.00	0.00
39,000	0.00	0.00	0.00	0.00	0.00	0.00	0.00	0.00	0.00	0.00
40,000	0.00	0.00	0.00	0.00	0.00	0.00	0.00	0.00	0.00	0.00
41,000	0.00	0.00	0.00	0.00	0.00	0.00	0.00	0.00	0.00	0.00

Table 4.24: Tandem-Axle Load Spectra for Year 4

Axle Load (lb)	Vehicle Class									
	4	5	6	7	8	9	10	11	12	13
6,000	1.34	0.00	3.83	79.19	12.70	1.77	0.82	0.00	0.29	4.13
8,000	1.65	0.00	15.90	0.00	11.47	4.49	0.49	0.00	0.44	3.85
10,000	3.84	0.00	17.39	0.00	11.59	7.42	2.29	0.00	3.62	6.23
12,000	4.29	0.00	11.18	0.76	17.02	10.16	4.22	0.00	9.59	6.02
14,000	7.02	0.00	12.06	0.00	16.52	9.93	5.95	0.00	9.51	7.48
16,000	7.95	0.00	7.47	0.00	10.53	6.56	8.18	0.00	14.99	9.68
18,000	5.23	0.00	4.08	0.00	6.74	5.03	9.94	0.00	22.19	8.42
20,000	4.86	0.00	3.13	0.00	4.58	4.50	10.34	0.00	20.35	9.40
22,000	6.68	0.00	2.46	0.00	2.98	4.18	9.44	0.00	11.75	8.74
24,000	10.41	0.00	2.59	0.76	2.08	4.13	8.74	0.00	5.15	7.29
26,000	11.92	0.00	2.67	0.00	1.34	4.88	8.19	0.00	1.50	4.27
28,000	10.75	0.00	2.65	3.33	0.88	6.62	7.20	0.00	0.46	6.00
30,000	7.40	0.00	2.54	0.76	0.50	8.74	6.37	0.00	0.13	4.17
32,000	4.98	0.00	2.59	1.39	0.31	9.08	5.51	0.00	0.02	3.78
34,000	3.32	0.00	2.47	0.00	0.23	6.72	3.92	0.00	0.01	2.23
36,000	2.44	0.00	2.20	5.20	0.14	3.56	2.95	0.00	0.00	2.13
38,000	1.77	0.00	1.69	0.00	0.11	1.43	2.19	0.00	0.00	1.51
40,000	1.43	0.00	1.16	0.00	0.07	0.51	1.21	0.00	0.00	0.88
42,000	1.01	0.00	0.84	0.00	0.08	0.17	0.76	0.00	0.00	1.09
44,000	0.65	0.00	0.48	1.67	0.04	0.07	0.44	0.00	0.00	0.81
46,000	0.36	0.00	0.30	2.08	0.03	0.03	0.34	0.00	0.00	0.52
48,000	0.25	0.00	0.13	0.00	0.02	0.01	0.23	0.00	0.00	0.52
50,000	0.20	0.00	0.10	0.00	0.01	0.01	0.14	0.00	0.00	0.00
52,000	0.09	0.00	0.05	0.00	0.00	0.00	0.06	0.00	0.00	0.00
54,000	0.07	0.00	0.03	2.08	0.00	0.00	0.01	0.00	0.00	0.52
56,000	0.04	0.00	0.01	0.00	0.00	0.00	0.02	0.00	0.00	0.00
58,000	0.01	0.00	0.00	2.78	0.00	0.00	0.02	0.00	0.00	0.31
60,000	0.02	0.00	0.00	0.00	0.00	0.00	0.01	0.00	0.00	0.00
62,000	0.01	0.00	0.00	0.00	0.00	0.00	0.00	0.00	0.00	0.00
64,000	0.01	0.00	0.00	0.00	0.00	0.00	0.01	0.00	0.00	0.03
66,000	0.00	0.00	0.00	0.00	0.00	0.00	0.00	0.00	0.00	0.00
68,000	0.00	0.00	0.00	0.00	0.00	0.00	0.01	0.00	0.00	0.00
70,000	0.00	0.00	0.00	0.00	0.00	0.00	0.00	0.00	0.00	0.00
72,000	0.00	0.00	0.00	0.00	0.00	0.00	0.00	0.00	0.00	0.00
74,000	0.00	0.00	0.00	0.00	0.00	0.00	0.00	0.00	0.00	0.00
76,000	0.00	0.00	0.00	0.00	0.00	0.00	0.00	0.00	0.00	0.00
78,000	0.00	0.00	0.00	0.00	0.00	0.00	0.00	0.00	0.00	0.00
80,000	0.00	0.00	0.00	0.00	0.00	0.00	0.00	0.00	0.00	0.00
82,000	0.00	0.00	0.00	0.00	0.00	0.00	0.00	0.00	0.00	0.00

Table 4.25: Tridem-Axle Load Spectra for Year 4

Axle Load (lb)	Vehicle Class									
	4	5	6	7	8	9	10	11	12	13
12,000	0.00	0.00	0.00	6.59	0.00	0.00	113.24	1.08	0.00	1.91
15,000	0.00	0.00	0.00	1.38	0.00	0.00	136.43	0.99	0.00	0.64
18,000	0.00	0.00	0.00	1.00	0.00	0.00	158.95	0.89	0.00	1.30
21,000	0.00	0.00	0.00	0.92	0.00	0.00	182.82	0.79	0.00	1.07
24,000	0.00	0.00	0.00	2.06	0.00	0.00	207.11	0.63	0.00	2.05
27,000	0.00	0.00	0.00	3.49	0.00	0.00	232.58	0.55	0.00	2.25
30,000	0.00	0.00	0.00	3.52	0.00	0.00	257.40	0.48	0.00	2.72
33,000	0.00	0.00	0.00	7.92	0.00	0.00	282.19	0.75	0.00	5.02
36,000	0.00	0.00	0.00	9.21	0.00	0.00	306.17	0.47	0.00	6.42
39,000	0.00	0.00	0.00	14.93	0.00	0.00	329.58	0.45	0.00	7.63
42,000	0.00	0.00	0.00	16.21	0.00	0.00	353.35	0.36	0.00	11.66
45,000	0.00	0.00	0.00	13.11	0.00	0.00	377.60	0.35	0.00	11.53
48,000	0.00	0.00	0.00	8.06	0.00	0.00	401.66	0.22	0.00	10.72
51,000	0.00	0.00	0.00	5.95	0.00	0.00	426.11	0.17	0.00	10.68
54,000	0.00	0.00	0.00	2.32	0.00	0.00	450.58	0.11	0.00	9.00
57,000	0.00	0.00	0.00	1.69	0.00	0.00	475.58	0.02	0.00	5.33
60,000	0.00	0.00	0.00	0.40	0.00	0.00	500.12	0.01	0.00	4.13
63,000	0.00	0.00	0.00	0.46	0.00	0.00	525.09	0.01	0.00	2.65
66,000	0.00	0.00	0.00	0.48	0.00	0.00	550.05	0.00	0.00	1.45
69,000	0.00	0.00	0.00	0.06	0.00	0.00	575.02	0.00	0.00	0.74
72,000	0.00	0.00	0.00	0.00	0.00	0.00	600.01	0.00	0.00	0.42
75,000	0.00	0.00	0.00	0.17	0.00	0.00	625.00	0.00	0.00	0.32
78,000	0.00	0.00	0.00	0.06	0.00	0.00	650.00	0.00	0.00	0.27
81,000	0.00	0.00	0.00	0.00	0.00	0.00	675.00	0.00	0.00	0.00
84,000	0.00	0.00	0.00	0.00	0.00	0.00	700.00	0.00	0.00	0.09
87,000	0.00	0.00	0.00	0.00	0.00	0.00	725.01	0.00	0.00	0.00
90,000	0.00	0.00	0.00	0.00	0.00	0.00	750.00	0.00	0.00	0.00
93,000	0.00	0.00	0.00	0.00	0.00	0.00	775.00	0.00	0.00	0.00
96,000	0.00	0.00	0.00	0.00	0.00	0.00	800.00	0.00	0.00	0.00
99,000	0.00	0.00	0.00	0.00	0.00	0.00	825.00	0.00	0.00	0.00
102,000	0.00	0.00	0.00	0.00	0.00	0.00	850.00	0.00	0.00	0.00

Table 4.26: Quad-Axle Load Spectra for Year 4

Axle Load (lb)	Vehicle Class									
	4	5	6	7	8	9	10	11	12	13
12,000	0.00	0.00	0.00	0.00	0.00	0.00	7.98	0.00	0.00	0.00
15,000	0.00	0.00	0.00	0.00	0.00	0.00	5.24	0.00	0.00	0.00
18,000	0.00	0.00	0.00	0.00	0.00	0.00	11.24	0.00	0.00	0.00
21,000	0.00	0.00	0.00	0.00	0.00	0.00	13.07	0.00	0.00	0.00
24,000	0.00	0.00	0.00	0.00	0.00	0.00	11.74	0.00	0.00	0.00
27,000	0.00	0.00	0.00	0.00	0.00	0.00	9.94	0.00	0.00	0.00
30,000	0.00	0.00	0.00	0.00	0.00	0.00	6.98	0.00	0.00	0.00
33,000	0.00	0.00	0.00	0.00	0.00	0.00	3.68	0.00	0.00	0.00
36,000	0.00	0.00	0.00	0.00	0.00	0.00	5.26	0.00	0.00	0.00
39,000	0.00	0.00	0.00	0.00	0.00	0.00	5.61	0.00	0.00	0.00
42,000	0.00	0.00	0.00	0.00	0.00	0.00	5.46	0.00	0.00	0.00
45,000	0.00	0.00	0.00	0.00	0.00	0.00	4.52	0.00	0.00	0.00
48,000	0.00	0.00	0.00	0.00	0.00	0.00	2.49	0.00	0.00	0.00
51,000	0.00	0.00	0.00	0.00	0.00	0.00	0.80	0.00	0.00	0.00
54,000	0.00	0.00	0.00	0.00	0.00	0.00	1.64	0.00	0.00	0.00
57,000	0.00	0.00	0.00	0.00	0.00	0.00	1.12	0.00	0.00	0.00
60,000	0.00	0.00	0.00	0.00	0.00	0.00	1.12	0.00	0.00	0.00
63,000	0.00	0.00	0.00	0.00	0.00	0.00	0.97	0.00	0.00	0.00
66,000	0.00	0.00	0.00	0.00	0.00	0.00	0.69	0.00	0.00	0.00
69,000	0.00	0.00	0.00	0.00	0.00	0.00	0.00	0.00	0.00	0.00
72,000	0.00	0.00	0.00	0.00	0.00	0.00	0.14	0.00	0.00	0.00
75,000	0.00	0.00	0.00	0.00	0.00	0.00	0.17	0.00	0.00	0.00
78,000	0.00	0.00	0.00	0.00	0.00	0.00	0.00	0.00	0.00	0.00
81,000	0.00	0.00	0.00	0.00	0.00	0.00	0.00	0.00	0.00	0.00
84,000	0.00	0.00	0.00	0.00	0.00	0.00	0.00	0.00	0.00	0.00
87,000	0.00	0.00	0.00	0.00	0.00	0.00	0.00	0.00	0.00	0.00
90,000	0.00	0.00	0.00	0.00	0.00	0.00	0.00	0.00	0.00	0.00
93,000	0.00	0.00	0.00	0.00	0.00	0.00	0.00	0.00	0.00	0.00
96,000	0.00	0.00	0.00	0.00	0.00	0.00	0.13	0.00	0.00	0.00
99,000	0.00	0.00	0.00	0.00	0.00	0.00	0.00	0.00	0.00	0.00
102,000	0.00	0.00	0.00	0.00	0.00	0.00	0.00	0.00	0.00	0.00

Table 4.27: Summary of Mix Properties for the Collected Loose HMA Mixes (Hossain et al., 2013)

Properties	**S3 Mix**	**S4 Mix**
Aggregate Gradation (Sieve Size)	***Passing (%)***	***Passing (%)***
1.0 in.	100	100
¾ in.	98	100
½ in.	87	98
⅜ in	80	89
No. 4	58	63
No. 8	37	40
No. 16	25	28
No. 30	19	22
No. 50	12	14
No. 100	4	6
No. 200	2.9	3.7
Binder Information	**S3 Mix**	**S4 Mix**
Binder Type	PG 64-22	PG 64-22
Binder Content	4.1	4.6
Binder Specific Gravity	1.01	1.0173
Aggregate Property	**S3 Mix**	**S4 Mix**
Maximum Aggregate Size (MAS)	1.0 in.	¾ in.
Nominal Maximum Size (NMS)	¾ in.	½ in.
Sand Equivalent	94	70
L.A. Abrasion % Wear	28.0	11.0
Durability	71	63
Ignition Oven Correction Factor (IOC)	0.14	0.26
Fractured Faces	100/100	100/100
Effective Specific Gravity (Gse)	2.671	2.678
Mixture Property	**S3 Mix**	**S4 Mix**
Voids in the Mineral Aggregate (VMA) (%)	13.6	14.1
Indirect Tensile Strength (psi)	158.8	110.5
Gse (Effective specific gravity of aggregate)	2.671	2.678
Gsb (Bulk specific gravity of aggregate)	2.645	2.658
Gmm (Maximum theoretical specific gravity of mix)	2.502	2.490

Table 4.28: Dynamic Modulus Data for S3 and S4 Mixes (Hossain et al., 2016)

S3 Mix (Dynamic Modulus, psi)						
Temp (°F)	**0.1 Hz**	**0.5 Hz**	**1 Hz**	**5 Hz**	**10 Hz**	**25 Hz**
10	2,194,482	2,395,862	2,472,903	2,629,875	2,688,509	2,758,336
40	995,548	1,307,273	1,464,214	1,817,892	2,013,348	2,025,775
70	306,328	494,014	571,255	822,116	901,579	948,270
100	86,215	126,454	156,197	255,138	301,891	361,526
130	40,825	51,128	60,620	86,963	121,483	153,106
S4 Mix (Dynamic Modulus, psi)						
Temp (°F)	**0.1 Hz**	**0.5 Hz**	**1 Hz**	**5 Hz**	**10 Hz**	**25 Hz**
10	1,976,749	2,248,836	2,361,669	2,610,177	2,710,590	2,836,667
40	761,210	1,059,477	1,180,146	1,404,441	1,513,592	1,662,424
70	210,084	352,080	416,131	600,179	659,885	745,122
100	65,742	95,197	115,086	181,825	213,554	261,165
130	30,947	43,577	49,294	71,907	85,008	98,958

Table 4.29: DSR test data on PG 64-22 Binder (Hossain et al., 2016)

Temperature (°F)	**Angular Frequency = 10 rad/sec**	
	G* (Pa)	**δ (°)**
142	6153	77
147	3930	18
153	2713	79

Table 4.30: Resilient Modulus Values of the 12% CFA-Stabilized Subgrade Soil Specimen at OMC

		M_r (psi) @ OMC				
σ_3 (psi)	σ_d (psi)	2-day	8-day	16-day	23-day	30-day
6	1.8	120,955	150,609	175,146	184,386	189,430
6	3.6	101,200	145,032	161,564	176,745	177,369
6	5.4	103,218	140,698	155,854	170,115	172,560
6	7.2	98,384	138,275	155,374	168,630	169,780
6	9.0	92,000	138,166	148,290	165,991	165,891
4	1.8	113,664	144,116	171,959	179,970	181,801
4	3.6	97,960	139,566	158,112	167,580	175,600
4	5.4	96,565	138,446	153,659	166,209	168,243
4	7.2	96,327	138,199	151,789	165,210	165,434
4	9.0	93,035	136,614	148,215	160,313	161,269
2	1.8	112,369	139,178	161,377	176,760	177,321
2	3.6	96,885	136,846	155,247	165,773	168,231
2	5.4	96,960	133,180	152,711	165,212	167,232
2	7.2	95,633	132,843	148,089	163,014	163,329
2	9.0	92,053	132,222	145,334	160,815	160,712
k_1		121,609	147,881	177,284	185,967	190,532
k_2		-0.13	-0.04	-0.08	-0.06	-0.07
R^2		0.82	0.48	0.84	0.77	0.81
Design[a] M_r		96,340	137,653	153,609	167,012	168,073

σ_d : Deviator Stress; σ_3 : Confining Pressure; [a]$M_r = k_1 (\sigma_d \wedge k_2)$ (σ_d = 6 psi, σ_3 = 4 psi)

Table 4.31: Resilient Modulus Values of the 12% CFA-Stabilized Subgrade Soil Specimen at OMC + 2%

		M_r (psi) @ OMC + 2%				
σ_3 (psi)	σ_d (psi)	2-day	8-day	16-day	23-day	30-day
6	1.8	69,738	104,221	113,625	117,186	117,667
6	3.6	69,041	98,103	109,152	109,606	109,651
6	5.4	63,802	98,523	106,478	106,728	106,205
6	7.2	58,558	94,283	100,573	103,629	103,778
6	9.0	54,464	90,165	97,254	100,294	100,286
4	1.8	62,055	99,682	106,812	112,890	112,817
4	3.6	61,061	97,720	104,417	104,527	104,656
4	5.4	57,672	94,433	99,131	100,147	102,019
4	7.2	55,398	91,058	97,740	98,611	98,792
4	9.0	52,755	89,156	94,568	98,707	99,182
2	1.8	59,477	97,170	100,293	101,767	101,648
2	3.6	60,381	97,093	98,013	98,167	99,253
2	5.4	56,381	93,008	96,500	96,861	97,280
2	7.2	55,871	91,435	94,764	96,023	96,208
2	9.0	51,837	89,379	94,004	95,128	96,171
k_1		69,986	105,469	112,268	114,894	114,960
k_2		-0.11	-0.07	-0.07	-0.07	-0.07
R^2		0.54	0.77	0.52	0.50	0.51
Design[a] M_r		57,466	93,037	99,034	101,350	101,409

σ_d : Deviator Stress; σ_3 : Confining Pressure; [a]$M_r = k_1 (\sigma_d \wedge k_2)$ (σ_d = 6 psi, σ_3 = 4 psi)

Table 4.32: Resilient Modulus Values of Natural Subgrade Soil Specimens

σ_3 (psi)	σ_d (psi)	M_r (psi)	
		OMC	OMC+2%
6	1.8	20,447	15,907
6	3.6	19,741	15,172
6	5.4	18,488	13,786
6	7.2	17,690	12,695
6	9.0	16,957	11,755
4	1.8	18,687	14,688
4	3.6	18,259	13,821
4	5.4	17,499	12,860
4	7.2	16,851	12,107
4	9.0	16,312	11,480
2	1.8	17,354	13,406
2	3.6	16,750	12,662
2	5.4	16,154	11,858
2	7.2	15,609	11,170
2	9.0	15,189	10,646
k_1		20,185	16,498
k_2		-0.10	-0.16
R^2		0.70	0.66
Design[a] M_r		17,008	12,327

[a]$M_r = k_1 \times \sigma_d \wedge k_2$ (σ_d = 6 psi, σ_3 = 4 psi); σ_d : Deviator Stress; σ_3 : Confining Pressure

Table 4.33: Weather Stations and Their Distances from Test Section

Weather Station	Latitude	Longitude	Distance from Test Section (approximate)
Will Rogers Airport	35.389427°	-97.598853°	26 miles
Wiley Post Airport	35.532970°	-97.650250°	37 miles
Guthrie Airport	35.850349°	-97.415295°	55 miles
Lawton Airport	34.567801°	-98.415961°	67 miles
Stillwater Airport	36.160209°	-97.085217°	78 miles
McAlester Airport	34.880904°	-95.764152°	92 miles
Hobart Airport	34.995559°	-99.052163°	95 miles

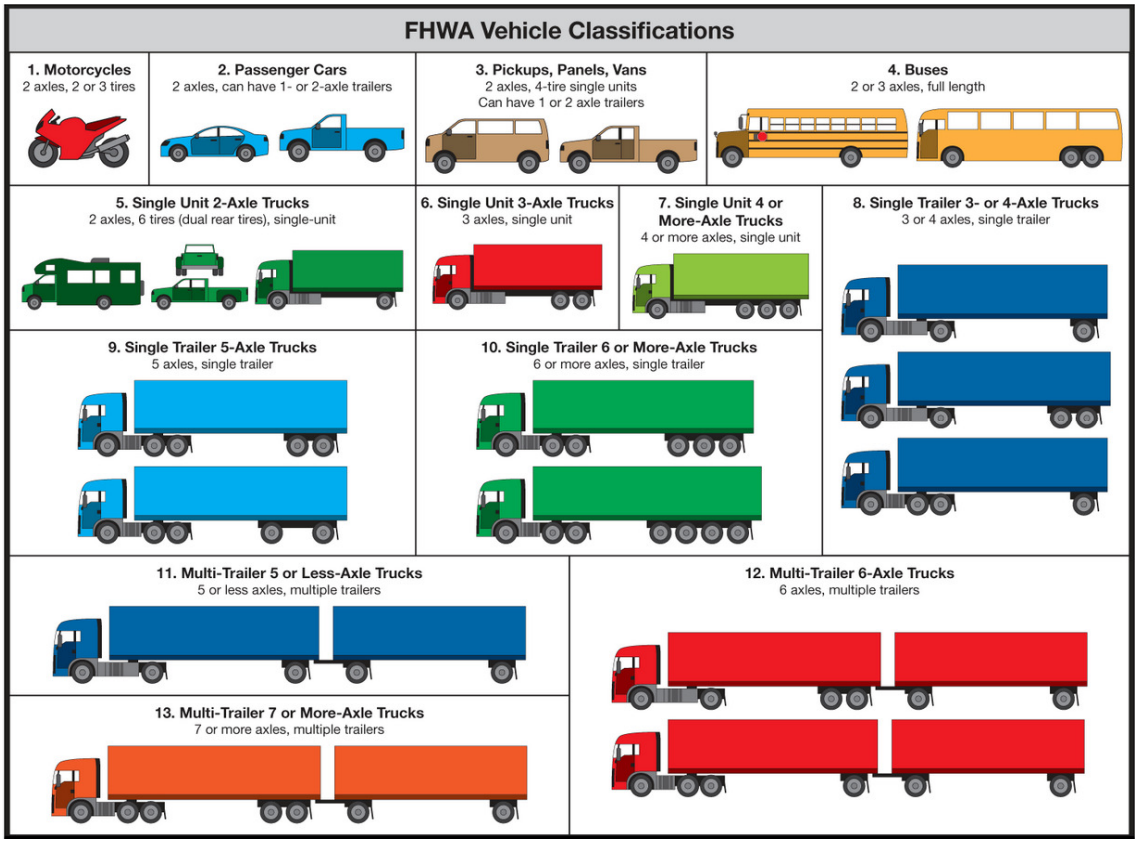

Figure 4.1: FHWA Vehicle Classification

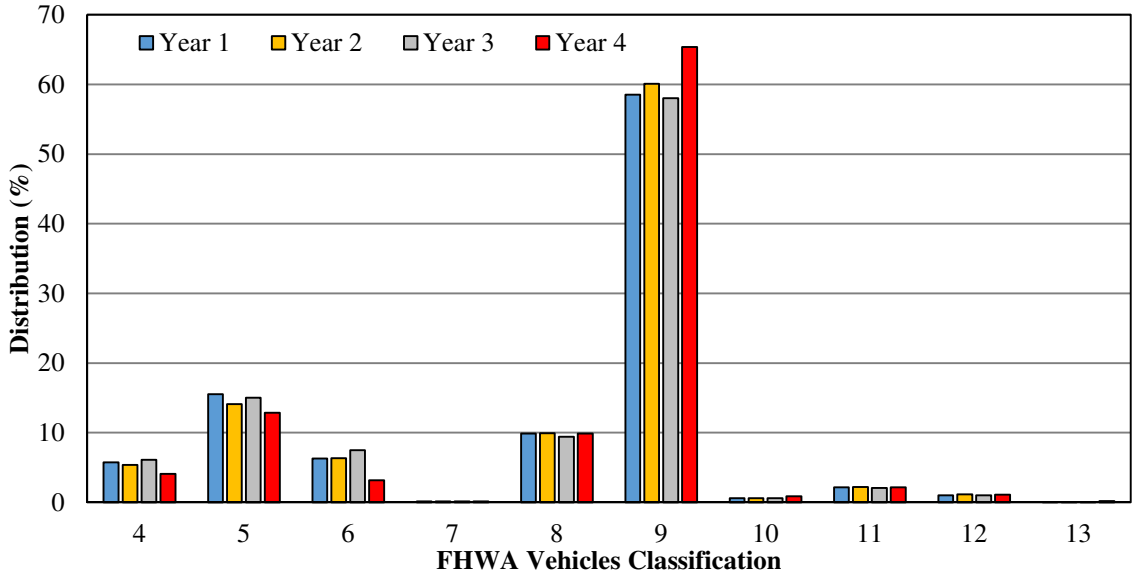

Figure 4.2: Vehicle Class Distribution on the Test Section

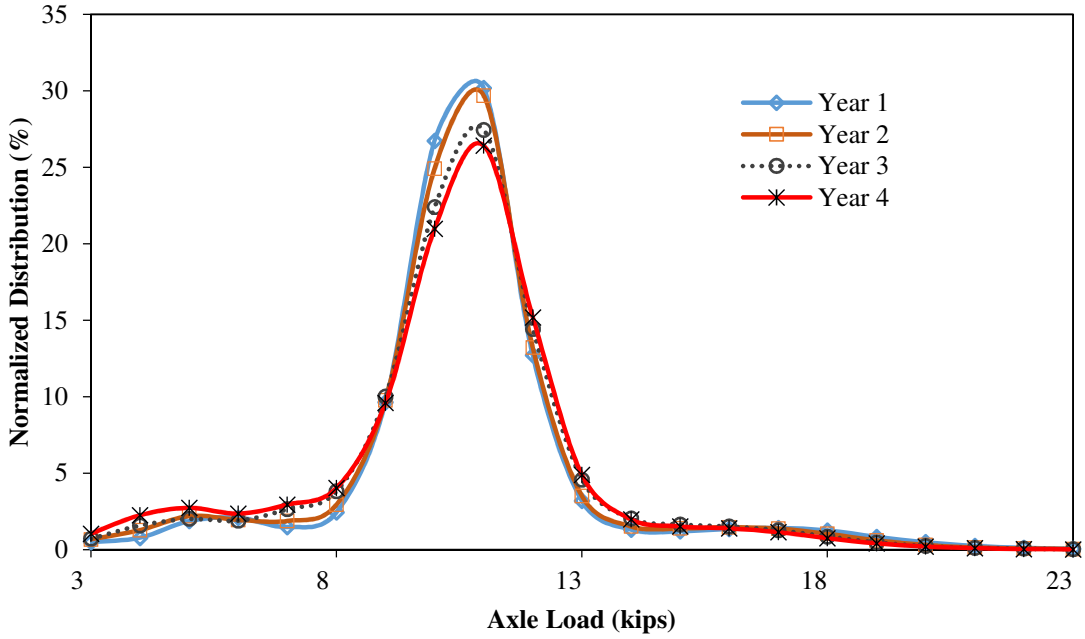

Figure 4.3: Axle Load Spectra for Single Axles of Class 9

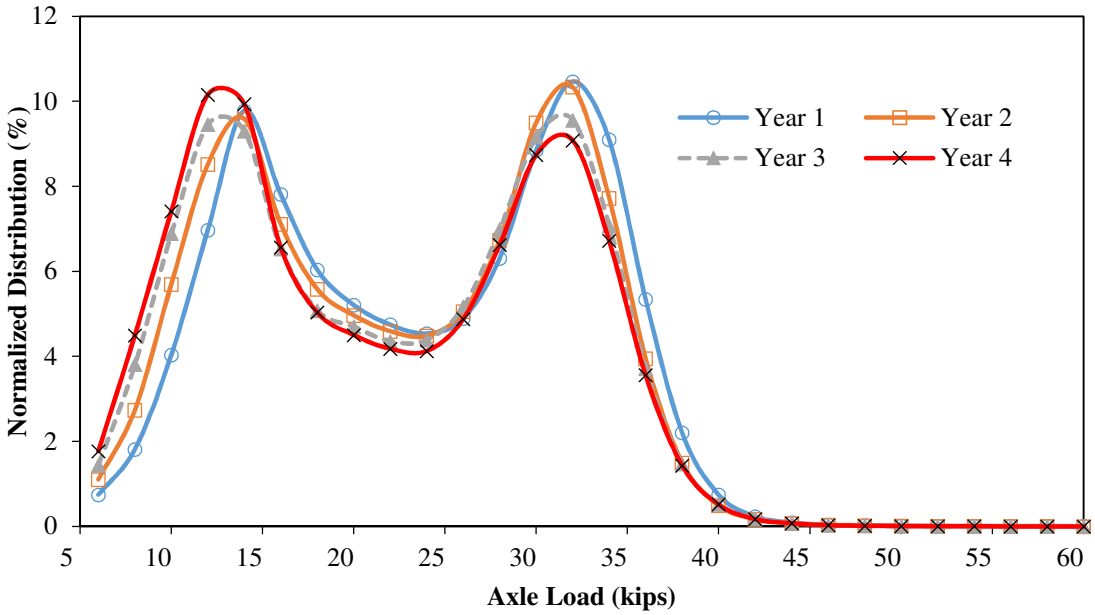

Figure 4.4: Axle Load Spectra for Tandem Axles of Class 9

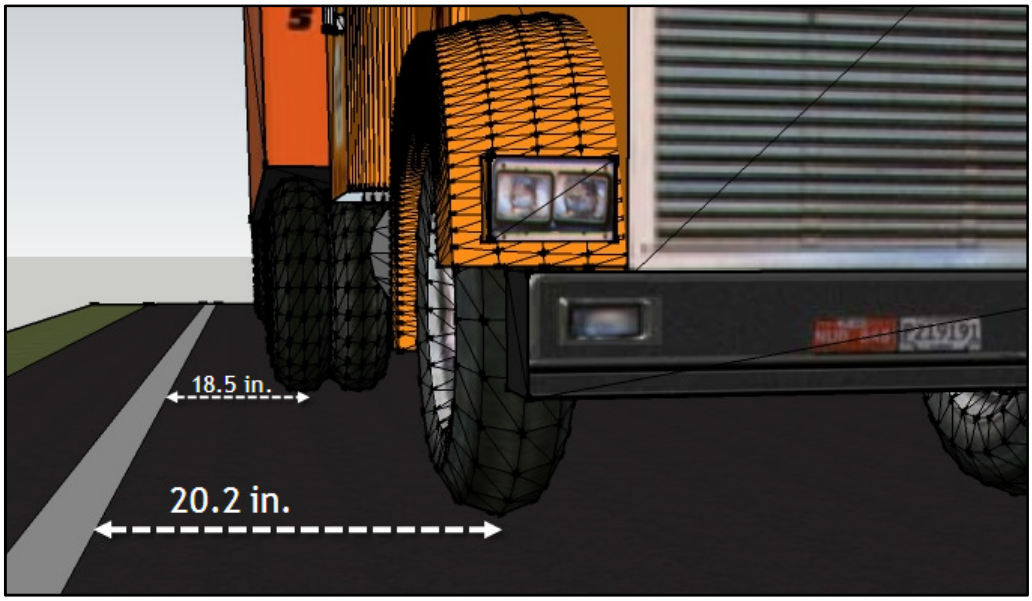

Figure 4.5: Distances Used in Calculating Wheel Wander

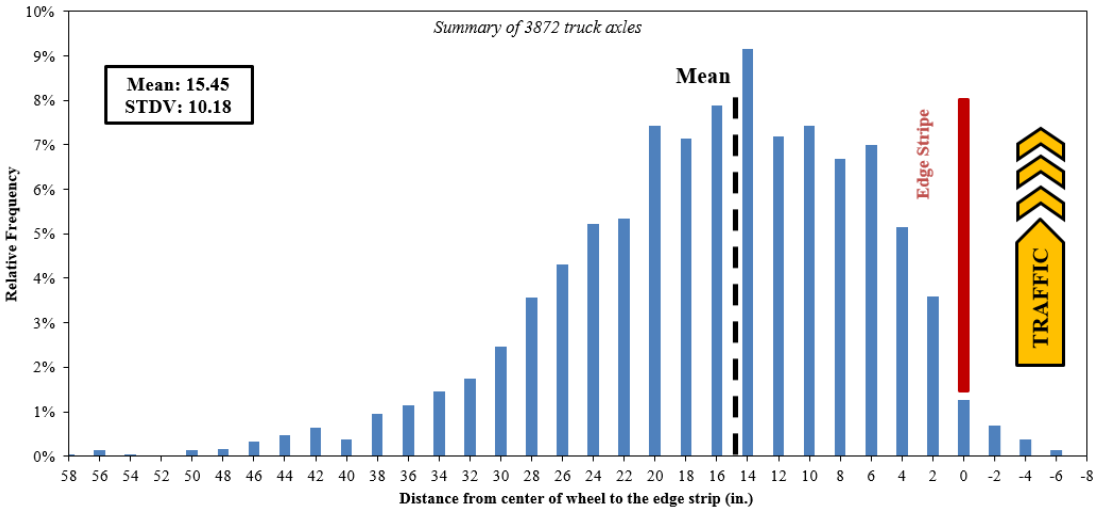

Figure 4.6: Statistical Distributions of Lateral Traffic Wander Data (Solanki et al., 2013)

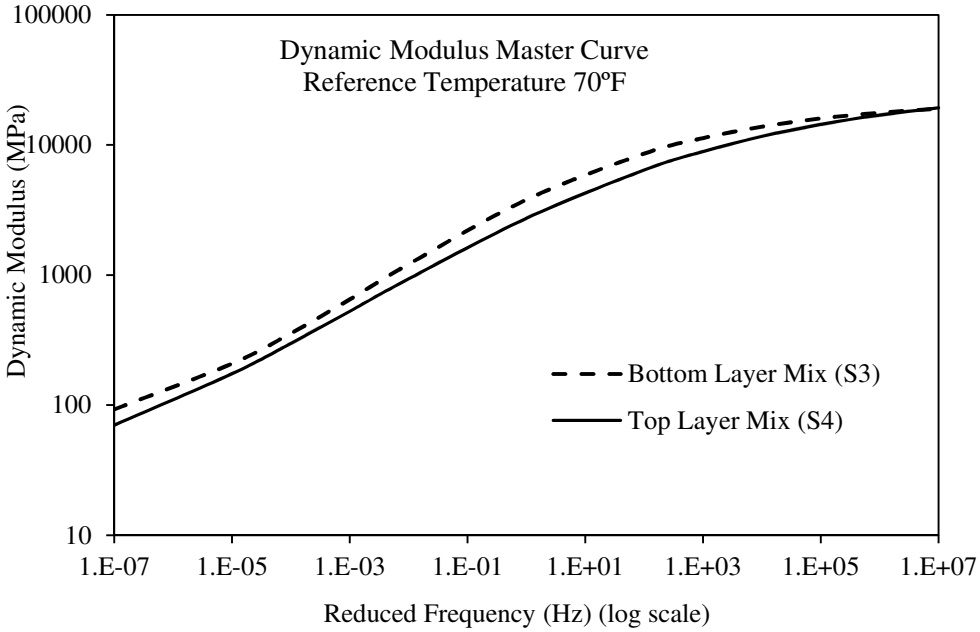

Figure 4.7: Dynamic Modulus Master Curve for S4 and S3 Mixes

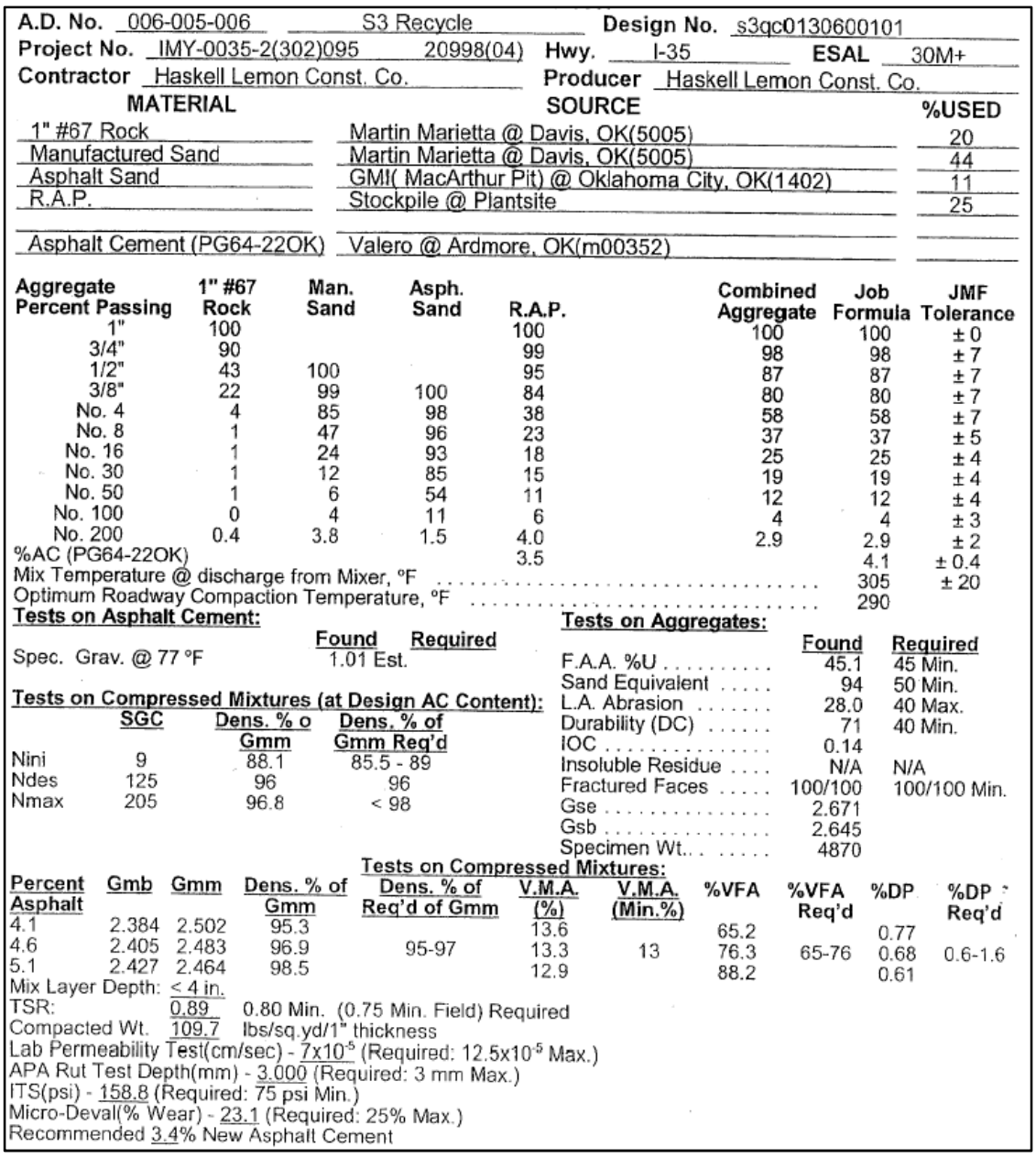

A.D. No. 006-005-006 S3 Recycle Design No. s3qc0130600101
Project No. IMY-0035-2(302)095 20998(04) Hwy. I-35 ESAL 30M+
Contractor Haskell Lemon Const. Co. Producer Haskell Lemon Const. Co.

MATERIAL	SOURCE	%USED
1" #67 Rock	Martin Marietta @ Davis, OK(5005)	20
Manufactured Sand	Martin Marietta @ Davis, OK(5005)	44
Asphalt Sand	GMI(MacArthur Pit) @ Oklahoma City, OK(1402)	11
R.A.P.	Stockpile @ Plantsite	25
Asphalt Cement (PG64-22OK)	Valero @ Ardmore, OK(m00352)	

Aggregate Percent Passing	1" #67 Rock	Man. Sand	Asph. Sand	R.A.P.	Combined Aggregate	Job Formula	JMF Tolerance
1"	100			100	100	100	± 0
3/4"	90			99	98	98	± 7
1/2"	43	100		95	87	87	± 7
3/8"	22	99	100	84	80	80	± 7
No. 4	4	85	98	38	58	58	± 7
No. 8	1	47	96	23	37	37	± 5
No. 16	1	24	93	18	25	25	± 4
No. 30	1	12	85	15	19	19	± 4
No. 50	1	6	54	11	12	12	± 4
No. 100	0	4	11	6	4	4	± 3
No. 200	0.4	3.8	1.5	4.0	2.9	2.9	± 2
%AC (PG64-22OK)				3.5		4.1	± 0.4
Mix Temperature @ discharge from Mixer, °F						305	± 20
Optimum Roadway Compaction Temperature, °F						290	

Tests on Asphalt Cement:

	Found	Required
Spec. Grav. @ 77 °F	1.01 Est.	

Tests on Compressed Mixtures (at Design AC Content):

	SGC	Dens. % o Gmm	Dens. % of Gmm Req'd
Nini	9	88.1	85.5 - 89
Ndes	125	96	96
Nmax	205	96.8	< 98

Tests on Aggregates:

	Found	Required
F.A.A. %U	45.1	45 Min.
Sand Equivalent	94	50 Min.
L.A. Abrasion	28.0	40 Max.
Durability (DC)	71	40 Min.
IOC	0.14	
Insoluble Residue	N/A	N/A
Fractured Faces	100/100	100/100 Min.
Gse	2.671	
Gsb	2.645	
Specimen Wt.	4870	

Tests on Compressed Mixtures:

Percent Asphalt	Gmb	Gmm	Dens. % of Gmm	Dens. % of Req'd of Gmm	V.M.A. (%)	V.M.A. (Min.%)	%VFA	%VFA Req'd	%DP	%DP Req'd
4.1	2.384	2.502	95.3		13.6		65.2		0.77	
4.6	2.405	2.483	96.9	95-97	13.3	13	76.3	65-76	0.68	0.6-1.6
5.1	2.427	2.464	98.5		12.9		88.2		0.61	

Mix Layer Depth: < 4 in.
TSR: 0.89 0.80 Min. (0.75 Min. Field) Required
Compacted Wt. 109.7 lbs/sq.yd/1" thickness
Lab Permeability Test(cm/sec) - $7x10^{-5}$ (Required: $12.5x10^{-5}$ Max.)
APA Rut Test Depth(mm) - 3.000 (Required: 3 mm Max.)
ITS(psi) - 158.8 (Required: 75 psi Min.)
Micro-Deval(% Wear) - 23.1 (Required: 25% Max.)
Recommended 3.4% New Asphalt Cement

Figure 4.8: Mix Design Sheet for S3 Mix (Courtesy: Haskell Lemon Construction Co., Norman)

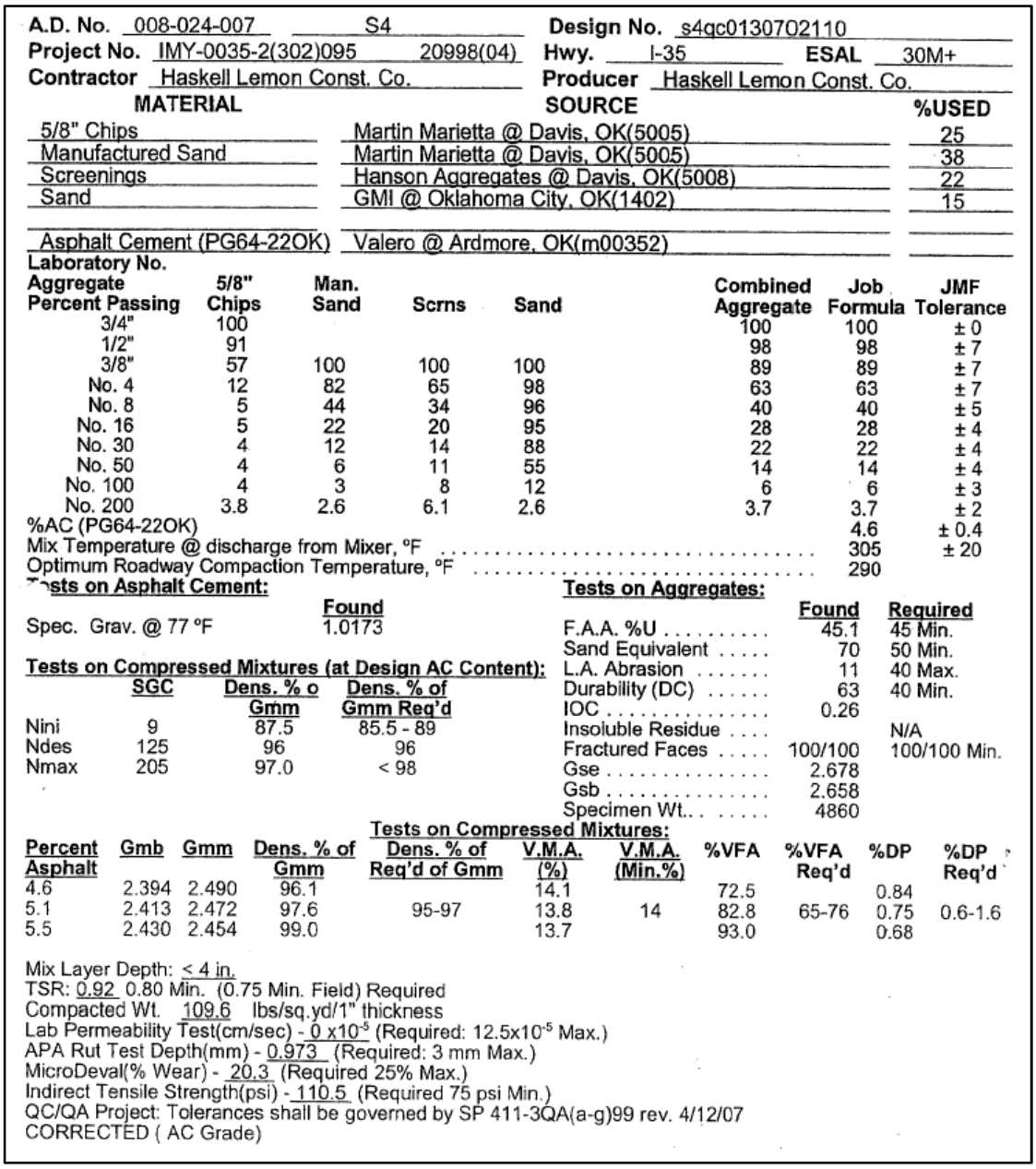

A.D. No. 008-024-007 S4 Design No. s4qc0130702110
Project No. IMY-0035-2(302)095 20998(04) Hwy. I-35 ESAL 30M+
Contractor Haskell Lemon Const. Co. Producer Haskell Lemon Const. Co.

MATERIAL	SOURCE	%USED
5/8" Chips	Martin Marietta @ Davis, OK(5005)	25
Manufactured Sand	Martin Marietta @ Davis, OK(5005)	38
Screenings	Hanson Aggregates @ Davis, OK(5008)	22
Sand	GMI @ Oklahoma City, OK(1402)	15
Asphalt Cement (PG64-22OK)	Valero @ Ardmore, OK(m00352)	

Laboratory No.

Aggregate Percent Passing	5/8" Chips	Man. Sand	Scrns	Sand	Combined Aggregate	Job Formula	JMF Tolerance
3/4"	100				100	100	± 0
1/2"	91				98	98	± 7
3/8"	57	100	100	100	89	89	± 7
No. 4	12	82	65	98	63	63	± 7
No. 8	5	44	34	96	40	40	± 5
No. 16	5	22	20	95	28	28	± 4
No. 30	4	12	14	88	22	22	± 4
No. 50	4	6	11	55	14	14	± 4
No. 100	4	3	8	12	6	6	± 3
No. 200	3.8	2.6	6.1	2.6	3.7	3.7	± 2
%AC (PG64-22OK)						4.6	± 0.4
Mix Temperature @ discharge from Mixer, °F						305	± 20
Optimum Roadway Compaction Temperature, °F						290	

Tests on Asphalt Cement:

	Found
Spec. Grav. @ 77 °F	1.0173

Tests on Aggregates:

	Found	Required
F.A.A. %U	45.1	45 Min.
Sand Equivalent	70	50 Min.
L.A. Abrasion	11	40 Max.
Durability (DC)	63	40 Min.
IOC	0.26	
Insoluble Residue		N/A
Fractured Faces	100/100	100/100 Min.
Gse	2.678	
Gsb	2.658	
Specimen Wt.	4860	

Tests on Compressed Mixtures (at Design AC Content):

	SGC	Dens. % of Gmm	Dens. % of Gmm Req'd
Nini	9	87.5	85.5 - 89
Ndes	125	96	96
Nmax	205	97.0	< 98

Tests on Compressed Mixtures:

Percent Asphalt	Gmb	Gmm	Dens. % of Gmm	Dens. % of Req'd of Gmm	V.M.A. (%)	V.M.A. (Min.%)	%VFA	%VFA Req'd	%DP	%DP Req'd
4.6	2.394	2.490	96.1		14.1		72.5		0.84	
5.1	2.413	2.472	97.6	95-97	13.8	14	82.8	65-76	0.75	0.6-1.6
5.5	2.430	2.454	99.0		13.7		93.0		0.68	

Mix Layer Depth: < 4 in.
TSR: 0.92 0.80 Min. (0.75 Min. Field) Required
Compacted Wt. 109.6 lbs/sq.yd/1" thickness
Lab Permeability Test(cm/sec) - 0 x10^{-5} (Required: 12.5x10^{-5} Max.)
APA Rut Test Depth(mm) - 0.973 (Required: 3 mm Max.)
MicroDeval(% Wear) - 20.3 (Required 25% Max.)
Indirect Tensile Strength(psi) - 110.5 (Required 75 psi Min.)
QC/QA Project: Tolerances shall be governed by SP 411-3QA(a-g)99 rev. 4/12/07
CORRECTED (AC Grade)

Figure 4.9: Mix Design Sheet for S4 Mix (Courtesy: Haskell Lemon Construction Co., Norman)

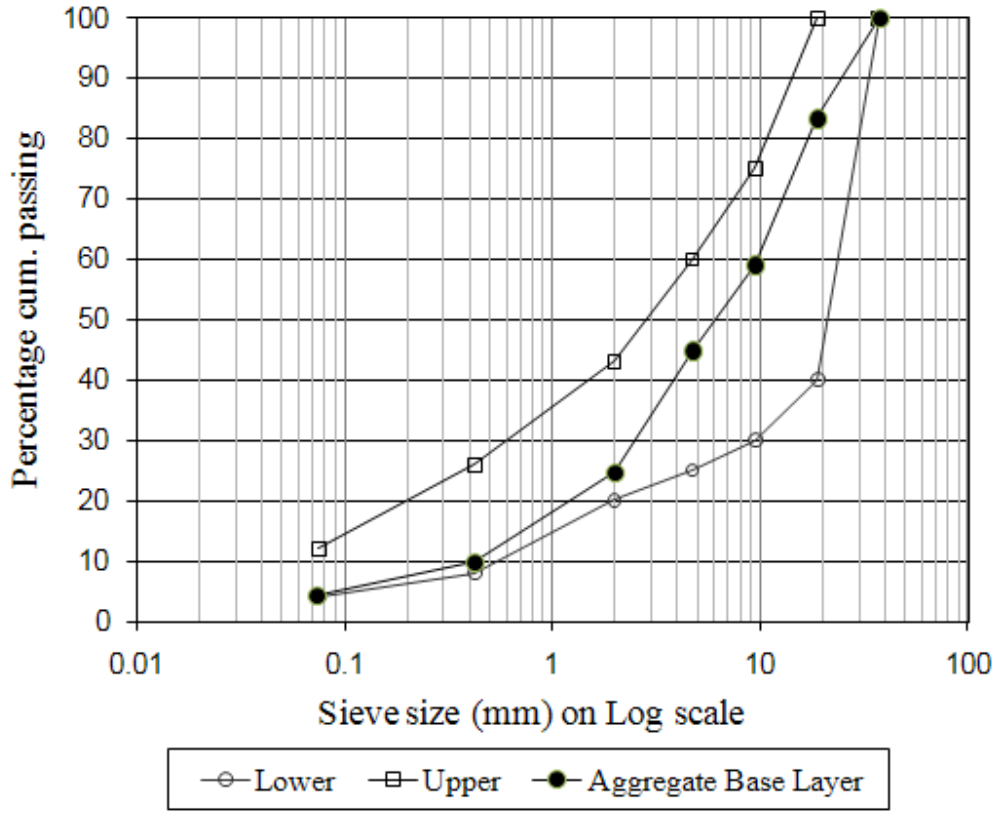

Figure 4.10: Gradation of Aggregate Base Layer

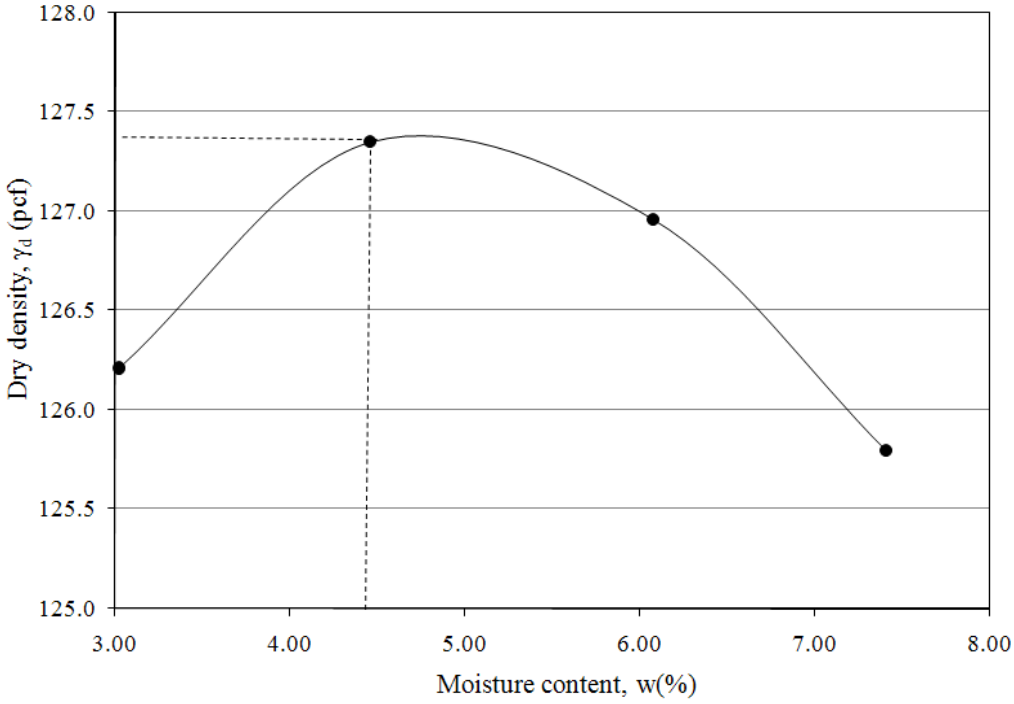

Figure 4.11: Moisture-Density Relationship of Aggregate Base (Solanki et al., 2013)

Figure 4.12 Compacted Resilient Modulus Specimen of Aggregate Base

Figure 4.13: Setup for Resilient Modulus Testing on Aggregate Base Specimen

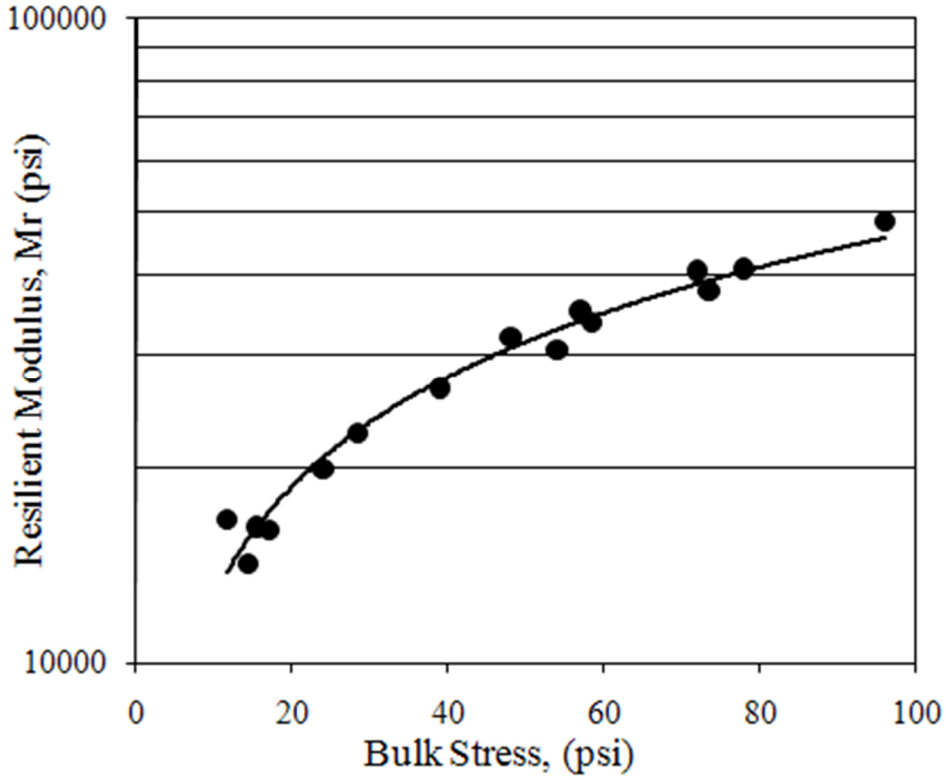

Figure 4.14: Variation of Resilient Modulus with Bulk Stress for Aggregate Base (Solanki et al., 2013)

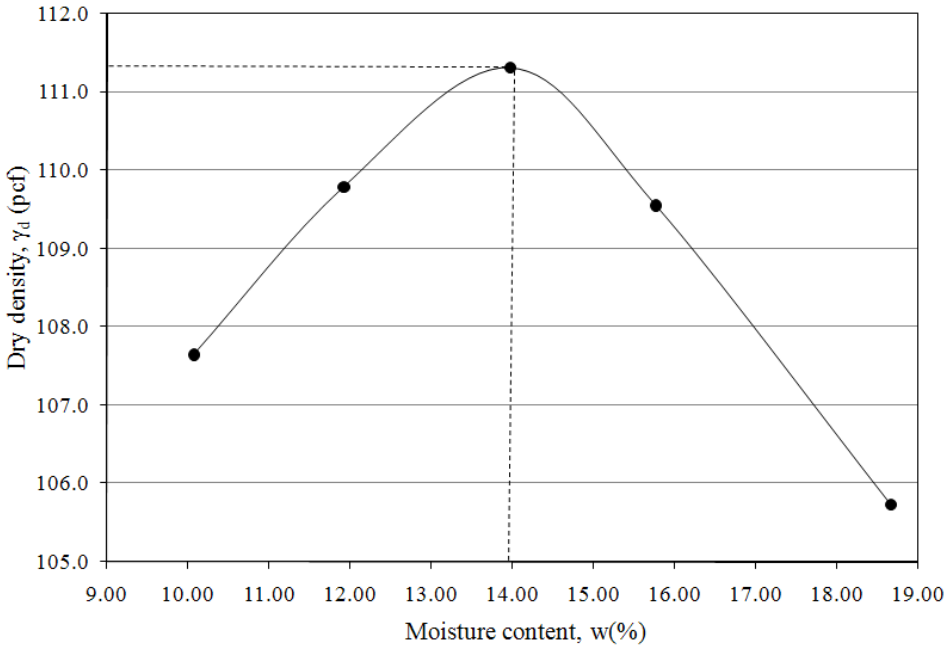

Figure 4.15: Moisture-Density Relationship of Subgrade Soil-CFA Mix (Solanki et al., 2013)

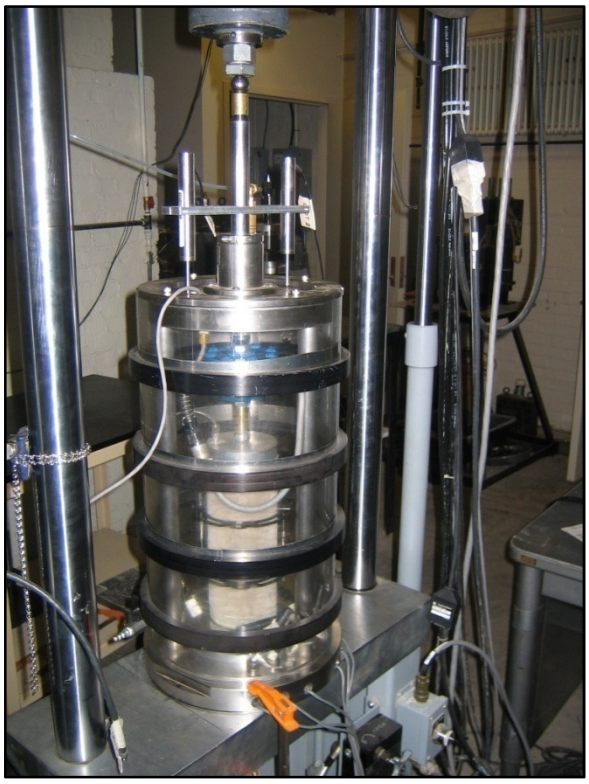

Figure 4.16: Setup for Resilient Modulus Testing on Natural and Stabilized Subgrade Soil Specimen

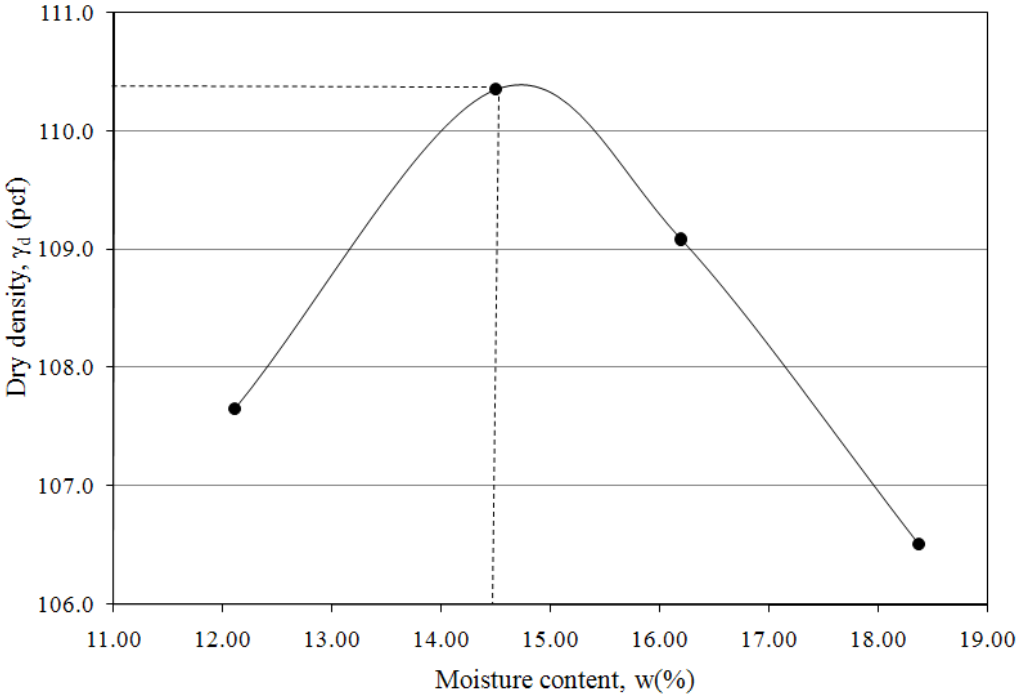

Figure 4.17: Moisture-Density Relationship of Subgrade Soil (Solanki et al., 2013)

Figure 4.18: Weather Stations near Interstate-35 Test Section

CHAPTER

5

Sensitivity of Level 1 Input Parameters on Pavement Performance

5.1 Introduction

This chapter provides an overview of the need for developing Level 1 input parameters for traffic and materials. Sensitivity of different input levels is also discussed. In addition, comparisons between default (Level 1) and site specific (Level 3) inputs and their influence on rut prediction are presented and the most sensitive traffic parameters identified for better prediction of pavement performance relative to rut.

5.2 Prediction of Rut using Default Input Parameters

The test section used in this study exhibited significant rutting (approximately 0.9 in.) and minimal cracking (less than 1% of the total area) during its service life. The sensitivity of the levels of input parameters was studied by comparing rut values predicted by AASHTOWare® with the rut values measured in the field. Nationally calibrated (AASHTO, 2004) rut models were used for this purpose.

As discussed in Section 3.9.1, a total of 18 rut measurements were performed at the test section. Table 5.1 shows the measured rut values at all stations during each field test. Since variations were observed among different stations within the test section, it was decided to take the average rut values of all six stations for a particular field visit and use that value as the representative value for the entire test section. These average rut values were then compared with the corresponding values predicted by the MEPDG.

Default (Level 3) inputs for both traffic and materials were used first to predict rut using AASHTOWare®. Figure 5.1 shows a graphical comparison between the measured and predicted ruts. Table 5.2 shows the difference between the measured and predicted ruts. It is observed from Figure 5.1 and Table 5.2 that the MEPDG over-predicted the rut values in all cases. The level of error ranges between 15% and 66%, with an average error of about 37%. For statistical characterization, student pair t-test was conducted for different periods of the year. The null hypothesis for this analysis was that the difference in predicted and measured rut values was equal to zero and the alternative hypothesis was that the rut values were not equal. A significance level of 0.05 was assumed. Thus, p-value of 0.05 or less indicates rejection of the null hypothesis. The p-value here was found to be less than 0.05 ($p = 0.0001$; $p < 0.05$), indicating that statistically significant differences exist between the predicted and measured rut values. These results also indicate that the use of default input parameters (Level 3) can lead to erroneous results and limit the utility of MEPDG in performance predictions. Subsequently, Level 1input parameters were developed to examine the performance of the MEPDG.

For consistency in comparing the significance of errors between the measured and predicted rut values, the following definitions were followed in this study:

- Very significant difference: Difference $\geq 30\%$,
- Moderately significant difference: $10\% \leq$ Difference $\leq 30\%$,
- Not significant difference: Difference $\leq 10\%$.

5.3 Pavement Performance Prediction using Different Levels of Traffic and Material Input Parameters

To examine the sensitivity of different input parameters in the MEPDG, rut predictions were performed using three different combinations of inputs:

(1) Combination 1: Level 1 material and Level 3 traffic inputs;

(2) Combination 2: Level 3 material and Level 1 traffic inputs; and

(3) Combination 3: Level 1 inputs for both material and traffic.

Selection of these combinations was partly dictated by the agency needs. For example, a transportation agency may have Level 1 traffic data but not Level 1 materials data. Similarly, an agency may have Level 1 materials data but may not have Level 1 traffic data. Therefore, these scenarios were examined in this study and the corresponding differences with the measured rut were determined.

5.3.1 Combination 1: Level 1 Materials and Level 3 Traffic Inputs

For this combination, the predicted rut values were compared with the average rut values measured in the field, as shown in Figure 5.2. The difference between measured and predicted rut values was found to be in the range of 10% to 59%, with an average of approximately 30%. Statistical analyses were conducted using a Student's t-test. The p-value was found to be less than 0.05 ($p = 0.001$; $p < 0.05$), indicating a significant difference between measured and predicted rut values. The results show that use of Level 1 material and Level 3 traffic input parameters with nationally calibrated rut models can lead to very significant error in rut prediction (difference $\geq 30\%$).

5.3.2 Combination 2: Level 3 Materials and Level 1 Traffic Inputs

For this combination, differences between the MEPDG predicted rut values using Level 3 materials and Level 1 traffic inputs are found to range between 2% and 41%,

with an average of approximately 16%. So, Combination 2 has 14% less error than Combination 1. Figure 5.3 shows a graphical comparison for this combination. Student's t-test results show that moderately significant difference exists ($p = 0.03$; $p < 0.05$) ($10\% \leq$ Difference $\leq 30\%$) between the measured and predicted rut. However, the difference was smaller compared to that for Combination 1.

5.3.3 Combination 3: Level 1 Inputs for both Materials and Traffic

When using Level 1 input parameters for both traffic and materials, the average error was found to be approximately 10%, showing a significant improvement in rut prediction using the MEPDG software. Figure 5.4 shows a graphical comparison between the measured and predicted ruts for all three scenarios. Student's t-test results show a p-value of slightly less than 0.05 ($p = 0.045$; $p < 0.05$), indicating that the difference is still significant. However, for practical purposes and based on the convention used is this study, this difference cannot be considered as significant (difference $\leq 10\%$).

From the aforementioned combinations, it was observed that Level 1 input significantly improved the rut prediction using the MEPDG. For example, the average error in rut prediction reduced from approximately 37% (when Level 3 inputs were used) to 10% (with Level 1 inputs). It was also observed that the MEPDG rut prediction was more sensitive to Level 1 input parameters for traffic than Level 1 input parameters for materials. For example, using Level 3 materials the average error in rut prediction was about 30% compared to about 16% when Level 1 traffic inputs were used. Because, traffic inputs were found to be more sensitive, an effort was made to further examine the differences between Level 1 and Level 3 input parameters for traffic.

5.4 Comparison of Developed Level 1 Traffic Inputs with Level 3 Inputs

5.4.1 Axle Load Spectra

Axle load spectra (ALS) for four axle types (single, tandem, tridem and quad) were developed in this study for all vehicles. Since Class 9 vehicles are dominant among all vehicle classes, the axle load distribution for Class 9 vehicles was analyzed further. Figures 5.5 and 5.6 show the axle load spectra (Level 1) for the single and tandem axles of Class 9 vehicles for four years, respectively. It is observed that, for single axles, the distribution peaks around 11 kips, which is the expected range for Class 9 single axles (Oh et al., 2014; Tran and Hall, 2007). Detailed analyses of the axle load spectra for single axles showed similar results for other vehicle classes. From Figure 5.6, it can be observed that there are two distinct peaks for the tandem axle distribution: one between 10 and 16 kips, and the other between 28 and 36 kips. This observation is also consistent with previous studies (Faruk et al., 2016; Oh et al., 2014; Papagiannakis et al., 2006; Timm et al., 2006).

Figures 5.5 and 5.6 also show a graphical comparison of axle load spectra between default (Level 3) and site-specific values (Level 1). Only single and tandem axles for Class 9 vehicles are presented here. It is observed that frequency of the peak values for site-specific axle load distribution is higher than the default values. For example, in case of single axles, the site-specific peak frequency was found to be approximately 30% compared to the default value of approximately 18%. In case of tandem axles, the frequencies of the site-specific peak values were approximately 9% and 10% compared to the default values of approximately 8% and 6%, respectively.

It can be observed from the combination mentioned at Section 5.3.3 that only 10% difference was observed between the measured and predicted rut values when Level 1

inputs were used for all traffic and materials parameters. However, to examine the effects of Level 3 and Level 1 ALS on predicted rut values, a comparative analysis was performed. For this analysis, Level 1 inputs were used for all traffic and materials except the ALS. The ALS were used as Level 3 input. It was found that, using Level 3 ALS inputs, MEPDG over-predicts the rut values by approximately 13% compared to using Level 1 ALS inputs.

5.4.2 Vehicle Class Distribution (VCD) Factors

Figure 5.7 shows a graphical comparison of VCD between Level 3 and Level 1 inputs. Significant differences were observed between the default and site-specific (i.e., Level 1) values. For example, differences of about 20% and 25% were observed between the default and actual values for Class 5 and 9 vehicles, respectively. It is also observed that the highest percentage of vehicle for the test section is of Class 9 vehicles (approximately 60%), followed by Class 5 vehicles (approximately 15%). This observation is consistent with the previous studies (Faruk et al., 2016; Tran and Hall, 2007). From the Level 1 traffic data, it was observed that the VCD data matches closely with the Truck Traffic Classification (TTC) for Group 2.

Similar to Section 5.4.1, to examine the effects of Level 1 VCDs on MEPDG rut prediction, a comparative analysis was performed using Level 1 inputs for all the traffic and materials except the VCD. Level 3 inputs were used for the VCD. It was found that, using Level 3 VCD inputs, the MEPDG over-predicts the rut values by approximately 5% compared to using Level 1 VCD inputs.

5.4.3 Monthly Adjustment Factors (MAF)

Figure 5.8 shows a graphical comparison of MAF values between Level 3 and Level 1 inputs for the Class 9 vehicles. It can be observed that the default MAF value (Level 3) is 1.00, irrespective of the month of a year and the vehicle class. Whereas, the actual MAF values (Level 1) for Class 9 vehicles varied from 0.57 to 1.18, indicating the importance of developing MAF parameters for Level 1 input. A similar trend was observed for other classes of vehicles.

A comparative analysis of predicted rut was conducted using Level 1 inputs for all traffic and materials except Level 3 input was used for MAF. It was found that using Level 3 MAF inputs, MEPDG over-predicts the rut values by about 2% compared to using Level 1 MAF inputs.

5.4.4 Hourly Distribution Factors (HDF)

Significant differences were observed between the Level 1 and Level 3 HDFs. Figure 5.9 shows a graphical comparison of HDF between MEPDG Level 3 (default) input and Level 1 inputs. The default HDFs (Level 3) is found to be constant at a value of 2.3 for hours 0 to 5, then increasing sharply to 5 for hours 6 to 9 and then increasing sharply again to 6. Whereas, the HDF obtained from the Level 1 input shows a gradual increase and decrease with time. Since, the MEPDG does not use the HDFs for design of flexible pavements anymore, no comparative study could be performed to examine the effects of Level 1 HDFs on rut prediction.

5.4.5 Lateral Traffic Wander

As noted previously, three lateral positioning sensors (LPS) were installed in a "Z"-shaped form at the test section to measure the lateral traffic wander. Figure 5.10

shows the distribution of traffic wander, which was generated using 3,872 truck axles (steering and tandem). It was found that the mean wheel location was 15.5 in. from the lane marking. The standard deviation for the traffic wander was 10.2 in. Comparatively, the default (Level 3) input for this parameter is 18 in. and the standard deviation is 10 in.

5.5 Comparison of Traffic Inputs for Different Years

The developed Level 1 traffic inputs were compared for the four consecutive years. Four major traffic inputs were selected for this task: HDF, MDF, VCD and ALS.

5.5.1 Comparison of Different Years of ALSs

Although the ALS distributions were developed for all the vehicle classes (Class 4 to Class 13), only the ALS distributions for Class 9 vehicles are presented in this study for comparison purposes.

Figure 5.5 presents four years of average ALS distributions for Class 9 single axles. It is seen that that the highest peak value for the Class 9 single axles was approximately 30% in Year 1 and the lowest peak value was approximately 26.5% in Year 4. The peak values for the other two years (Year 2 and 3) fall in between these two values. Therefore, there is approximately 3.5% difference in the peak values for single axles over the four-year period.

From the ALS distributions for Class 9 tandem axles (Figure 5.6), it is observed that the highest peak value for tandem axles was approximately 10.5% in Year 1 and the lowest peak value was approximately 9% in Year 4. Therefore, there was approximately 1.5% difference in peak values for tandem axles over the four-year period. Overall, it is noted that the ALSs of different years were not much different.

5.5.2 Comparison of Different Years of VCDs

Figure 5.7 shows a graphical comparison of VCD distribution for Year 1 through Year 4. Approximately 1% to 5% differences were observed in the VCD values for different vehicle classes over the four-year period. The highest variation in the VCDs was observed for Class 9 vehicles and the lowest variations were observed for Class 7 vehicles. It can be observed that slight differences (1% to 5%) exist between different years of VCD. However, this difference is much less than their differences with the Level 3 distribution. For example, in case of Class 9 vehicles Level 3 VCD is approximately 36%, whereas the Level 1 distribution was approximately 60%.

5.5.3 Comparison of Different Years of MAFs

Figure 5.8 shows the MAF distribution for Year 1 through Year 4. It can be observed that the lowest MAF for Class 9 vehicles was observed in June of Year 2, whereas the highest MAF was observed in May of Year 2. The average MAF value was found to be 1, as expected. The standard deviations varied from approximately 0.05 to 0.49. The variations in the MAF value for Class 9 vehicles were the highest in Year 2 and the lowest in Year 4.

5.5.4 Comparison of Different Years of HDFs

Figure 5.9 shows the HDFs for Year 1 through 4. It was observed from the four years of HDFs that the maximum HDF values for these years varies from 5.93 to 6.03, whereas the minimum HDF values varied from 1.87 to 1.96. In general, around 10 a.m. the test section experienced the most traffic, whereas around 1 a.m. the test section experienced the least traffic on any given day. It can be stated that although the

developed Level 1 HDF values are very different from the default (Level 3) values, the HDFs for four consecutive years were not much different.

5.6 Sensitivity of Different Traffic Inputs on Pavement Performance

Since it was observed that significant differences (as high as 36%) exist between the Level 1 and Level 3 traffic inputs, an effort was made to analyze the sensitivity of different inputs for traffic. Rut prediction was performed using the AASHTOWare® for three different traffic input combinations. Level 1 materials input parameters were used for this exercise. The following combination of traffic inputs were considered:

(1) Combination 1: Level 1 ALS and Level 3 other traffic inputs (MAF and VCD),

(2) Combination 2: Level 1 VCD and Level 3 other traffic inputs (ALS and MAF), and

(3) Combination 3: Level 1 MAF and Level 3 other traffic inputs (ALS and VCD).

5.6.1 Combination 1: Level 1 ALS and Level 3 Other Traffic Inputs (MAF and VCD)

Under this combination, Level 1 ALS data and Level 3 MAF and VCD data were used to predict the MEPDG rut. The predicted rut values were compared with the average field measured rut values. Differences between the measured and the MEPDG predicted rut values were found to be in the range of 2% to 41%, with an average error of approximately 16%. Also, the Sum of Squared Errors (SSE), which represents the squared sum of differences between the observed and predicted rut values, were evaluated. The SSE was found to be 0.081 for this combination. Statistical analyses were conducted using a Student's t-test. The p-value was found to be less than 0.05 ($p = 0.04$;

$p < 0.05$), indicating a statistically significant difference between measured and predicted rut. A summary of the results for this combination is presented in Table 5.3.

5.6.2 Combination 2: Level 1 VCD and Level 3 Other Traffic Inputs (ALS and MAF)

Level 1 VCD data and Level 3 ALS and VCD data were used to predict the MEPDG rut for this combination. The differences between measured and MEPDG predicted rut values were found to be in the range of 6% to 52%, with an average error of approximately 24%. A SSE value of 0.189 and a p-value less than 0.05 ($p = 0.005$; $p < 0.05$) were found for this combination. Table 5.3 represents a summary of this combination.

5.6.3 Combination 3: Level 1 MAF and Level 3 Other Traffic Inputs (ALS and VCD)

For this combination, Level 1 MAF data and Level 3 ALS and VCD data were used to predict the MEPDG rut. The differences between measured and MEPDG predicted rut values were found to be in range of 10% to 58%, with an average error of approximately 29%. A SSE value of 0.284 and a p-value less than 0.05 ($p = 0.001$; $p < 0.05$) was found for this combination. Table 5.3 represents a summary of this combination.

It can be observed from Table 5.3 that Combination 1 (with Level 1 ALS data) outperformed Combination 2 (with Level 1 VCD data) and Combination 3 (with Level 1 MAF data). In addition, Combination 2 was found to perform better than Combination 3. Therefore, this can be stated that ALS is the most sensitive traffic input parameter followed by VCD and MAF.

5.7 Sensitivity of Different Years of Level 1 Traffic Inputs on Pavement Performance

It was observed that some traffic inputs (e.g., ALS) are more sensitive than other traffic inputs (e.g., MAF, VCD) in predicting rut. Therefore, it was decided to further analyze the sensitivity of traffic inputs year-wise. Because developing Level 1 traffic inputs involves significant investment in terms of time and human resource, it is important for the state agencies to know the frequency of developing the traffic inputs for pavement design. To investigate whether pavement performance are sensitive to different years of Level 1 inputs, multiple rut predictions were performed using the AASHTOWare® by changing one particular type of input developed for different years (i.e., Years 1, 2, 3 and 4), while keeping the other traffic inputs at Year 1. For this exercise, Level 1 inputs for materials were used for all the different runs.

5.7.1 Different Years of MAF Data

For this exercise, at first, rut was predicted using Year 1's MAF data, while keeping the other traffic inputs from Year 1. Then rut was predicted using Year 2, Year 3 and Year 4's MAF data while keeping the other traffic inputs unchanged at Year 1's data. From Table 5.4, it can be observed that some differences (0.003 in. to 0.05 in.) exist among the predicted rut values using different years of MAF data. To examine if these difference in rut values are significant or not, student's paired t-test (two-sample assuming unequal variances) was conducted. The null hypothesis for this analysis was that the difference in rut values for two years was equal to zero and an alternative hypothesis was that rut values were not equal. A significance level of 0.05 was assumed. A p-value of 0.05 or more indicates acceptance of the null hypothesis. As indicated in

Table 5.4, all the p-values (two-tail) were found to be more than 0.05 ($p > 0.05$), indicating that the differences were not statistically significant.

5.7.2 Different Years of VCD Data

For this exercise, rut values were predicted using Year 1's VCD data first, while keeping the other traffic inputs from Year 1 as well. Then rut was predicted using Year 2, Year 3 and Year 4's VCD data while keeping the other traffic inputs unchanged at Year 1's data. Table 5.5 presents the predicted rut values using different years of VCD data. Minimal differences (0.001 in. to 0.009 in.) were observed among different years of rut values. When rut was compared between two consecutive years, the p-values from Student's t-test were found to be more than 0.05, which indicates that no significance difference exists between the data.

5.7.3 Different Years of ALS Data

When rut was predicted using different years of ALS data, it was found that some differences (0.003 in. to 0.2 in.) exist among the predicted rut values for different years of ALS. However, student's t-test results did not show significant differences between the data.

It is evident from the above exercise that significant differences do not exist between consecutive years of Level 1 input parameters for traffic. Consequently, it can be stated that a longer data collection effort (say ten years) may be needed to better understand the frequency for Level 1 traffic input.

5.8 Summary

Differences between Level 1 and Level 3 MEPFG input parameters and their effects on rut prediction were discussed in this chapter. Sensitivity of different traffic inputs were also discussed in this chapter.

The following conclusions can be drawn from this chapter:

- The MEPDG predicted rut using the default input parameters (Level 3) with nationally calibrated rut model shows very significant differences with the measured rut. The average difference was about 37%. Use of Level 1 input parameters in the rut models improved the accuracy of prediction, and the average error reduced to around 10%. It was also observed that the MEPDG rut prediction was slightly more sensitive towards Level 1 traffic input parameters.
- Significant differences were observed between the Level 1 and Level 3 HDFs. For example, the default HDFs (Level 3) was found to be constant at 2.3 for hours 0 to 5, then increasing sharply to 5 for hours 6 to 9 and then increasing sharply again to 6. Whereas, the HDF obtained from the Level 1 input shows a gradual increase and decrease with time.
- The default MAF value (Level 3) is 1.00, irrespective of the month of a year and the vehicle class, whereas the actual MAF values (Level 1) for Class 9 vehicles varied from 0.57 to 1.18, indicating the importance of developing MAF parameters for Level 1 input.
- Significant differences were observed in the VCD factors between the default and site-specific (i.e., Level 1) values. For example, a difference of about 25% was observed between the default and actual values for Class 9 vehicles.

- Significant differences were observed between default and Level 1 ALS as well. For example, in case of single axles of Class 9 vehicles, Level 1 peak value was found to be approximately 30%, compared to the default value of approximately 18%. In case of tandem axles, the frequency of Level 1 peak values were approximately 9% and 10% compared to the default values of approximately 8% and 6%, respectively.
- Comparative analyses were performed for four years of different traffic inputs. It was observed that although the developed Level 1 HDF, VCD, MAF, and ALS values are very different from the default (Level 3) values, the Level 1 inputs for four consecutive years were not very different from each other.
- A sensitivity analysis was performed to find out the most sensitive traffic input parameter. It was found that the ALS is the most sensitive traffic input, followed by VCD and MAF.
- Although there were numerical differences observed in the developed Level 1 MAF, VCD, and ALS values in different years, the differences were not statistically significant ($p > 0.05$). Therefore, it can be stated that a longer data collection effort (say ten years) may be needed to better understand the required frequency for developing Level 1 traffic inputs for Oklahoma.

Table 5.1: Rut Measurements on the Test Section

Date	Rut (in.)						
	Sta. 144	**Sta. 235**	**Sta. 319**	**Sta. 540**	**Sta. 738**	**Sta. 900**	**Average**
31-May-08	0	0	0	0	0	0	
21-Aug-08	0.2	0.3	*0.4*	0.3	0.300	0.200	**0.283**
3-Dec-08	0.3	0.3	*0.35*	0.2	0.200	0.200	**0.258**
8-Jan-09	0.3	*0.35*	0.25	0.2	0.200	0.200	**0.250**
19-May-09	0.390	*0.444*	0.425	0.363	0.395	0.280	**0.383**
28-Oct-09	0.418	0.468	0.444	0.393	*0.483*	0.310	**0.419**
16-Feb-10	0.419	0.465	0.431	0.381	*0.476*	0.307	**0.413**
10-Mar-10	0.409	0.465	0.429	0.384	*0.483*	0.304	**0.412**
18-May-10	0.427	0.469	0.437	0.388	*0.501*	0.303	**0.421**
10-Aug-10	0.409	0.424	0.509	0.409	*0.612*	0.317	**0.447**
22-Nov-10	0.441	0.439	0.545	0.457	*0.678*	0.359	**0.487**
14-Feb-11	0.440	0.400	0.532	0.435	*0.653*	0.361	**0.470**
7-Jun-11	0.421	0.405	0.538	0.441	*0.663*	0.377	**0.474**
18-Oct-11	0.441	0.485	0.606	0.48	*0.714*	0.435	**0.527**
22-Feb-12	0.476	0.461	0.598	0.47	0.712	0.421	**0.523**
2-May-12	0.479	0.491	0.600	0.456	0.712	0.410	**0.525**
8-Nov-12	0.487	0.471	0.580	0.457	0.767	0.446	**0.535**
11-Apr-13	0.487	0.500	0.639	0.463	0.776	0.442	**0.551**
22-Jul-13	0.501	0.499	0.597	0.473	0.791	0.452	**0.552**
28-Oct-13	0.520	0.512	0.657	0.486	0.803	0.469	**0.575**
26-Mar-14	0.515	0.510	0.648	0.486	0.827	0.472	**0.576**
21-Jul-14	0.544	0.495	0.660	0.525	0.822	0.480	**0.588**

Table 5.2: Comparison of Measured and Predicted Rut using Level 3 Inputs

Date	Measured Average Rut (in.)	MEPDG Predicted Rut (in.)	Difference (%)
Aug, 2008	0.283	0.3809	34.4
Dec, 2008	0.258	0.4142	60.3
Jan, 2009	0.250	0.4161	66.4
May, 2009	0.383	0.4422	15.5
Oct, 2009	0.419	0.5629	34.2
Feb, 2010	0.413	0.5666	37.1
Mar, 2010	0.412	0.5676	37.7
May, 2010	0.421	0.5760	36.9
Aug, 2010	0.447	0.6243	39.8
Nov, 2010	0.487	0.6348	30.5
Feb, 2011	0.470	0.6364	35.4
Jun, 2011	0.474	0.6529	37.7
Oct, 2011	0.527	0.6956	32.0
Feb, 2012	0.523	0.6971	33.3
May, 2012	0.525	0.7037	34.1
Aug, 2012	0.565	0.7406	31.0
Nov, 2012	0.535	0.7470	39.7
Apr, 2013	0.551	0.7495	36.0

Table 5.3: Comparison of Different Levels of Traffic Inputs

Combination #	Combination Type	Difference between Measured and Predicted Rut				
		Average	Minimum	Maximum	SSE	p-value
1	Level 1 ALS, Level 3 MAF & VCD	16%	2%	41%	0.081	< 0.05
2	Level 1 VCD, Level 3 ALS & MAF	24%	6%	52%	0.189	< 0.05
3	Level 1 MAF, Level 3 ALS & VCD	29%	10%	58%	0.284	< 0.05

Table 5.4: Rut Prediction using MAFs from Different Years

Predicted Rut (in.) using MAFs of Different Years				
Date	**Year 1**	**Year 2**	**Year 3**	**Year 4**
Aug, 2008	0.344	0.320	0.341	0.340
Dec, 2008	0.369	0.351	0.367	0.364
Jan, 2009	0.371	0.352	0.368	0.366
May, 2009	0.390	0.375	0.386	0.385
Oct, 2009	0.494	0.468	0.491	0.488
Feb, 2010	0.496	0.471	0.493	0.490
Mar, 2010	0.497	0.472	0.494	0.491
May, 2010	0.504	0.479	0.500	0.497
Aug, 2010	0.549	0.519	0.545	0.542
Nov, 2010	0.557	0.529	0.554	0.550
Feb, 2011	0.558	0.530	0.555	0.551
Jun, 2011	0.571	0.542	0.567	0.564
Oct, 2011	0.610	0.581	0.607	0.603
Feb, 2012	0.611	0.582	0.608	0.604
May, 2012	0.616	0.588	0.612	0.609
Aug, 2012	0.650	0.617	0.647	0.643
Nov, 2012	0.655	0.623	0.652	0.648
Apr, 2013	0.657	0.625	0.654	0.650
p-value (Year 1 & 2)		0.44		
p-value (Year 1 & 3)		0.92		
p-value (Year 1 & 4)		0.85		
p-value (Year 2 & 3)		0.50		
p-value (Year 2 & 4)		0.56		
p-value (Year 3 & 4)		0.93		

Table 5.5: Rut Prediction using VCDs from Different Years

Predicted Rut (in.) using VCDs of Different Years				
Date	**Year 1**	**Year 2**	**Year 3**	**Year 4**
Aug, 2008	0.344	0.344	0.343	0.346
Dec, 2008	0.369	0.369	0.369	0.372
Jan, 2009	0.371	0.370	0.370	0.374
May, 2009	0.390	0.391	0.390	0.395
Oct, 2009	0.494	0.494	0.494	0.499
Feb, 2010	0.496	0.497	0.496	0.501
Mar, 2010	0.497	0.498	0.497	0.502
May, 2010	0.504	0.504	0.503	0.509
Aug, 2010	0.549	0.549	0.548	0.554
Nov, 2010	0.557	0.557	0.556	0.563
Feb, 2011	0.558	0.558	0.557	0.564
Jun, 2011	0.571	0.572	0.570	0.578
Oct, 2011	0.610	0.611	0.609	0.617
Feb, 2012	0.611	0.612	0.610	0.618
May, 2012	0.616	0.617	0.615	0.624
Aug, 2012	0.650	0.651	0.649	0.657
Nov, 2012	0.655	0.656	0.654	0.663
Apr, 2013	0.657	0.658	0.656	0.665
p-value (Year 1 & 2)		0.99		
p-value (Year 1 & 3)		0.99		
p-value (Year 1 & 4)		0.87		
p-value (Year 2 & 3)		0.97		
p-value (Year 2 & 4)		0.88		
p-value (Year 3 & 4)		0.86		

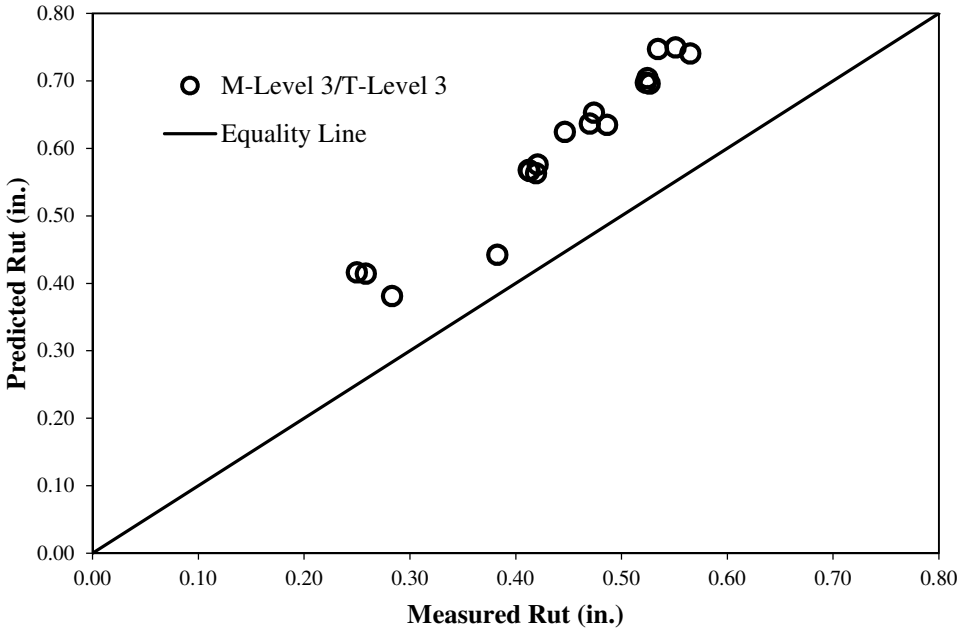

Figure 5.1: Comparison of Measured and Predicted Rut for Level 3 Input Parameters
(M = Material, T = Traffic)

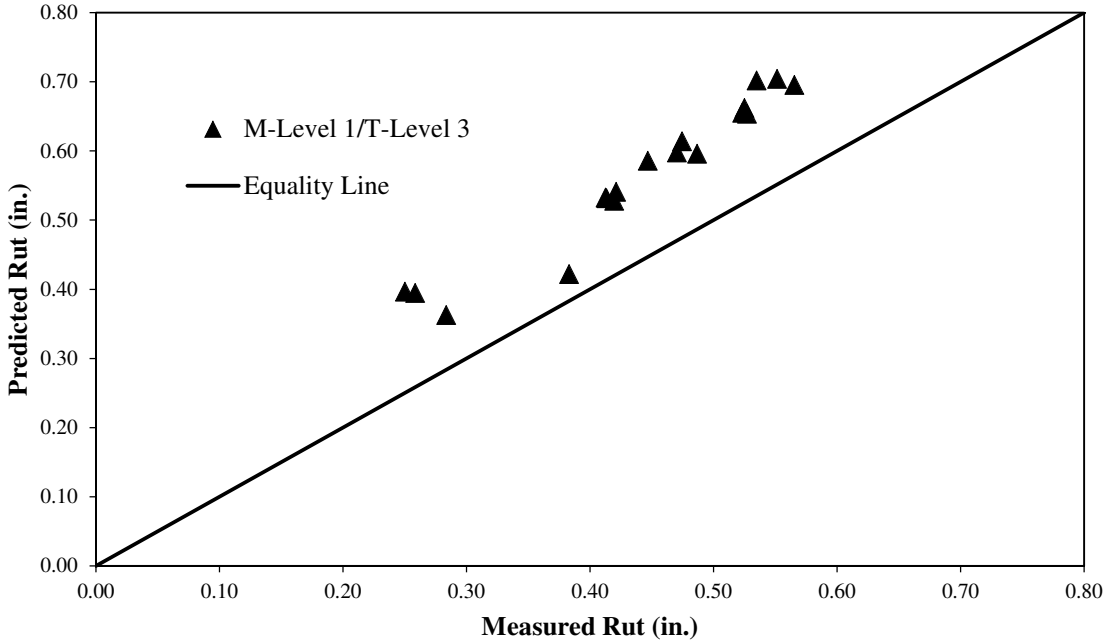

Figure 5.2: Comparison of Measured and Predicted Rut for Level 1 Material and Level 3 Traffic Input Parameters (M = Material, T = Traffic)

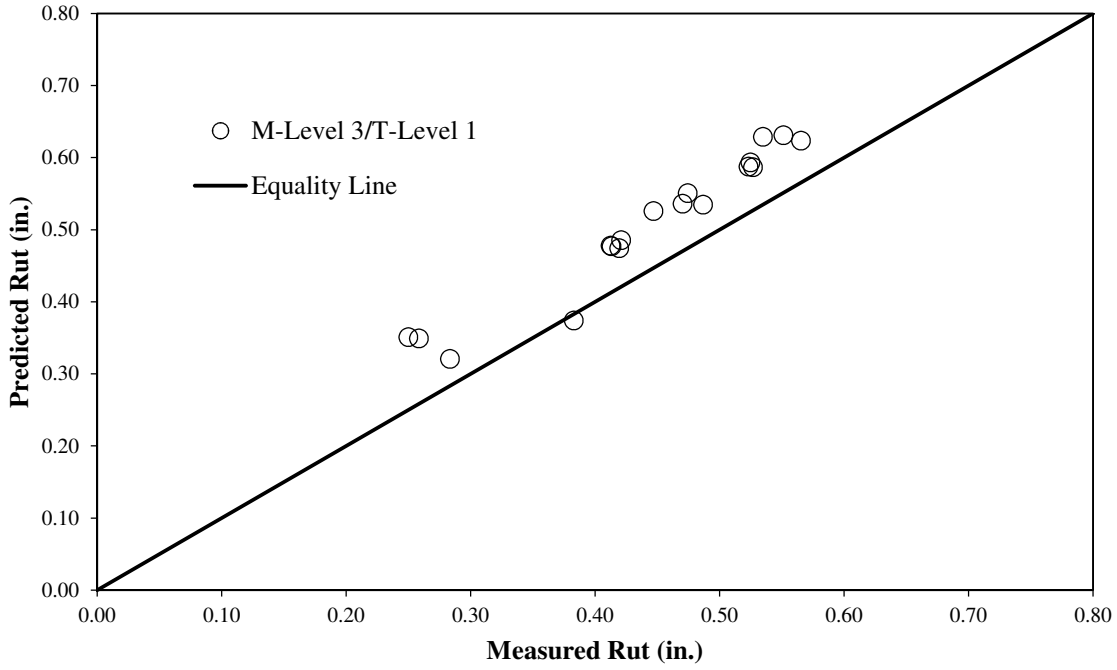

Figure 5.3: Comparison of Measured and Predicted Rut for Level 3 Material and Level 1 Traffic Input Parameters (M = Material, T = Traffic)

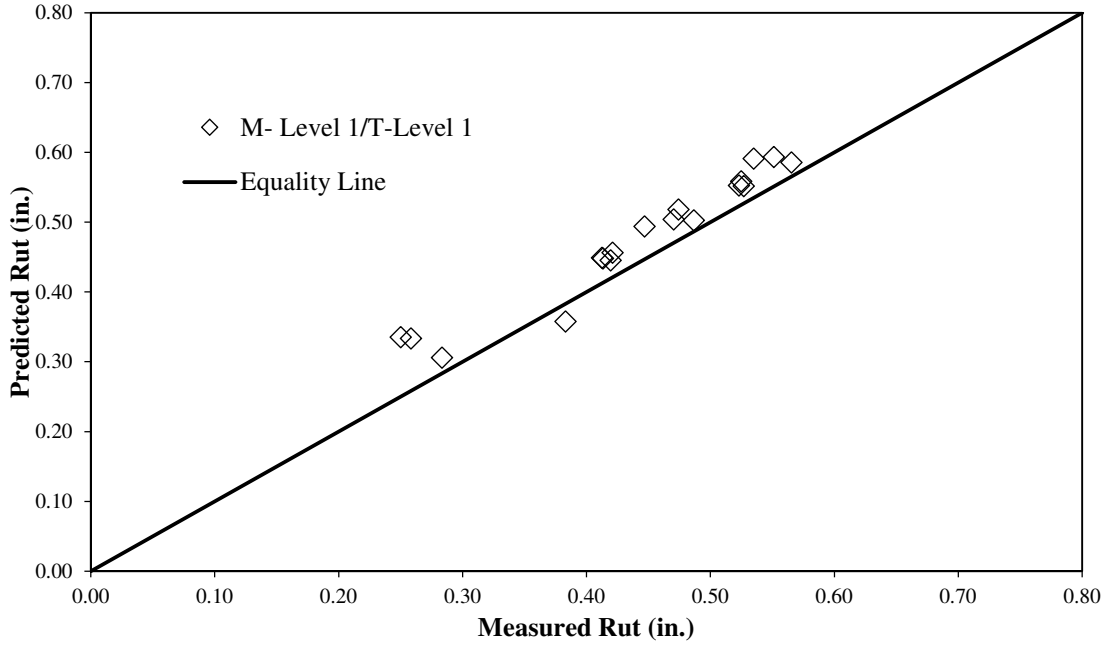

Figure 5.4: Comparison of Measured and Predicted Rut for Level 1 Material and Level 1 Traffic Input Parameters (M = Material, T = Traffic)

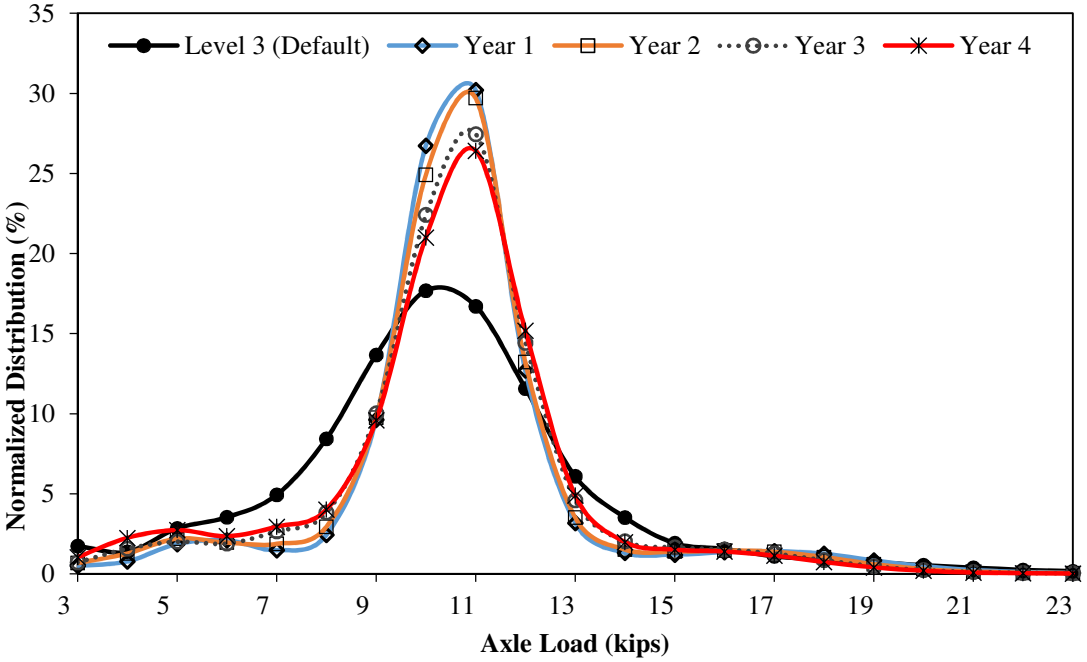

Figure 5.5: Comparison of Level 3 and Level 1 Axle Load Spectra (For Class 9 Single Axle)

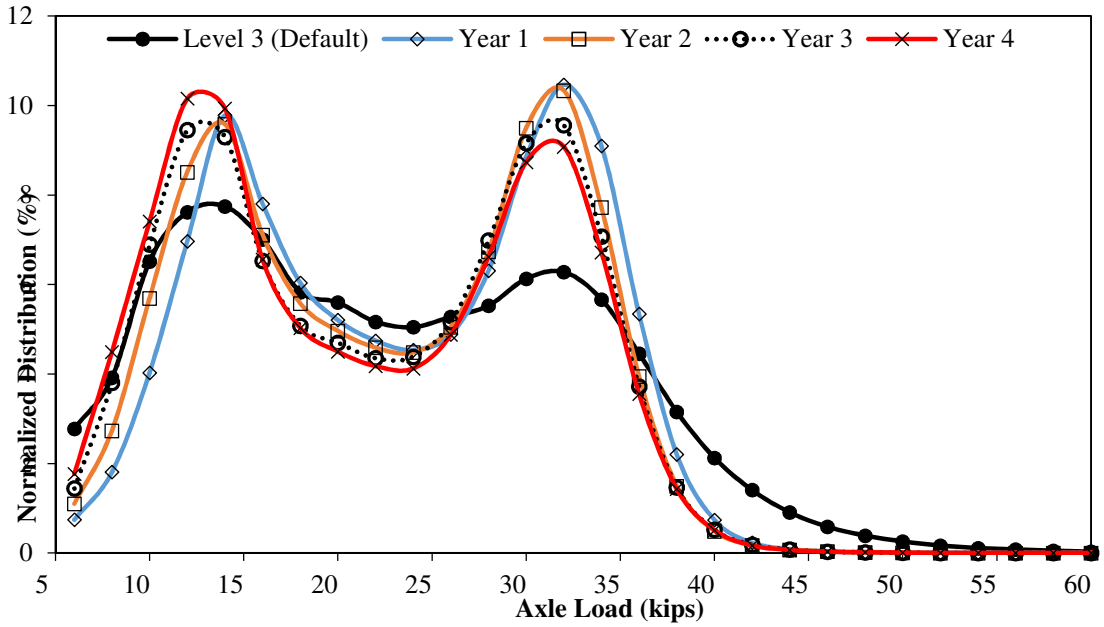

Figure 5.6: Comparison of Level 3 and Level 1 Axle Load Spectra (For Class 9 Tandem Axles)

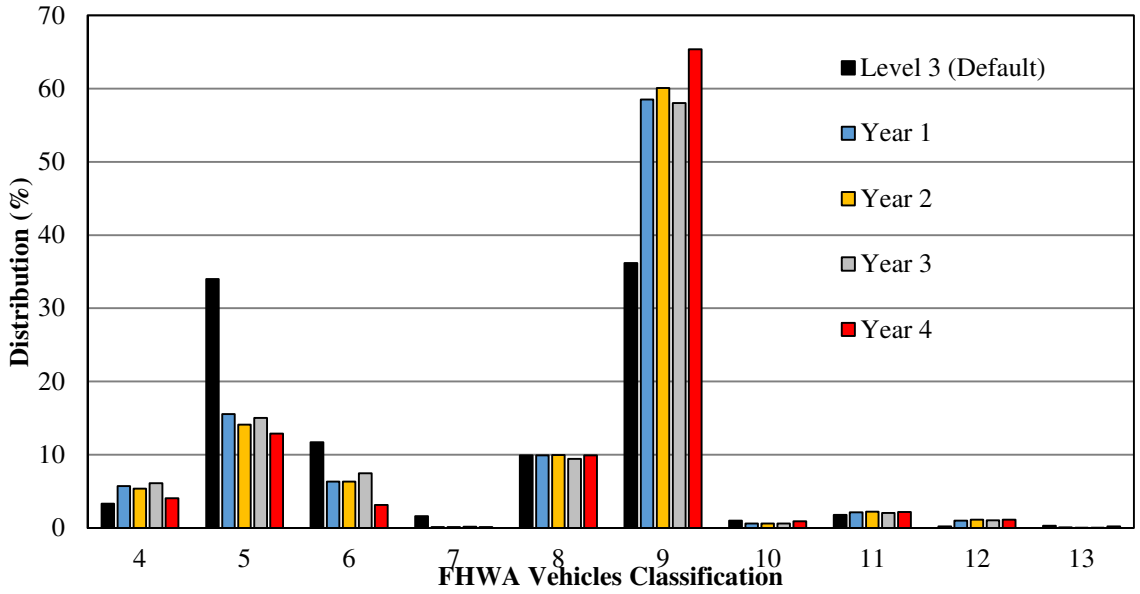

Figure 5.7: Comparison of Level 3 and Level 1 Vehicle Class Distribution Factors

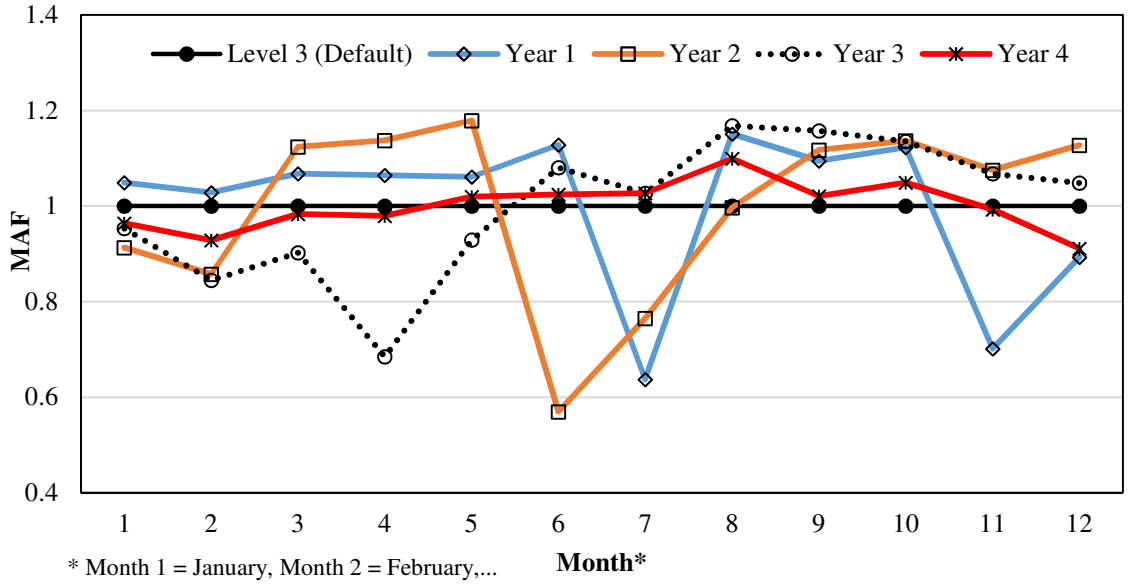

Figure 5.8: Comparison of Level 3 and Level 1 Monthly Adjustment Factors (for Class 9 Vehicles)

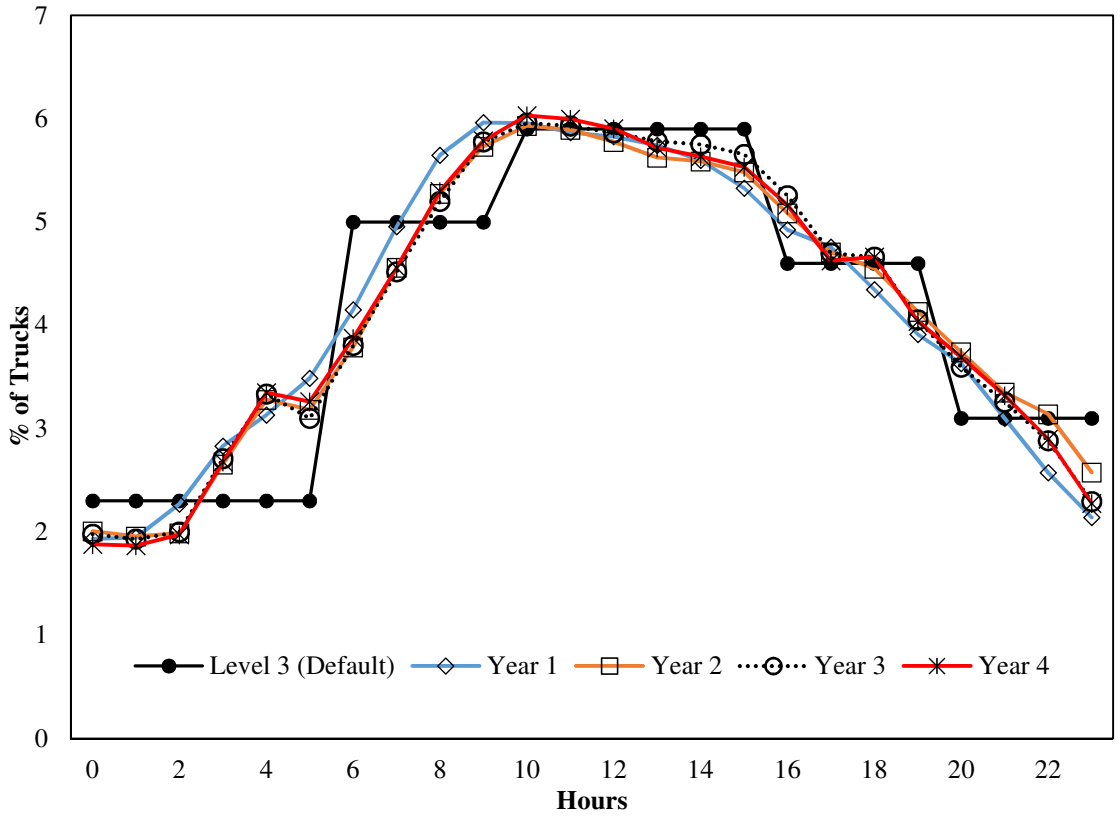

Figure 5.9: Comparison of Level 3 and Level 1 Hourly Distribution Factors

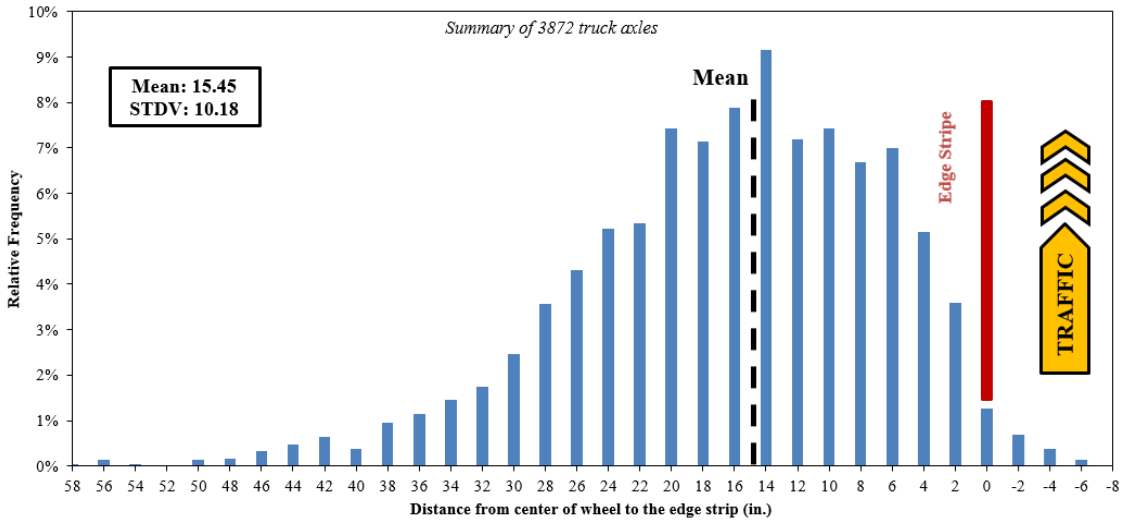

Figure 5.10: Statistical Distributions of Lateral Traffic Wander Data (Solanki et al., 2013)

CHAPTER

6

Local Calibration of MEPDG Rut Models

6.1 Introduction

As discussed in Chapter 5, developing Level 1 input parameters for both materials and traffic improved the prediction of rut using the MEPDG significantly. For example, the average error in prediction was reduced from 37% to 10% when Level 1 inputs were used instead of Level 3. However, differences between the measured and predicted rut still existed. Therefore, efforts were made in this study to calibrate the (nationally calibrated) MEPDG rut models for local conditions in Oklahoma. This chapter provides a brief discussion of the MEPDG rut models, need for the local calibration of these models, nationwide local calibration efforts and a methodology for local calibration of the rut models for Oklahoma.

6.2 Rut Models in the MEPDG

The MEPDG uses an incremental damage concept to predict total rut depth in a pavement structure. The total rut depth is calculated as the summation of rut depths accumulated in all unbound (loose) and bound (asphalt and/or cement/asphalt-treated base) layers. Equation 6.1 is used in the MEPDG to calculate total rut depth (RD):

$$RD = \sum_{i=1}^{n} \varepsilon_{p,i} h_i \quad (6.1)$$

where:

n = Total number of sublayers,

i = Sublayer number,

$\varepsilon_{p,i}$ = Plastic strain in sublayer i, and

h_i = Thickness of sublayer i.

Equation 6.2 is used in the MEPDG to determine permanent deformations (rut) in asphalt layers:

$$\frac{\varepsilon_p}{\varepsilon_r} = K_z \beta_{r1} 10^{k_{r1}} T^{\beta_{r2} k_{r2}} N^{\beta_{r3} k_{r3}} \quad (6.2)$$

where:

ε_p = Plastic strain (in./in.),

ε_r = Resilient strain (in./in.),

T = Temperature of layer at middepth (°F),

N = Number of load repetitions,

$\beta_{r1}, \beta_{r2}, \beta_{r3}$ = Local calibration coefficients,

k_{r1}, k_{r2}, k_{r3} = National coefficients (k_{r1} = -3.35412, k_{r2} = 1.5606, k_{r3} = 0.4791), and

K_z = Depth confinement factor that adjusts the permanent strain for the confining pressure.

Likewise, Equation 6.3 is used to estimate rut contributed by unbound base and subgrade layers:

$$\delta_a = \beta_{s1} k_1 \varepsilon_v h \left(\frac{\varepsilon_0}{\varepsilon_r}\right) \left| e^{-\left[\frac{\rho}{N}\right]^{\beta}} \right| \quad (6.3)$$

where:

δ_a = Permanent deformation for the layer,

ε_v = Average vertical strain (in./in.),

h = Thickness of the layer,

ε_0,β, ρ = Material properties, and

β_{s1} = Calibration coefficient to optimize for both base and subgrade layers.

Therefore, the total rut of a pavement section can be estimated by adding the contribution of rut occurring in each layer:

$$RD = h_{AC}\varepsilon_r K_z \beta_{r1} 10^{k_{r1}} T^{\beta_{r2}k_{r2}} N^{\beta_{r3}k_{r3}} + \beta_{GB}k_{GB}\varepsilon_v h_{GB}\left(\frac{\varepsilon_0}{\varepsilon_r}\right)\left|e^{-\left[\frac{\rho}{N}\right]^{\beta}}\right| + \beta_{SG}k_{SG}\varepsilon_v h_{SG}\left(\frac{\varepsilon_0}{\varepsilon_r}\right)\left|e^{-\left[\frac{\rho}{N}\right]^{\beta}}\right| \quad (6.4)$$

where:

h_{AC} = Thickness of asphalt layer,

h_{GB} = Thickness of granular base layer, and

h_{SG} = Thickness of subgrade layer.

From Equation 6.4 it is evident that there are five coefficients (β_{r1}, β_{r2} and β_{r3} for the asphalt layer, β_{GB} for the granular base layer, and β_{SG} for the subgrade layer) for local calibration of the rut models.

6.3 Need for Calibration of the Rut Models in the MEPDG

Local calibration is an important step for the implementation of the MEPDG for pavement design (FHWA, 2010, AASHTO, 2004). The purpose of local calibration is to address the differences in construction and maintenance practices, traffic and environmental conditions, maintenance policies, and material specifications across the United States (Mehta et al., 2008; Hoegh et al., 2010). Although, ODOT can use the performance models with nationally calibrated "default" coefficients, the outcome may

not reflect actual field measurements. A higher level of precision and economically optimum outcomes can be achieved by local calibration of rut model coefficients to represent the local conditions (traffic, materials and environment) prevalent in Oklahoma. In the present study, the rut models in the MEPDG were calibrated using data from the Interstate-35 test section. The calibrated model can be assumed to represent the local conditions of Oklahoma.

6.4 Local Calibration Efforts in the Unites States

A number of states (Colorado, New Mexico, Arkansas, Texas, North Carolina, Minnesota, and Washington) have conducted research on the local calibration of the MEPDG rut models. Two different approaches have been used: (1) calibration using the total rut, (2) calibration using the layer-wise rut. Tarefder and Rodriguez-Ruiz. (2013), Hall et al. (2011), Banerjee et al. (2009) adopted the total rut approach whereas, Bhattacharya et al. (2015), Hoegh et al. (2010), Muthadi et al. (2008), and Li et al. (2009) used the layer-wise rut approach for the local calibration.

Bhattacharya et al. (2015) used a total of 93 new and rehabilitated flexible pavement sections from the LTPP and Colorado Department of Transportation's (CDOT) pavement management database. Since, Level 1 data for materials and traffic were not available, they used Level 3 data to calibrate the rut models in the MEPDG. They used the trenching data from different sections for layer-wise calibration of the MEPDG rut models. The goodness of fit (R^2), standard deviation and p-values were used to quantify the differences between the measured and predicted ruts in the calibration process. Final calibration coefficients for rutting in Colorado were reported as: β_{r1} = 4.3, β_{r2} = 1, β_{r3} = 1, β_{GB}= 0.22, and β_{SG}= 0.37.

Tarefder and Rodriguez-Ruiz (2013) used the Level 3 database from New Mexico for both traffic and materials to calibrate the rut prediction models. They calibrated the rut models using 13 Hot Mix Asphalt (HMA) pavement sections from different regions in New Mexico. Since rut data for each individual layer was not available, total rut approach was used to calibrate the rutting models using iterative process. They optimized the coefficients β_{r2} and β_{r3} in the first set of iterations. This was done by varying and permuting the two nonlinear calibration coefficients (β_{r2} and β_{r3}) while the other three coefficients β_{r1},β_{GB}, and β_{SG} were set to a default value of 1.0. Once the corresponding sum of squared errors (SSE) and mean residual error (MRE) were minimized between the measured and predicted rut, the β_{r2} and β_{r3} values were fixed to certain values. In the second series of iterative runs, the values of β_{r1},β_{GB}, and β_{SG} were varied and permuted and the final set of calibration coefficients were obtained for New Mexico.

Hall et al. (2011) performed the local calibration using data obtained from 26 flexible pavement sections across five different regions in Arkansas. They used default (Level 3) inputs in most cases because of lack of site-specific (Level 1) data. Hall et al. (2011) recommended that additional sites be established and a more robust data collection procedure be implemented for future calibration efforts. Iterative runs of the MEPDG were performed with different combinations of coefficients to optimize the rutting model. Hall (2011) hypothesized that rutting mainly occurs in the HMA layers and subgrade and hence assumed that the national rutting models for granular base can be directly used for Arkansas; therefore, the default coefficient for rutting in the granular base was not adjusted. Only $\beta_{r1}$and β_{r3} values for HMA layers and β_{SG} for subgrade layers were

calibrated for Arkansas. Final calibration coefficients for rutting in Arkansas were reported as: β_{r1} = 1.2, β_{r2} = 1, β_{r3} = 0.8, β_{GB}= 1, and β_{SG}= 0.5.

Hoegh et al. (2010) calibrated the MEPDG rutting prediction model by using the Level 2 and Level 3 data because of the lack of Level 1 data. They used data from 12 hot mix asphalt (HMA) pavement sections from the full-scale pavement research facility MnROAD in Minnesota. Rutting was measured manually by MnROAD staff three times per year using the straightedge method. Trenches were cut at the selected sections to study the level of rutting occurring in individual layers of the pavement. Therefore, a layer-wise approach was used for calibration. It was observed that most of the rutting occurred in the HMA while the granular base and the subgrade remained unaffected. Hoegh et al. (2010) observed that the MEPDG predicts accurately the rutting due to the HMA, but the overestimates the base and subgrade ruts. Therefore, they recommended that the associated coefficients be modified.

Banerjee et al. (2009) focused their study to develop Level 2 and Level 3 calibration factors of the MEPDG rut models for five different regions in Texas. Banerjee used a total of 18 LTPP test sections for this exercise. For this calibration, β_{r2} was kept constant under the assumption that the temperature dependency of the specific material should be determined in the laboratory for a given mix. Since no specific mix was available for this study, the default (Level 3) was assumed to be correct. After reviewing the calibration procedure of the MEPDG when performed at the national scale, Banerjee et al. (2009) decided that a range of $\beta_{r1}$and β_{r3} be chosen for local calibration. At the end, a set of calibration factors for Texas was recommended. These experiments were

representative of five regions with different environmental conditions: wet-warm, wet-cold, dry-warm, dry-cold and mixed.

Li et al. (2009) performed calibration of the MEPDG rut models using data obtained from the Washington State Pavement Management System (WSPMS). The split-sample and the jackknife testing approaches were combined in the calibration process. Trenches in WSDOT routes have shown that very limited rutting occurs in the subgrade. Therefore, the corresponding calibration coefficients were set to 0. Only β_{r1}, β_{r2} and β_{r3} values for the asphalt layer were calibrated using the layer-wise approach. Their results showed that the calibration factors β_{r2} and β_{r3} were more importatnt than β_{r1}.

Muthadi and Kim (2008) calibrated the MEPDG rut models for local materials, conditions and practices used in the flexible pavements of North Carolina. A total of 53 pavement sections were selected and a layer-wise approach was used for calibration. Because trenches and cores from these pavements were unavailable, predictions rather than actual measurements were used to distribute the total rut depth measurements to each pavement layer. The total measured rut depth was distributed to each pavement layer on the basis of the ratio of the predicted total rut depth to the predicted permanent deformation in each layer. Using Microsoft Excel solver program, β_{r1}, β_{GB} and β_{SG} (the global calibration coefficients for asphalt layers and local calibration coefficient for subgrade layer) were reported for North Carolina.

6.5 Methodology for Local Calibration

In the present study, both the total rut and layer-wise rut were used to calibrate the MEPDG rut models. In this chapter, the local calibration using total rut approach is discussed. The layer-wise calibration approach will be discussed in Chapter 7.

The local calibration was done by comparing the measured rut with the MEPDG predicted rut over time. These analyses were first done for the default (Level 3) calibration parameters and then adjusted so as to reduce difference between the observed and the predicted rut values progressively (Hossain et al., 2016). The best fit minimizes the difference between the observed and the MEPDG predictions.

In this study, β_{r2} was kept constant at 1, as observed in similar studies conducted by Banerjee et al. (2009) and Hall et al. (2011). The range of β_{r1} and β_{r3} was selected based on the recommendations by Muthdai and Kim (2008), Banerjee et al. (2009), Hall et al. (2011) and Tarefder and Rodriguez-Ruiz (2013). The calibration coefficient β_{r1} is a shift factor that modifies the intercept term of the permanent deformation model. This factor primarily captures differences in the distress predictions caused by the varying thicknesses of the HMA layers and other initial conditions. β_{r3} captures the differences resulting from the number of load repetitions; thus, it represents the rate or progression of permanent deformation. From the literature review of the calibration coefficients of granular base (β_{GB}) and natural subgrade (β_{SG}), it was decided that the value for β_{GB} and β_{SG} will be assumed as 1 and 0.5, respectively, for this study. The calibration coefficients β_{GB} and β_{SG} capture the deviation in predictions from the observed distresses that may arise from differences in the material properties.

Trial runs were performed with multiple combinations of calibration coefficients. The model output and best fit were estimated as Sum of Squared Errors (SSE), which represents the squared sum of the differences between the observed and the predicted rut values. In the iterative process, one calibration coefficient was varied at a time while others were kept constant. The goal was to reduce the SSE and increase the goodness of fit (R^2 values) between the measured and predicted rut.

6.6 Results and Discussion

From the literature review, it was found that the values of the calibration coefficients for asphalt β_{r1}, β_{r2}, and β_{r3} varied from 1 to 4.3, from 1 to 1.1, and from 0.8 to 1.1, respectively. Similarly, the literature review showed that the values for aggregate base and subgrade calibration coefficients β_{GB} and β_{SG} varied from 0.22 to 1, and 0 to 1.2, respectively. Therefore, these values were used to start the calibration process in this study. Multiple runs were performed until the SSE values between the measured and predicted ruts were minimized and R^2 values optimized.

Table 6.1 lists a total of 14 trials runs with respective SSE, average error between the measured and predicted rut, and R^2 values. It can be observed that trial run No. 14 produced the least SSE and the second best R^2 values. The final calibration coefficients that produced the least SSE were: β_{r1} = 2, β_{r2} = 1, β_{r3} = 0.93, β_{GB} = 1 and β_{SG} = 0.5. In the national calibration, at default (Level 3) value of 1.00 is set for for each of these coefficients. The calibration coefficients, obtained through the local calibration effort in this study, were thus different than the Level 3 (default) values. Figure 6.1 shows a visual comparison between rut predicted using the calibrated models and the measured rut from the test section. It can be seen that the differences between the MEPDG predicted rut and

measured rut have reduced considerably as the points are closer to the equality line. For example, when Level 3 coefficients were used, the average error in rut prediction, SSE and R^2 values were found to be 10%, 0.032, and 0.89, respectively. After the local calibration exercise, the average error in rut prediction, SSE and R^2 values were found to be less than 5%, 0.010, and 0.95, respectively. Student's t-test was performed on the measured and predicted rut values with these calibration coefficients and the p-value was found to be 0.71, which is greater than 0.05. It means there was no statistically significant difference between the measured and predicted rut values. The average error between the measured and predicted rut after the calibration was less than 5%, which indicates the goodness of prediction.

In this calibration exercise, it was found that the rut predictions were very sensitive to β_{r3} and not as sensitive to β_{r1}. For example, from Trial #2, Trial #3 and Trial #7, it was observed that that changing β_{r3} values from 0.75 to 1.2 changed the predictions significantly with the average error increasing from 13% to 145%. Figures 6.2, 6.3, and 6.4 show a graphical comparison of these three trials and the changes in the prediction trend line from right of the equality line to the left of it. On the contrary, a comparison of Trial #2, Trial #8, and Trial #13 shows that changing the β_{r1} values from 1 to 2 also changed the predictions with the average error increasing from 5% to 41%, which is much lower than the corresponding change for the case of β_{r3}. Figures 6.2, 6.5 and 6.6 show a graphical comparison of these three trials. These results are reasonable because β_{r3} relates to the number of wheel passes and this happens to be a much bigger number than $K_z 10^{k_{r1}}$ (responsible for the initial prediction of the permanent deformation), which is

accounted through β_{r1} (Equation 6.2). Similar observations were reported in some of the previous studies (Tarefder and Rodriguez-Ruiz, 2013 and Banerjee et al., 2009).

6.7 Summary

The following conclusions can be drawn from this chapter:

- The calibration of MEPDG rutting models improved the rutting prediction significantly. Using the Level 1 traffic and material input, the average error between the measured and predicted rut reduced to approximately 5%.
- Statistical analyses performed on the calibrated models revealed no significant differences (p-value > 0) between the measured and predicted rut. For examples, when Student's t-test was performed between the measured and predicted rut, the p-value was found to be 0.71, which is greater than 0.05. This indicates a need of local calibration of rut models in Oklahoma.
- The sensitivity of different calibration factors was studied and it was found that the most sensitive calibration coefficient was β_{r3} followed by β_{r1}.

Table 6.1: SSE and R^2 of the Rutting Model for Different Calibration Coefficients

Trial	β_{r1}	β_{r2}	β_{r3}	β_{GB}	β_{SG}	SSE	Average Error	R^2
1	1	1	1	1	1	0.032	10 %	0.89
2	1	1	1	1	0.5	0.864	13 %	0.94
3	1	1	0.75	1	0.5	1.249	56 %	0.44
4	1	1	0.9	1	0.5	0.614	39 %	0.85
5	1	1	0.95	1	0.5	0.325	28 %	0.91
6	1	1	1.1	1	0.5	0.650	39 %	0.92
7	1	1	1.2	1	0.5	8.702	145 %	0.88
8	2	1	1	1	0.5	0.646	41 %	0.94
9	2	1	0.75	1	0.5	0.852	46 %	0.69
10	2	1	0.95	1	0.5	0.044	11 %	0.94
11	2	1	0.9	1	0.5	0.070	13 %	0.92
12	1.5	1	0.95	1	0.5	0.045	11 %	0.93
13	1.8	1	0.95	1	0.05	0.011	5 %	0.94
14	2	1	0.93	1	0.5	0.010	<5 %	0.95

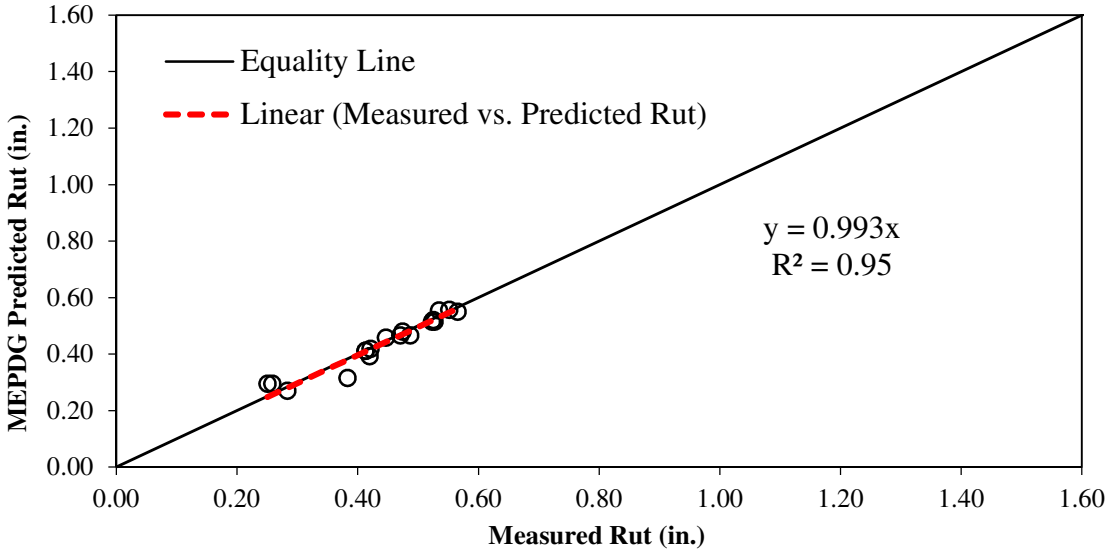

Figure 6.1: Comparison of Measured and Predicted Rutting after Calibration (Trial#14)

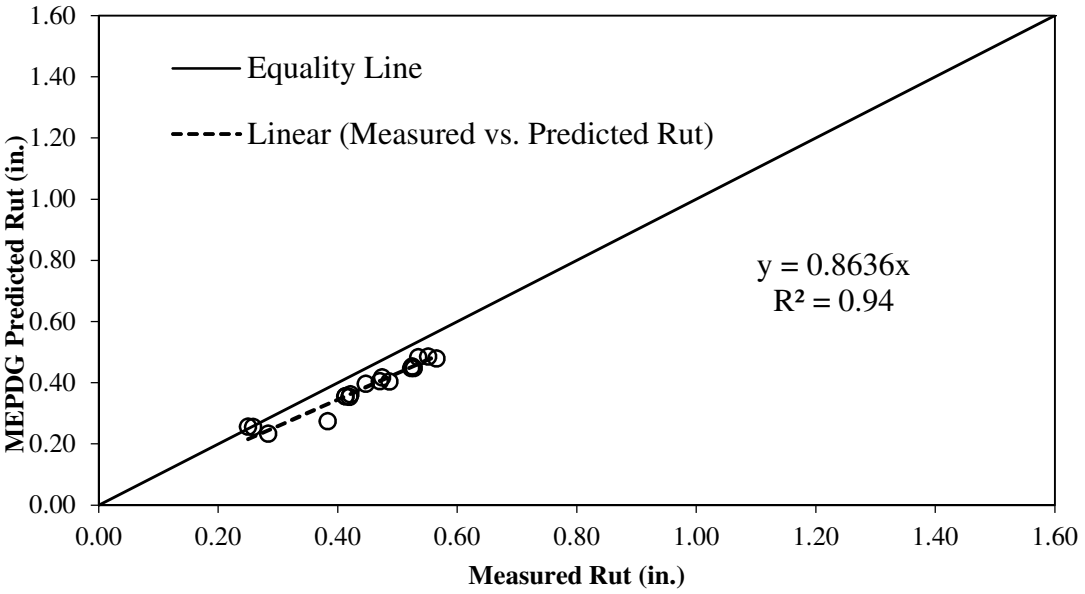

Figure 6.2: Comparison of Measured and Predicted Rutting after Calibration (Trial#2)

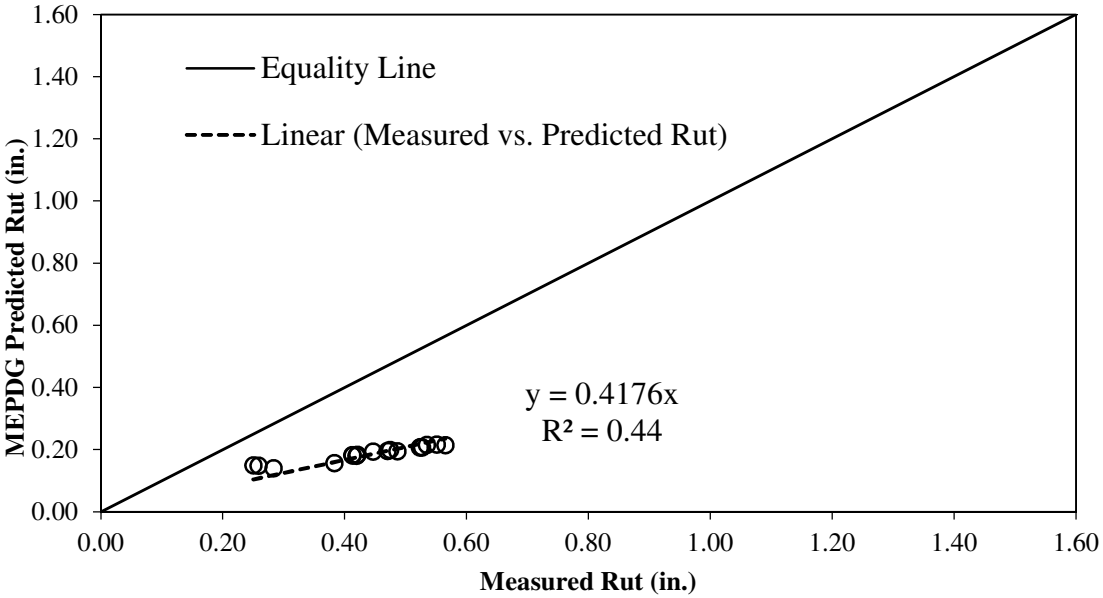

Figure 6.3: Comparison of Measured and Predicted Rutting after Calibration (Trial#3)

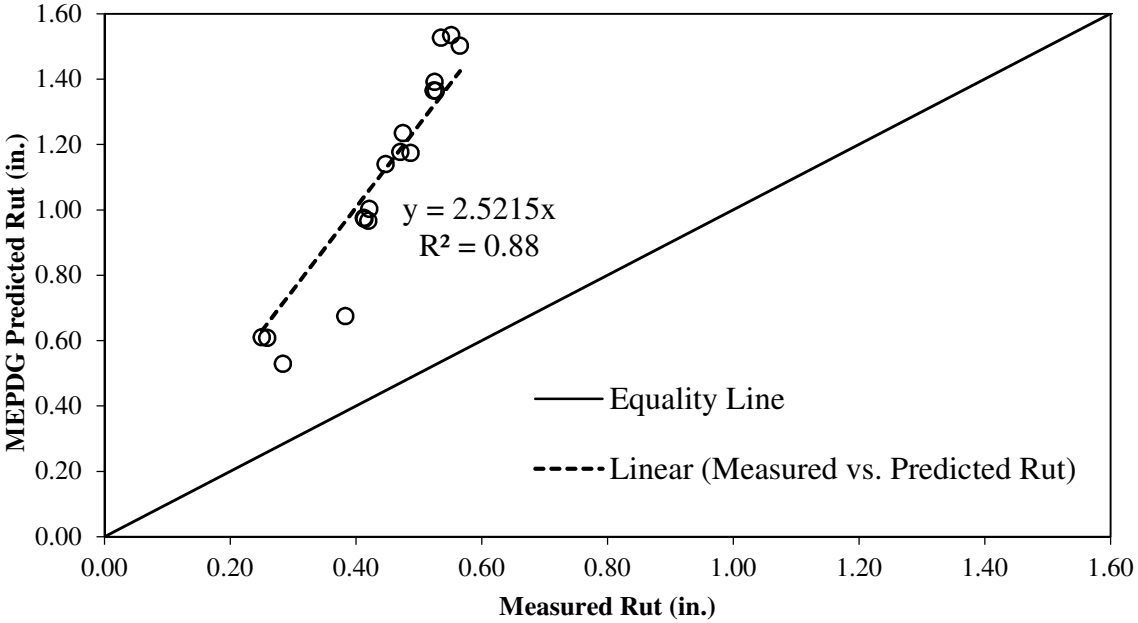

Figure 6.4: Comparison of Measured and Predicted Rutting after Calibration (Trial#7)

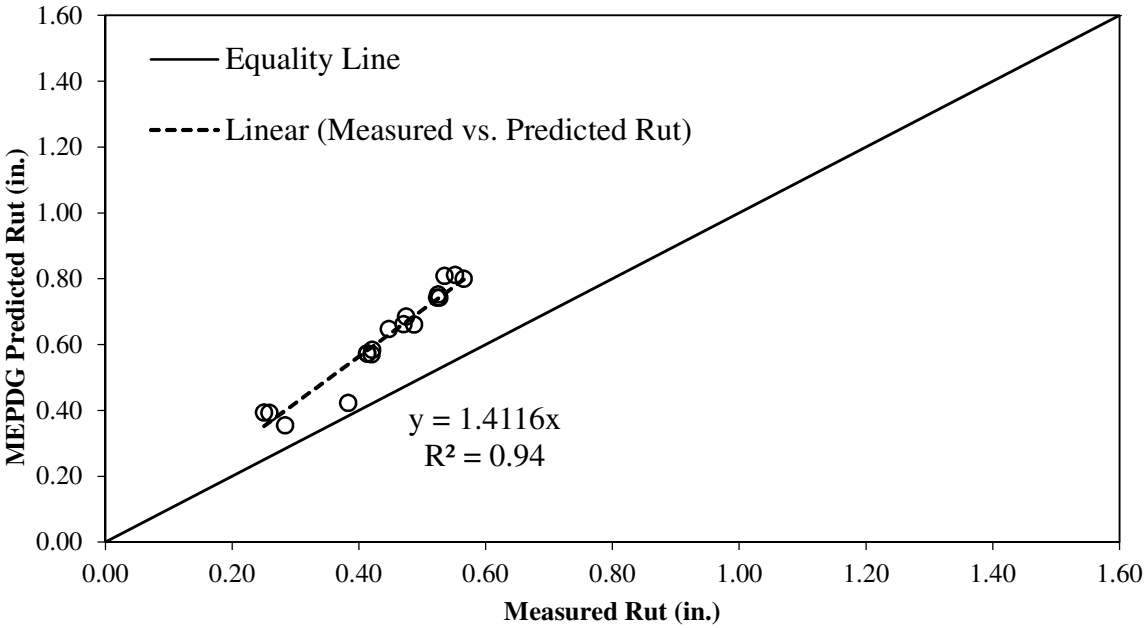

Figure 6.5: Comparison of Measured and Predicted Rutting after Calibration (Trial#8)

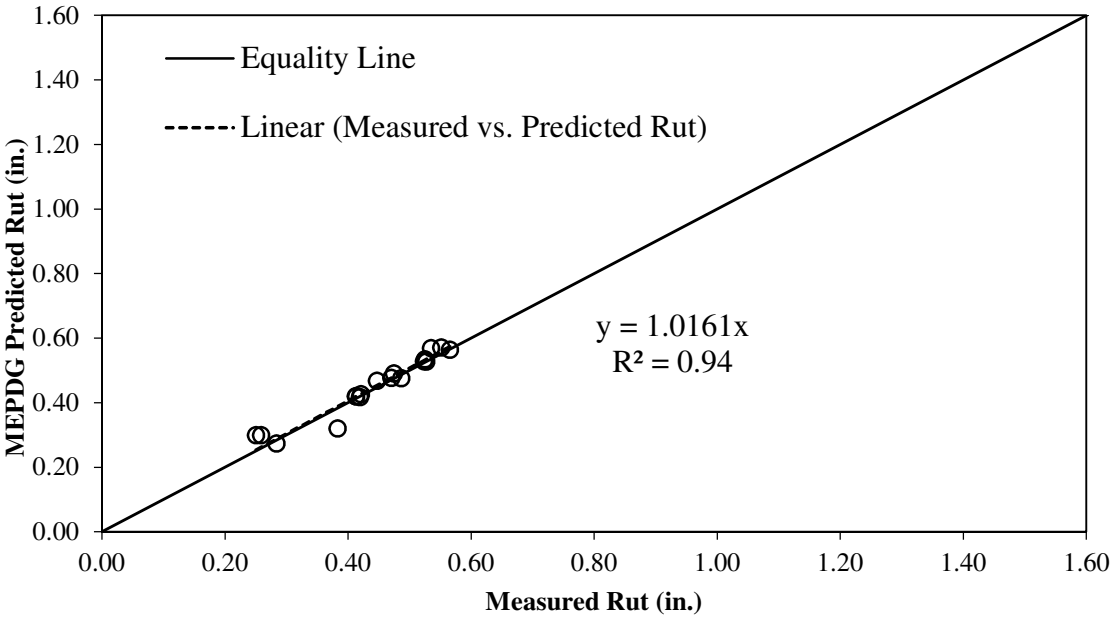

Figure 6.6: Comparison of Measured and Predicted Rutting after Calibration (Trial#13)

CHAPTER

7

Contribution of Different Structural Layers to Rutting

7.1 Introduction

Rutting and fatigue cracking are two major distresses in flexible pavements. The materials and structural strength of different layers play a vital role in minimizing pavement distresses. Permanent deformations of hot mix asphalt (HMA), aggregate and subgrade layers are primary contributors to rutting in flexible pavements. In order to achieve improved design and selection of material, it is important to understand the role of each pavement layer to rutting. Additionally, the Mechanistic Empirical Pavement Design Guide (MEPDG) depends on the contribution of each layer to estimate calibration factors associated with the distress models pertaining to rutting. Each layer has separate rutting calibration factors, which may or may not require calibration for a specific region or state (AASHTO, 2010). To accurately determine the calibration factors, one needs to have adequate knowledge of the contributing structural layers to pavement rutting. A forensic investigation can be extremely helpful in this regard.

This chapter provides an overview of the pavement profiles and their comparisons with a major previous study, "National Cooperative Highway Research Program Report 468" (NCHRP, 2002). This chapter also includes forensic investigation on the test section and local calibration of the MEPDG rut models based on the data obtained from the forensic study.

7.2 Contribution of Structural Layers to Rutting: NCHRP Report 468

Forensic investigations through trenching are generally undertaken to examine the contribution of individual pavement layers to rutting. National Cooperative Highway Research Program (NCHRP) Report 468 (NCHRP, 2002) and National Center for Asphalt Technology (NCAT) Report 12-07 (Timm et al., 2012) are two important reference on this topic. Among these two reference, the NCHRP report covers a more comprehensive study that was undertaken to investigate the contribution of different pavement layers to rutting. States including Alabama, Minnesota, Mississippi, Nevada, North Carolina, Ohio and Texas were used to collect data from different test sections and in-service pavements to examine the contribution of individual structural layers to rutting. The study was focused on investigating the contribution of individual layers to rutting by monitoring and comparing the surface profile of the rutted pavements. The NCHRP study referenced the hypothesis of Simpson et al. (1995) which states that the area under the transverse surface profile could be used to predict the source of rutting from within the pavement structure. According to Simpson et al. (1995), the transverse surface profiles of rutted pavements can be classified under four general categories: subgrade rutting, base rutting, surface course rutting, and heave. Figure 7.1 (after NCHRP, 2002) shows the shape of the transverse surface profile for each category. The algebraic area between the transverse profile and the straight line connecting its end points can be used to determine which of the four categories fits a particular transverse profile. Area above the straight line connecting the profile end points was considered as positive, whereas the area below the line was considered as negative. From Figure 7.1, it can be observed that sections inside the subgrade category is entirely negative and sections inside the heave category is entirely positive. The NCHRP study attempted to

recognize base and surface rutting that included both positive and negative areas by utilizing a general perception that barely positive areas will be considered as surface rutting, while marginally negative areas will be considered as base rutting.

The transverse profile in Figure 7.1, however, may vary for a pavement with a stabilized layer or a HMA layer containing reclaimed asphalt pavement (RAP) similar to that used on the test section. In the present study, the contribution of different layers including stabilized soil and HMA layer(s) containing RAP was investigated. Surface transverse profiles were measured at approximately 100 to 150 ft. intervals (at Stations 144, 235, 319, 540, 738, and 900) to understand the contributions of different layers based on the aforementioned criteria (NCHRP, 2002). In addition, coring was performed on the test section to examine the depth and evidence of fatigue cracking. Trenching was performed to measure and quantify the contribution of each pavement layer to rutting and to compare the rut profiles with those in the NCHRP Report 468. The MEPDG rut models were then calibrated based on the observed rutting in each layer and the overall total rutting measured on the surface of the test section.

7.3 Comparison of Pavement Profile with the NCHRP Study

The overall shape of the pavement surface profile observed after rutting was very similar to the shape of the rutted profiles in the NCHRP Report 468. Figures 7.2, 7.3, and 7.4 show the surface profile of the test section for Stations 738, 900 and 235, respectively. Surface profiles at Stations 319 and 540 matched with the profiles from Stations 738 and 900, whereas the surface profile of Station 144 matched with the profile of Station 235.

Out of six stations, Station 738 experienced the highest rut, Station 900 experienced the lowest rut whereas Station 235 experienced somewhat average rut. If these three surface profiles are compared with the surface profiles in Figure 7.1, it can be observed that the surface profiles for Stations 738 and 900 are in agreement with the Type (c) failure mode, where the HMA layer was the only contributor to rutting. The surface profile obtained from Station 235 can be considered as a combination of Type (b) and Type (c) modes where the HMA layer and base layer are primary contributors to rutting (Figure 7.1).

Therefore, the initial hypothesis (prior to trenching) in this study was that the major contributor to rutting may be the HMA and/or aggregate base layers. Also, the test section had a stabilized subgrade layer above the natural subgrade to minimize the contribution of subgrade layer to rutting. To verify these initial hypotheses, a forensic investigation was performed. The forensic investigation was also expected to provide an insight of the effectiveness of using a stabilized subgrade layer or using RAP in HMA layers in controlling rutting.

7.4 Forensic Investigation of the Test Section

Based on the distress surveys performed over approximately six years (from 2008 through 2014), it was found that the section had undergone significant rutting (up to approximately 0.9 in.). However, very minimal cracking was observed (approximately 1% area). To analyze the contributing layers for rutting and cracking, a forensic study was performed on October 7, 2014, after approximately six years in service.

7.4.1 Extraction of Pavement Cores from the Cracked Locations

As previously mentioned, pavement cracks were mainly observed at the section approximately 4 ft. from the beginning of the section to approximately 132 ft. into test section. Pavement cores were obtained from some of the cracked locations to study the depth and source of cracking. First, cracked locations were marked with paint. Then a total of four 6 in. diameter cores were obtained from the cracked locations using diamond core barrel. Figures 7.5 (a) and (b) shows the plan and profile of the cores obtained from approximately 41 ft. from the starting point of the test section. It is seen that the cracks were only at the surface; no evidences of cracks below the pavement surface were seen (i.e., not a top-down or bottom-up crack). Therefore, it was concluded that the observed cracks may be either low temperature cracks or very premature top-down cracks.

7.4.2 Trenching for Rutting Measurements

To further investigate the nature and extent of rutting and to examine the contribution of different structural layers to total rut, trenches were cut at three selected locations (Stations 235, 738 and 900). As discussed previously, Station 738 had the highest rut, while Station 900 exhibited the lowest rut. Rut depths observed at Station 235 were average.

The trenching operations for the project were performed on October 7, 2014. The following steps briefly describe the trenching activities:

a) The trench locations were first marked on the test section (Figure 7.6). The research team originally discussed the possibility of trenching the entire width of the lane. However, as the test section is located on the right lane of the two-lane Interstate-35 with a very high traffic volume, trenching of the entire lane width

was not considered safe. Therefore, it was decided to trench half of the lane, starting from the shoulder to capture the contribution of the outside wheel path to rutting. As the rut depths were similar in the inside and outside wheel paths, trenching to examine rutting of the outside wheel path was considered reasonable.

b) Approximately 10 ft. by 3 ft. trenches were cut using a wet-saw cutting machine (Figure 7.7) at the selected stations. Depths of the trenches were approximately 3 ft. to 3½ ft. The pavement layers were removed from the trenches using a Caterpiller® 22 in. wide backhoe and a jackhammer (Figure 7.8).

c) After the pavement layers had been removed, the trench edges and faces were cleaned using a garden hose. The Face Dipstick® with 12 in. moonfoot spacing was then used to measure the surface profile on each side of the trench (Figure 7.9) and an average surface profile for each trench was determined. The locations of the moonfoots were marked on the pavement.

d) Depths of each construction lift in the pavement layers were visually marked on each face of the trench (Figure 7.10). Then, depths of each pavement layer (including each construction lift), from the respective surface, were measured using a carpenter square and a level (Figure 7.11). The depths were measured at the marked moonfoot spacing locations. Measurements were taken at eight locations in each trench.

e) The measured depths of the layers in the two faces of the trench were then averaged and reported as a single depth at each point. It was decided to measure the rut profile by construction lift thicknesses. Therefore, for each trench measurements were taken for one S4 layer, two S3 layers, and one aggregate base

layer. Figures 7.12, 7.13, and 7.14 show the rut profile of each layer at stations 738, 900, and 235, respectively.

7.5 Contribution of Different Layers to Rutting

Figures 7.12, 7.13, and 7.14 show a total of four pavement layers in each trench location. The topmost line at each profile represents the pavement surface, the line beneath it represents the bottom of S4 HMA layer, the line underneath represents the bottom of the first lift of S3 HMA layer, the line beneath it represents the bottom of the second lift of S3 layers, and the lowermost line represents the bottom of aggregate base layer. It can be observed that the wheel path falls between 2 and 4 feet far from the rut measurement starting point on the shoulder.

Figures 7.12, 7.13, and 7.14 show that almost all of the rutting was confined to only the surface layer, which is the S4 layer. Although, some movements were observed in the subsequent S3 and aggregate base layers, they did not align with the wheel path, as it did for the top S4 layer. As the movements in the S3 and aggregate base layers did not follow a consistent pattern like the S4 layer and because the movements were insignificant, it can be stated that the movements in the S3 and aggregate base layers were construction anomalies as one can expect in any construction.

Additionally, the test section includes a stabilized subgrade layer above the natural subgrade layer to minimize the contribution of subgrade layer to rutting. It appears that the stabilized subgrade acted as a firm support for the pavement and did not let the rut propagate beyond the asphalt layer. This is a significant observation for pavements with stabilized subgrade layers in Oklahoma. The trenching operations on

this test section justifies the inclusion of a stabilized subgrade layer for minimizations of rutting.

Moreover, very minimal ruts were observed in the S3 layers, which consisted of approximately 25% RAP. Presence of RAP has been found to increase stiffness of a mix and reduce rutting (Singh et al., 2016). Based on the aforementioned observations, it was concluded that the rut in the test section was contributed primarily by the top HMA layer (S4 layer).

7.6 Local Calibration of The MEPDG Rutting Models using Trenching Data

It was observed from the trenching operations that the rut was contained only in the HMA layers. Since contributions of the aggregate base and subgrade layers to rutting were found to be negligible, it was decided to re-calibrate the rut model coefficients (the calibration factors reported in Chapter 6) using the layer-wise approach. For this calibration effort, the factors for the aggregate base layer (β_{GB}) and the subgrade layers (β_{SG}) was assigned a minimal value (β_{GB}=0.05 and β_{SG}=0.05).

Trial runs were performed with multiple combinations of calibration coefficients. The model output and best fit were estimated as Sum of Squared Errors (SSE), which represent the squared sum of differences between the observed and the predicted rut values. It was an iterative process where one calibration coefficient from asphalt layers (β_{r1}, β_{r2}, β_{r3}) was varied at a time while the others were kept constant. The goal was to reduce the SSE and increase the goodness of fit (R^2 values) between the measured and predicted rut.

Table 7.1 lists a total of 15 trials runs with respective SSE, average error between the measured and predicted rut, and R^2 values. It can be observed that trial run No. 12

produced the least SSE and the second best R^2 values. The final calibration coefficients (using layer wise approach) that produced the least SSE were: β_{r1} = 1.25, β_{r2} = 1, β_{r3} = 1.05, β_{GB} = 0.05 and β_{SG} = 0.05. Figure 7.15 shows a visual comparison between predicted rut using the calibrated models and the measured rut from the test section (Trial No. 12). Student's t-test was performed between the measured and predicted rut using the final calibration coefficients. The p-value was found to be 0.83, which is greater than 0.05. It means that there is no significant difference between the measured and predicted rut values. The average error between the measured and predicted rut after the calibration was less than 5%, which indicates the goodness of prediction.

As noted before, two differenty approaches were used to perform the local calibration of the MEDG rut models in this study: 1) total rut approach, and 2) layer-wise rut approach. The total rut approach was utilised prior to the availability of the trenching data. The forensic study enabled using the layer-wise approach for rut calibration. Table 7.2 provides a side by side comparison of the calibration factors obtained uisng these two approaches.

7.7 Summary

The following conclusions can be drawn from this chapter:

- The Interstate-35 test section had undergone moderate to severe rutting and very minimal cracking in its service life of approximately six years. The rutted profiles of different stations on the test section were compared with the profiles reported in the NCHRP Report No. 468.
- When the rutting profiles were compared with the NCHRP profiles, in general, a close match was observed where the HMA layers are the major contributor

for rutting. Only one rutting profile at Station 235 showed a combination of HMA layer and base layer rutting according to NCHRP study. However, from the trenching data at three different locations confirmed that the HMA layer was the predominant contributor of almost all the rutting at the test section.

- It was concluded from the forensic study that that the stabilized subgrade layer and the HMA layer with RAP (S-3 layer) were effective in containing rutting to within the top HMA layer.
- Local calibration was performed for the MEPDG rutting models using the data from the forensic study. The final calibration factors were β_{r1} = 1.25, β_{r2} = 1, β_{r3} = 1.05, β_{GB} = 0.05 and β_{SG} = 0.05. It was observed that the stabilized subgrade layer acted as a firm support for the pavement and did not let the rut propagate beyond the asphalt layers. Therefore, it is expected that designing a similar pavement in Oklahoma may not need local calibration for the aggregate base and subgrade layers.

Table 7.1: SSE and R^2 of the Rutting Model for Different Calibration Coefficients

Trial	β_{r1}	β_{r2}	β_{r3}	β_{GB}	β_{SG}	SSE	Average Error	R^2
1	1	1	1	0.05	0.05	0.658	75 %	0.80
2	1.5	1	1.05	0.05	0.05	0.168	16 %	0.90
3	1.3	1	1.05	0.05	0.05	0.033	8 %	0.90
4	2	1	1.05	0.05	0.05	1.279	34 %	0.89
5	1.35	1	1	0.05	0.05	0.214	34 %	0.91
6	1	1.2	1	0.05	0.05	6.138	55 %	0.90
7	1.35	1	1.05	0.05	0.05	0.051	9 %	0.90
8	1.35	0.95	1.1	0.05	0.05	0.054	9 %	0.88
9	1.4	0.9	1.1	0.05	0.05	0.193	33 %	0.89
10	0.9	1	1.05	0.05	0.05	0.296	43 %	0.90
11	1.3	1	1	0.05	0.05	0.262	39 %	0.91
12	1.25	1	1.05	0.05	0.05	0.027	5 %	0.94
13	1.3	1	1.07	0.05	0.05	0.164	16 %	0.89
14	1.4	1	1.06	0.05	0.05	0.170	15 %	0.90
15	1.4	1	1.05	0.05	0.05	0.079	12 %	0.90

Table 7.2: Comparison of Rut Models Calibration Factors

MEPDG Rut Models Calibration Factors for Oklahoma			
Total Rut Approach		Layer-wise Rut Approach	
β_{r1}	2	β_{r1}	1.25
β_{r2}	1	β_{r2}	1
β_{r3}	0.93	β_{r3}	1.05
β_{GB}	1	β_{GB}	0.05
β_{SG}	0.5	β_{SG}	0.05

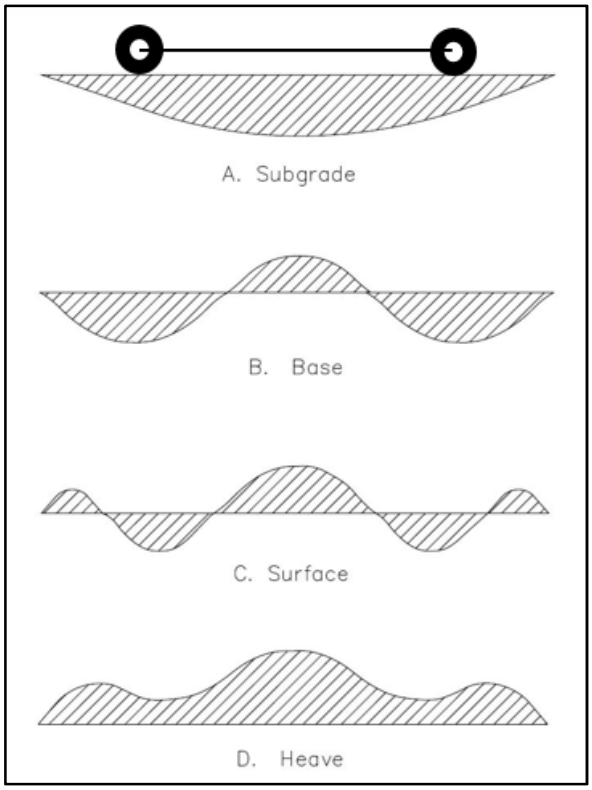

Figure 7.1: Rutting Failure Mode Observed from Transverse Surface Profile (Modified After (NCHRP, 2002)

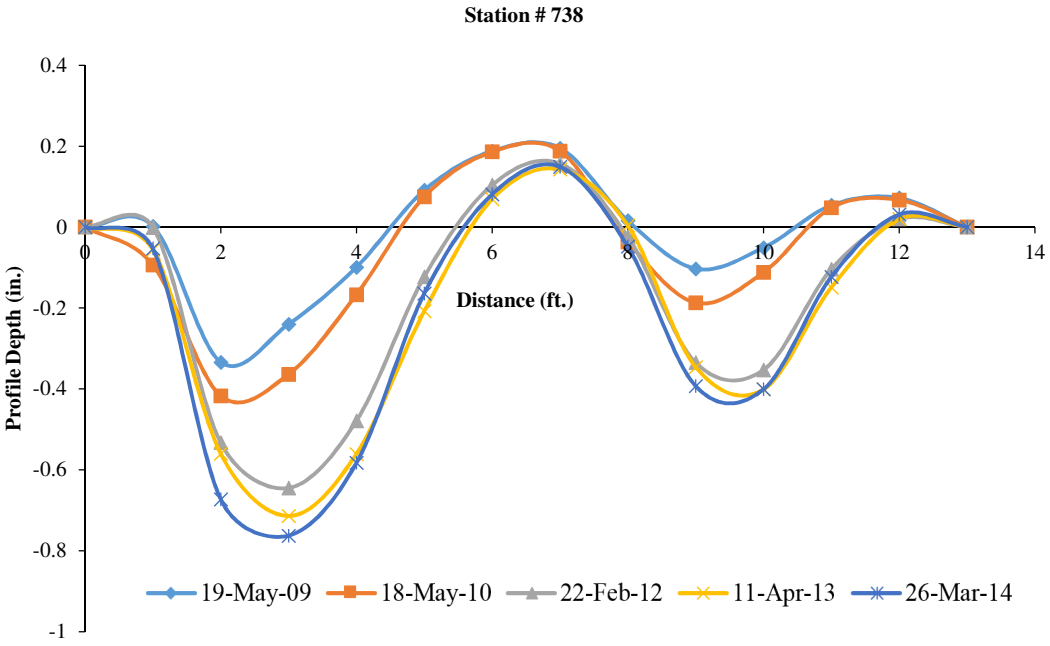

Figure 7.2: Pavement Surface Profiles at Station 738

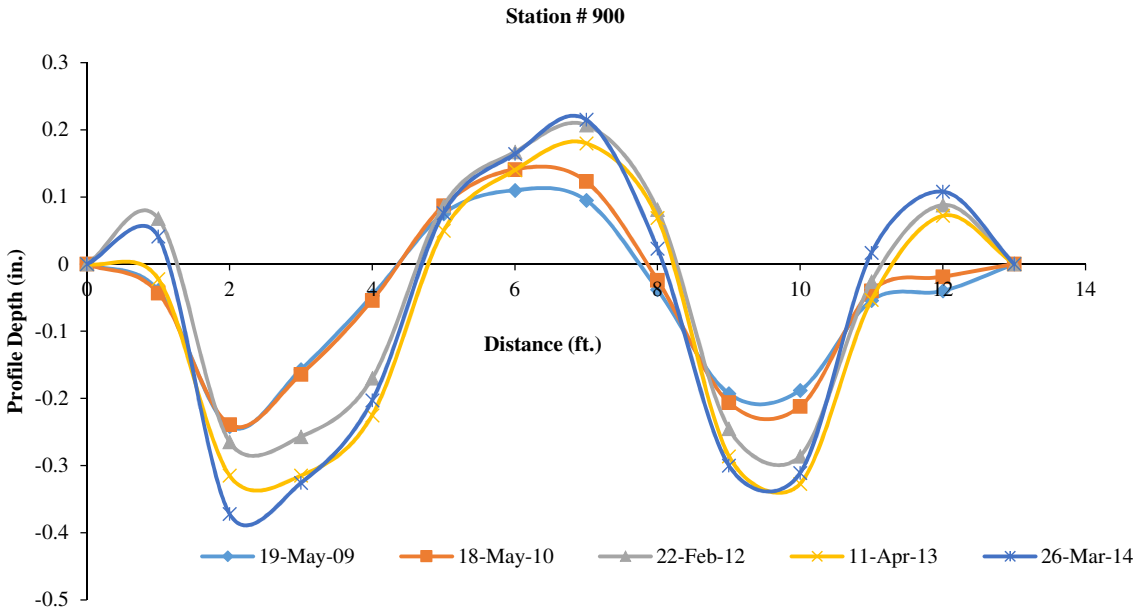

Figure 7.3: Pavement Surface Profiles at Station 900

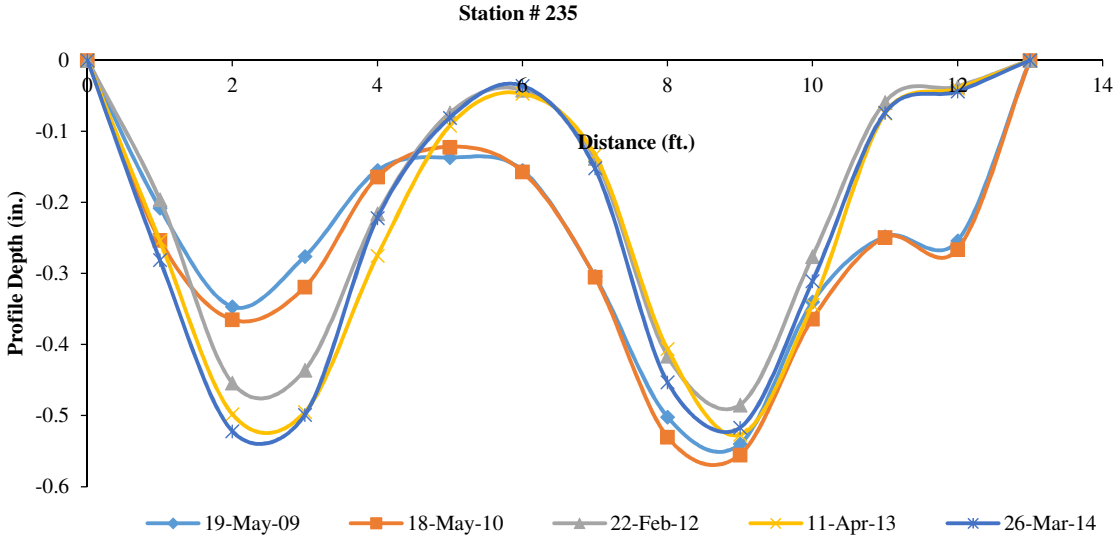

Figure 7.4: Pavement Surface Profiles at Station 235

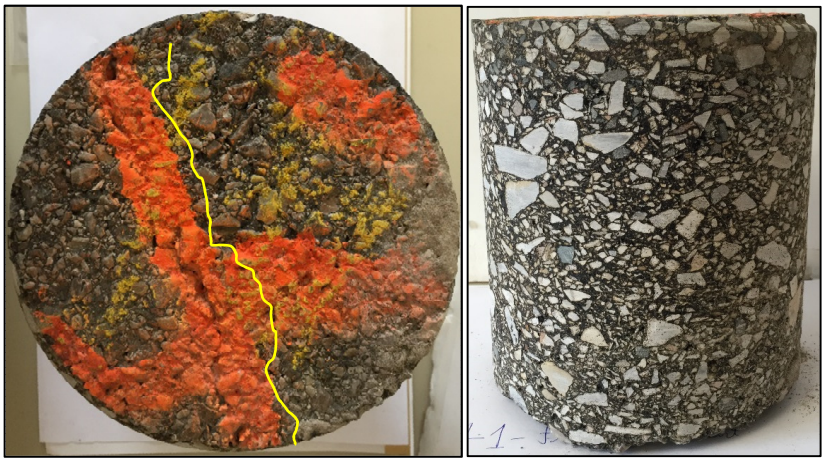

(a) (b)

Figure 7.5: Pavement Core Extracted 41 ft. from Starting Point (a) Plan View (b) Profile View

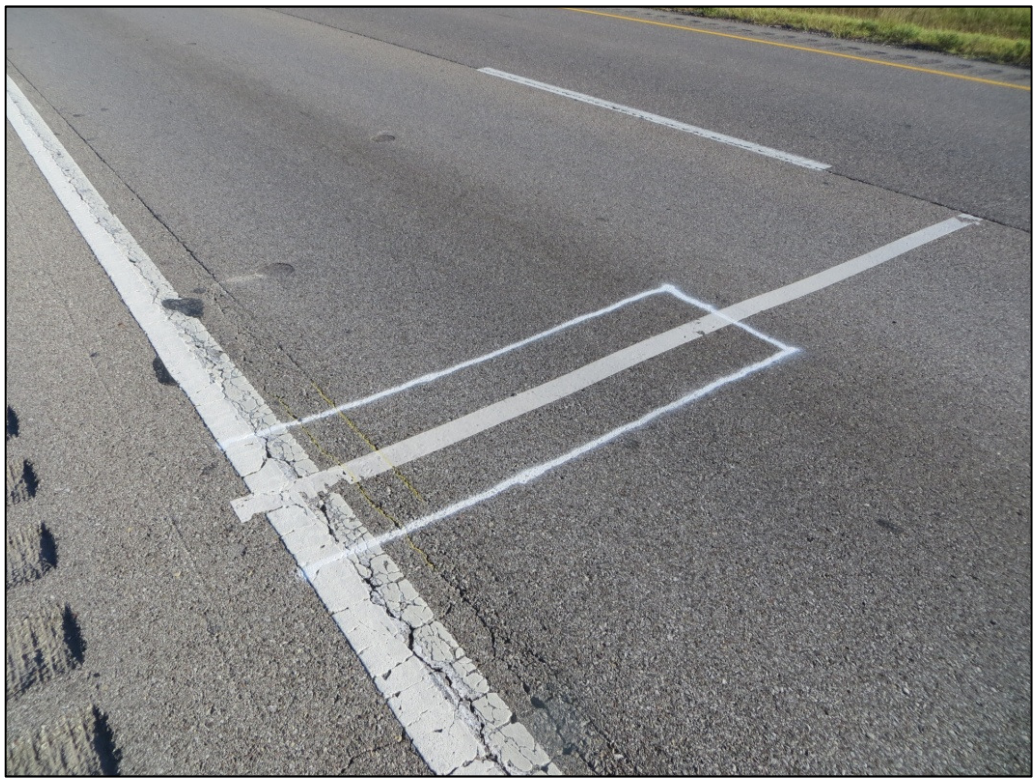

Figure 7.6: Marking on the Test Section before Trenching Operations

Figure 7.7: Cutting of Trench using Saw-cutting Machine

Figure 7.8: Removal of Pavement Materials using Back-Hoe

Figure 7.9: Rut Measurements using Face Dipstick®

Figure 7.10: Marking of Different Pavement Layers

Figure 7.11: Depth Measurements of Different Layers

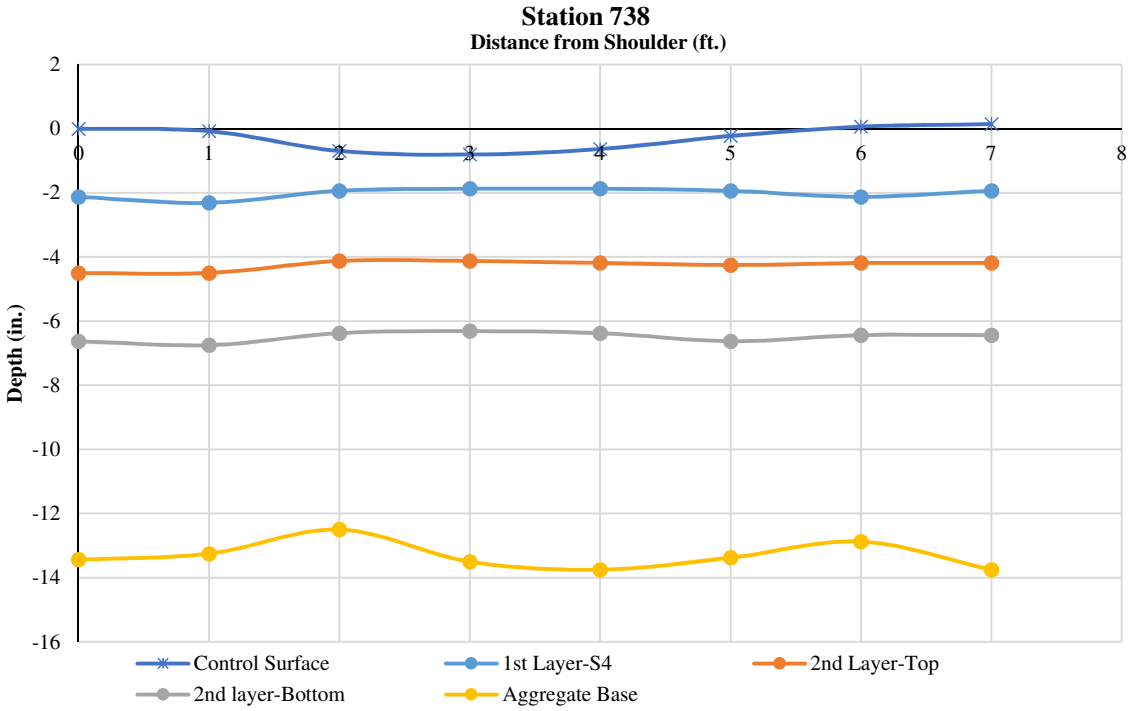

Figure 7.12: Average Profile of Pavement Layers after Trenching at Station 738

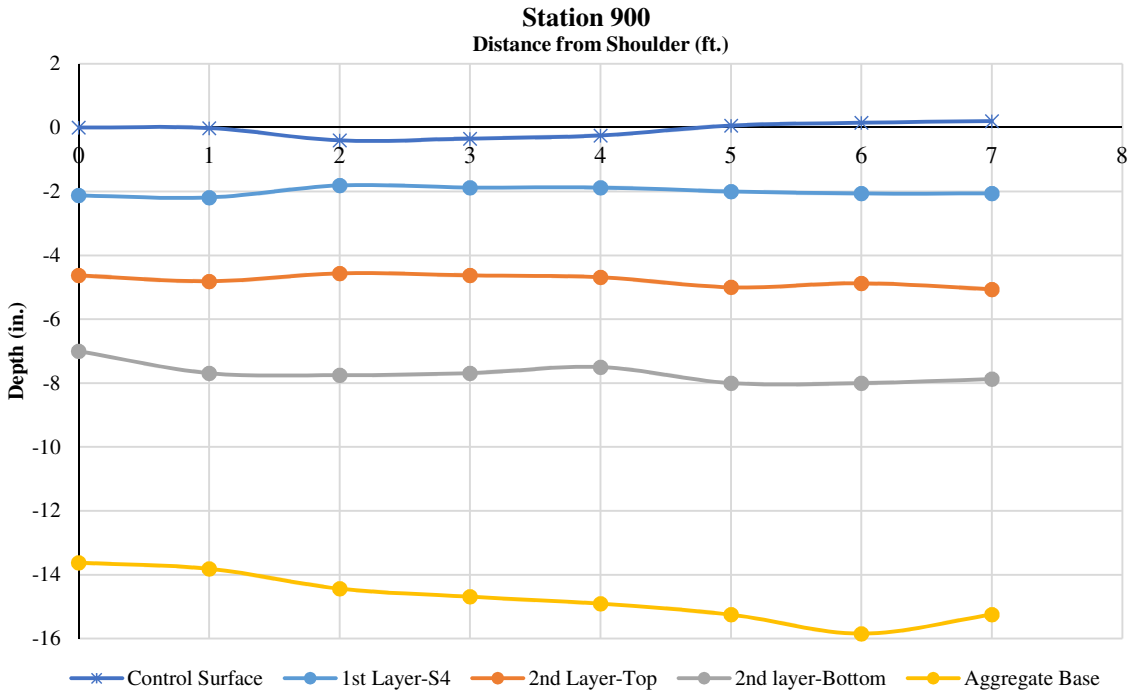

Figure 7.13: Average Profile of Pavement Layers after Trenching at Station 900

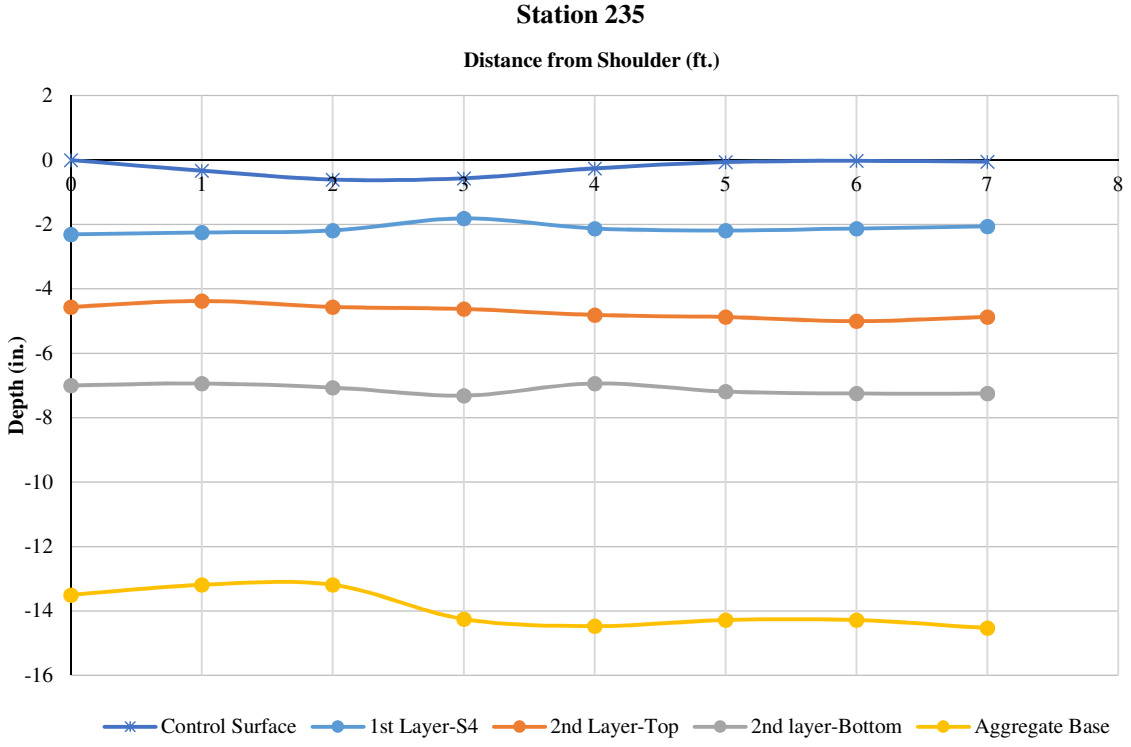

Figure 7.14: Average Profile of Pavement Layers after Trenching at Station 235

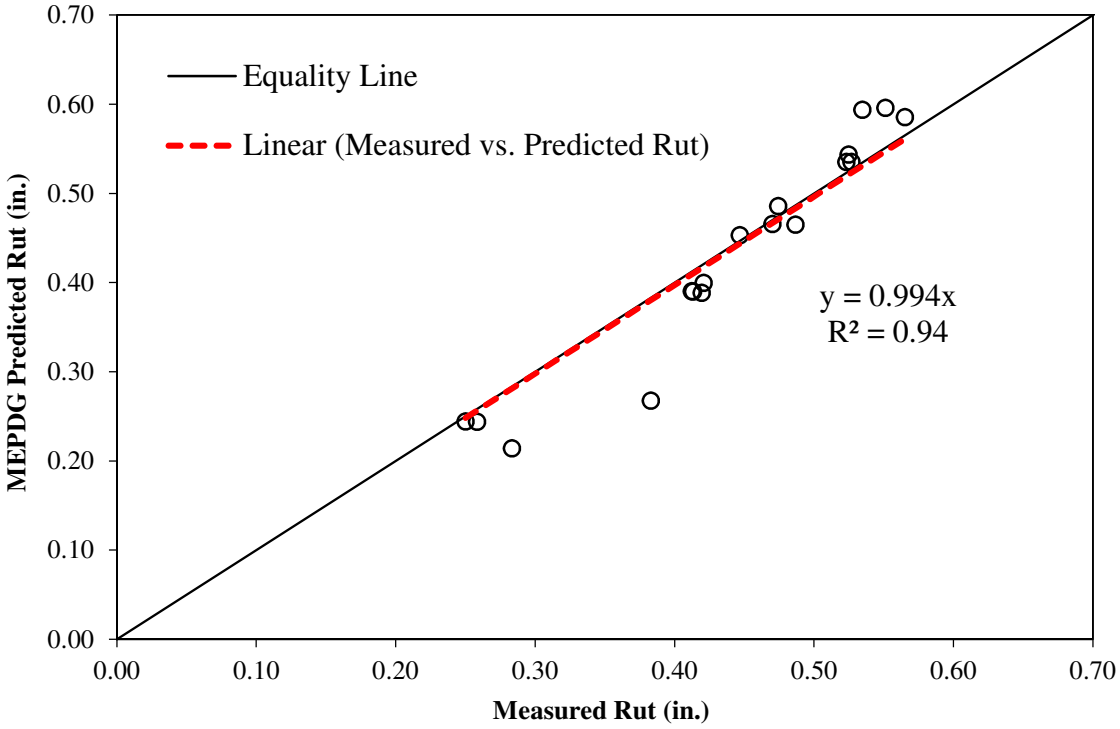

Figure 7.15: Comparison of Measured and Predicted Rutting after Calibration (Trial#12)

CHAPTER

8

Summary, Conclusions and Recommendations

8.1 Summary

In this study, a 1,000 ft. long test section was constructed by ODOT on the (right) southbound lane of Interstate-35 near Purcell, Oklahoma and was instrumented for traffic and field data collection. The materials used in the pavement construction were collected from the test section and laboratory tests were conducted to develop Level 1 input parameters for the MEPDG. Differences between the Level 3 (default) and Level 1 (site specific) input parameters and their significance in pavement performance prediction were analyzed in this study. Sensitivity of different input parameters in pavement design was conducted. Quarterly field measurements were performed to collect pavement performance data, namely rutting, fatigue cracking and International Roughness Index (IRI). At the end of the monitoring period, a forensic investigation was performed to determine the contribution of different pavement layers to rutting. Additionally, MEPDG rut models were calibrated for local conditions based on the data obtained from this study.

8.2 Conclusions

The conclusions from this study can be divided into three groups:

(4) Level 1 input generation and statistical analyses,

(5) Performance measurements at the test section,

(6) Forensic study of the test section, and

(7) Local calibration of the rut models in the MEPDG.

Conclusions for each category are given below:

(1) Level 1 Input Generation and Statistical Analyses

- Level 1 traffic inputs for the MEPDG were developed in this study. It was observed that the highest percentage of vehicle at this site was for Class 9 vehicles (approximately 60%) followed by Class 5 vehicles (approximately 15%). The MAFs varied from 0.25 to 2.47 in these four years, with Class 6 vehicles having the maximum variation in MAF values in the test section.
- An array of tests were conducted on the materials collected from the test section during construction to develop the MEPDG Level 1 material input parameters for this study. These tests included dynamic modulus tests on asphalt concrete, dynamic Shear rheometer tests on asphalt binder, volumetric tests of asphalt, resilient modulus (M_r) tests on aggregate base, stabilized subgrade and natural subgrade materials. The average air voids for the top S4 HMA layer and the bottom S3 HMA layer were found to be 9.1% and 8.0%, respectively. Effective asphalt contents (by volume) for the S4 and S3 layers were approximately 10.6% and 9.5%, respectively. The M_r values for aggregate base varied from approximately 14,000 to 50,000 psi with an average of 30,000 psi. The M_r values obtained for the natural subgrade materials compacted at OMC and OMC+2% provide a pavement design M_r values of 17,008 and 12,327 psi, respectively.

- Comparative analyses showed that the average difference between the measured and predicted rut using Level 3 inputs was approximately 37%. Use of Level 1 input parameters reduced the average error to approximately 10%. It was also observed that the MEPDG rut prediction was slightly more sensitive towards Level 1 traffic inputs than materials inputs.
- Significant differences were observed between the Level 1 and Level 3 traffic inputs. For example: the default MAF value (Level 3) is 1.00, irrespective of the month and vehicle class, whereas the actual MAF values (Level 1) for Class 9 vehicles varied from 0.57 to 1.18. Significant differences were observed in the VCD factors between the default and site-specific (i.e., Level 1) values. For example, a difference of about 25% was observed between the default and actual values for Class 9 vehicles. Significant differences were observed between default and Level 1 ALS as well. It was observed that frequency of the peak values of site-specific axle load distribution is much higher than the default values for Class 9 vehicles (approximately 4 to 12%).
- From the sensitivity analyses, it was found that the ALS is the most sensitive traffic input, followed by VCD and MAF. Therefore, if an agency has limited resources in developing Level 1 traffic inputs, they should prioritize in developing ALS first for more accurate pavement design.

(2) Performance Measurements at the Test Section

- Rut data was collected primarily by using Face Dipstick®. At the end of this monitoring period, the highest recorded rut value at the test section was 0.868 in. Although the rut values increased with time, most of the rut was

accumulated during the summer months, as seen in previous studies also (e.g., AASHO road test, NCAT test track). Also, the rate of rutting during the first summers months was much higher than in the second summer months, although the cumulative axles during each summer were similar (approximately 1.2 million). Field rut measurements show that all stations have undergone both primary and secondary rutting. No tertiary rutting was observed at any station.

- Cracks were observed on during the field trip in July, 2014, for the first time in approximately 6 years of monitoring life and after approximately 4.3 million Equivalent Single Axle Load (ESAL) applications. In addition, visible longitudinal cracks originating from the construction joint along the pavement edge stripe, and some minor aggregate loss were observed on the test section. However, no significant transverse, alligator or longitudinal cracks were observed within its six-year project life.
- The IRI for the test section was evaluated using the Face Dipstick®. The highest average IRI value observed on the test section was 154 in./mile. In general, the IRI values increased with time, which means that the road surface was getting rougher with time, as expected.

(3) Forensic Study of The Test Section

- To understand the contribution of different structural layers to rut, it was decided to compare the rutted profiles at selected locations with the profiles reported in the NCHRP report 468. In general, a close match was observed between the test sections' rutted profile and the profiles reported in the

NCHRP study where the HMA layers are the major contributor for rutting. However, to verify the rut contribution, a forensic study was performed on the test section after its six years of monitoring life. The trenching data at three different locations confirmed that the HMA layer was the predominant contributor of almost all the rutting that occurred on the test section. It was concluded from the forensic study that that the stabilized subgrade layer and the HMA layer with RAP (S3 layer) were effective in containing rut to within the top HMA layer. This is a very significant observation, especially, in terms of pavement with stabilized subgrade layers in Oklahoma. The trenching operations on this test section justifies the inclusion of a stabilized subgrade layer in terms of rut minimizations for Oklahoma pavements.

(4) Local Calibration of the Rut Models in the MEPDG

- Although developing Level 1 input parameters reduced the differences in rutting prediction significantly (average error reduced from 37% to 10%), it was observed that calibrating the rut models for Oklahoma local conditions further helps the accuracy of prediction. After the local calibration using the Level 1 traffic and material inputs, the average error between the measured and predicted rut reduced to approximately 5%.
- Since, the trenching operation showed that minimal to negligible rutting were observed in the aggregate base and subgrade layers, local calibration was performed for the rutting models on the MEPDG using forensic data. Final calibration factors for the rut models were β_{r1} = 1.25, β_{r2} = 1, β_{r3} = 1.05, β_{GB} = 0.05 and β_{SG} = 0.05. It was observed that the stabilized subgrade layer acted

as a firm support for the pavement and did not let the rut propagate beyond the asphalt layers. Therefore, it is expected that designing a similar pavement in Oklahoma may not need local calibration for the aggregate base and subgrade layers.

8.3 Recommendations

Based on this study, the following recommendations can be made for future studies:

- This study presents the data obtained from the first ever instrumented test section in Oklahoma. Level 1 traffic and materials data were used for the local calibration effort in this study. It is recommended that additional sites be collected for validation and further refinement of the rut parameters in the MEPDG. Future studies should consider different soil types, traffic and climatic conditions in Oklahoma.
- Local calibration of the fatigue cracking models were not pursued in this study because of minimal fatigue cracking (less than 1%) observed at the test section. It is recommended that future studies be performed to calibrate the fatigue models in the MEPDG for Oklahoma conditions.
- In this study, sensitivity of the traffic input parameters were analyzed using the observed rutting in the test section. Sensitivity of traffic input parameters should be studied using other distress parameters (e.g., fatigue, roughness).
- It is recommended that ODOT develops Level 1 traffic input parameters from the active WIM stations throughout the state. Level 1 materials input parameters should also be developed from the materials that are commonly

used in Oklahoma. After developing the Level 1 input parameters, the rut and fatigue models in the MEPDG could be calibrated for accurate and economical design of pavements in Oklahoma.

REFERENCES

AASHTO (2010). "Guide for the Local Calibration of the Mechanistic-Empirical Pavement Design Guide." National Cooperative Highway Research Program, Transportation Research Board, Washington, D.C.

AASHTO (2008). "Mechanistic-Empirical Pavement Design Guide – A Manual of Practice." American Association of State Highway and Transportation Officials (AASHTO), Washington, D.C.

AASHTO (2007). "Standard Method of Test for Determining Dynamic Modulus of Hot Mix Asphalt (HMA)." American Association of State Highway and Transportation Officials, AASHTO TP-62.

AASHTO (2007). "Standard Method of Test for Determining the Resilient Modulus of Soils and Aggregate Materials." American Association of State Highway and Transportation Officials, AASHTO T`307-99.

AASHTO (2004). "Guide for Mechanistic-Empirical Design of New and Rehabilitated Pavement Structures." National Cooperative Highway Research Program, Transportation Research Board, Washington, D.C.

ASTM (2012). "Standard Test Method for Laboratory Compaction Characteristics of Soil Using Standard Effort (12,400 ft-lbf/ft3 (600 kN-m/m3))." ASTM D698.

ASTM (2008). "Standard Test Method for Determining the Rheological Properties of Asphalt Binder Using a Dynamic Shear Rheometer." American Society for Testing and Materials, ASTM D7175.

ASTM (2001). "Standard Test Method for Sieve Analysis of Fine and Coarse Aggregates." American Society for Testing and Materials, ASTM C136.

Banerjee, A., Aguiar-Moya, J. P., and Prozzi, J. A. (2009). "Calibration of Mechanistic-Empirical Pavement Design Guide Permanent Deformation Models (Texas Experience with Long-Term Pavement Performance)." Transportation Research Record: Journal of the TRB, No. 2094, TRB of the National Academies, Washington, D.C. pp. 12–20.

Bhattacharya, B., Mallela, J., Titus-Glover, L., and Goldbaum, J. (2015). "Calibration of Pavement Rutting Prediction in Colorado using Layer-specific Rutting Model Coefficients for Hot-Mix Asphalt in AASHTOWare Pavement ME Design." Transportation Research Record, No. 2590, Journal of the Transportation Research Board, Washington, D.C., pp. 132 –141.

Bonaquist, R., and Christensen, D.W. (2005). "Practical Procedure for Developing Dynamic Modulus Master Curves for Pavement Structural Design." Transportation Research Record, No. 1929, Journal of the Transportation Research Board, Washington, D.C., pp. 208-217.

Cunagin, W., Reel, R., Ghanim, M., Roark, D., and Leggett, M., (2013). "Generating Site-Specific Axle Load Factors for the Mechanistic–Empirical Pavement Design Guide." Transportation Research Record, No. 2339, Journal of the Transportation Research Board, Washington, D.C., pp. 98–103.

Dean, J. (2008), Verbal Communication, Pavement Design Engineering at Oklahoma Department of Transportation, October, 2008.

Drumm, E. C., Reeves, J. S., Madgett, M. R., and Trolinger, W. D. (1997), "Subgrade Resilient Modulus Correction for Saturation Effects." Journal of Geotechnical and Geo-environmental Engineering, Vol. 23, No. 7.

Faruk, A. N. F., Liu, W., Lee, S., Naik, B., Chen, D., and Walubita, L. (2016). "Traffic Volume and Load Data Measurement Using a Portable Weight in Motion System: A Case Study." International Journal of Pavement Research and Technology, Vol. 9, pp. 202–213

FHWA (2015). "Towards Sustainable Pavement Systems: A Reference Document." FHWA-HIF-15-002, Federal Highway Administration, Washington, D.C.

FHWA (2010). "Local Calibration of the MEPDG Using Pavement Management Systems." FHWA-HIF-11-026, Federal Highway Administration, Washington, D. C.

FHWA (2010). "Local Calibration of The MEPDG using Pavement Management Systems." Federal Highway Administration, Final Report, Volume 1, Washington, D.C.

Flintsch, G. W., Loulizi, A., Diefenderfer, S. D., and Diefenderfer, B. K. (2008). "Asphalt Materials Characterization in Support of Mechanistic-Empirical Pavement Design Guide Implementation Efforts in Virginia." Transportation Research Board 87th Annual Meeting, CD-ROM, National Research Council, Washington, D.C.

Haider, S., Buch, N., Chatti, K., and Brown, J. (2011). "Development of Traffic Inputs for Mechanistic–Empirical Pavement Design Guide in Michigan." Transportation Research Record: Journal of the TRB, No. 2256, TRB of the National Academies, Washington, D.C. pp. 179–190.

Hajek, J., J., Billing, J., R., and Swan, D., J. (2011). "Forecasting Traffic Loads for Mechanistic–Empirical Pavement Design." Transportation Research Record: Journal of the TRB, No. 2256, TRB of the National Academies, Washington, D.C. pp. 151–158.

Hall, K., Xiao, D., and Wang, K. (2011). "Calibration of the MEPDG for Flexible Pavement Design in Arkansas." Transportation Research Record: Journal of the TRB, No. 2226, TRB of the National Academies, Washington, D.C. pp. 135–141.

Hoegh, K., Khazanovich, L., and Jensen, M. (2010). "Local Calibration of Mechanistic-Empirical Pavement Design Guide Rutting Model (Minnesota Road Research Project Test Sections)." Transportation Research Record: Journal of the TRB, No. 2180, TRB of the National Academies, Washington, D.C. pp. 130–141.

Huang, Y. H. (2004). "Pavement Analysis and Design" 2nd Edition, Prentice Hall, Inc. Englewood Cliffs, New Jersey.

Hossain, N., Singh, D., Zaman, M. (2016). "Enhancing Rutting Prediction of the Mechanistic – Empirical Pavement Design Guide by Using Data from a Field Test Section in Oklahoma." Transportation Research Record, No. 2590, Transportation Research Board, Washington, D.C., pp. 28-36.

Hossain, N., Singh, D., and Zaman, M. (2016). “Sensitivity of traffic input parameters on rutting performance of a flexible pavement using Mechanistic Empirical Pavement Design Guide.” International Journal of Pavement Research and Technology, Vol. 9, No. 6, pp. 405-459.

Hossain, N., Singh, D., Zaman, M., Alam, M., R., Shazzad, S., M., and Timm, D. (2015). “Field Performance Monitoring and Modeling of Instrumented Pavement on I-35 in McClain County (Phase 2).” Final Report, The University of Oklahoma, Norman, Oklahoma.

Hossain, N., Singh, D., Zaman, M., and Rassel, S. M. (2014). “Local Calibration of MEPDG Rut Models: Oklahoma’s Experience from an Instrumented Pavement Section.”, Proceedings of the 14th International Conference of International Association for Computer Methods and Recent Advances in Geomechanics (IACMAG), Kyoto, Japan.

Hossain, N., Singh, D., and Zaman, M. (2013). “Dynamic Modulus-based Field Rut Prediction Model from an Instrumented Pavement Section.”, 2nd Conference of Transportation Research Group of India (2nd CTRG), Agra, India. Elsevier Procedia- Social and Behavioral Sciences, No. 104, pp. 129-138.

Hossain, N. (2010). “Observed and Predicted Rut Behavior of an Instrumented Test Section on I-35.” M.S. Thesis, The University of Oklahoma, Norman, OK.

Ishak, S., Shin, H., Sridhar, B., and Zhang, Z. (2010). “Characterization and Development of Truck Axle Load Spectra for Implementation of New Pavement Design

Practices in Louisiana." Transportation Research Record: Journal of the TRB, No. 2153, TRB of the National Academies, Washington, D.C. pp. 121-129.

Li, J., Pierce, L., and Uhlmeyer, J. (2009). "Sensitivity of Axle Load Spectra in the Mechanistic–Empirical Pavement Design Guide for Washington State." Transportation Research Record: Journal of the TRB, No. 2093, TRB of the National Academies, Washington, D.C. pp. 50–56.

Li, J., Pierce, L., and Uhlmeyer, J. (2009). "Calibration of Flexible Pavement in Mechanistic-Empirical Pavement Design Guide for Washington State." Transportation Research Record: Journal of the TRB, No. 2095, TRB of the National Academies, Washington, D.C. pp. 73–83.

Lu, Q., and Harvey, J. (2006). "Characterization of Truck Traffic in California for Mechanistic-Empirical Design." Transportation Research Record: Journal of the TRB, No. 1945, TRB of the National Academies, Washington, D.C. pp. 61–72.

MTS System Corporation (2011). (http://www.mts.com) (Last accessed: May 31, 2013).

Mehta, Y., Sauber, R., Owad, J., and Krause, J. (2008). "Lessons Learned during Implementation of Mechanistic-Empirical Pavement Design Guide." Transportation Research Board 87th Annual Meeting, CD-ROM, Washington, D.C.

Muthadi, N., and Kim, Y. (2008). "Local Calibration of Mechanistic-Empirical Pavement Design Guide for Flexible Pavement Design." Transportation Research Record:

Journal of the TRB, No. 2087, TRB of the National Academies, Washington, D.C., pp. 131–141.

NCHRP (2004). "Guide for Mechanistic-Empirical Design of Pavement Structures, NCHRP Project 1-37A" National Cooperative Highway Research Program, Washington, D. C.

NCHRP Report 468 (2002). "Contributions of Pavement Structural Layers to Rutting of Hot Mix Asphalt Pavements." Transportation Research Board- National Research Council, Washington, D.C.

Oh, J., Walubita, L., and Leidy, J. (2014). "Establishment of Statewide Axle Load Spectra Data using Cluster Analysis" KSCE Journal of Civil Engineering, Vol 19, Issue 7, pp. 2083-2090.

Oklahoma Department of Transportation Standard Specifications, 2009.

Papagiannakis, A., Bracher, M., and Jackson, N. (2006). "Utilizing Cluster Techniques in Estimating Traffic Data Inputs for Pavement Design." Journal of Transportation Engineering, Vol. 132, No. 11, pp. 872-879.

PEEK TOPS (2010). PEEK Traffic Operations and Planning Software. (https://www.peektraffic.com/datasheets/TOPS.pdf)

Priest, A. L. (2005), "Calibration of Fatigue Transfer Functions for Mechanistic-Empirical Flexible Pavement Design." Master's Thesis, Auburn University, Auburn, Alabama.

Randell, J. (2016), Personal Communication, Pavement Design Engineering at Oklahoma Department of Transportation.

Romanoschi, S., Momin, S., Bethu, S., and Bendana, L. (2011). "Development of Traffic Inputs for New Mechanistic–Empirical Pavement Design Guide-Case Study." Transportation Research Record: Journal of the Transportation Research Board, No. 2256, Washington, D.C. pp. 142–150.

Shah, K. (2007), "Effects of Gradation and Compaction Energy on the Hydraulic Conductivity of an Aggregate Base Commonly used in Oklahoma." M. S. Thesis, The University of Oklahoma, Norman, OK.

Selvaraj, S.I. (2007). "Development of Flexible Pavement Rut Prediction Models from the NCAT Test Track Structural Study Sections Data." Ph.D. Dissertation, Auburn University, Auburn, Alabama.

Simpson, A. L., J. F. Daleiden, and W. O. Hadley (1995). "Rutting Analysis from a Different Perspective." In Transportation Research Record: Journal of the TRB, No. 1473, TRB of the National Academies, Washington, D.C.

Singh, D., and Sawant, D. (2016). "Understanding Effects of RAP on Rheological Performance and Chemical Composition of SBS Modified Binder using series of Laboratory Tests." International Journal of Pavement Research and Technology, pp. 178-189.

Singh, D. (2011). "A Laboratory Investigation and Modeling of Dynamic Modulus." Ph.D. Dissertation, The University of Oklahoma, Norman, Oklahoma.

Solanki, P., Hossain, N., Breidy, M., Singh, D., Zaman, M., and Muraleetharan, K. K. (2013). "Field Performance Monitoring and Modeling of Instrumented Pavement on I-35 in McClain County." Final Report, The University of Oklahoma, Norman, Oklahoma.

Solanki, P., Zaman, M., and Dean, J. (2010). "Resilient Modulus of Clay Subgrades Stabilized with Lime, Class C Fly Ash, and Cement Kiln Dust for Pavement Design." Transportation Research Record, No. 2186, Journal of the Transportation Research Board, Washington, D.C., pp. 101-110.

Souliman, M., Mamlouk, M., El-Basyouy, M., and Zapata, C. (2010). "Calibration of the AASHTO MEPDG for Flexible Pavement for Arizona Conditions." Compendium of Papers of the 89th TRB Annual Meeting, CD-ROM, Washington, D.C.

Tam, W., and Quintus, H. (2003). "Use of Long-Term Pavement Performance Data to Develop Traffic Defaults in Support of Mechanistic-Empirical Pavement Design Procedures." Transportation Research Record: Journal of the Transportation Research Board, No. 1855, Washington, D.C. pp. 176–182.

Tarefder, R., and Rodriguez-Ruiz, J.I. (2013). "Local Calibration of MEPDG for Flexible Pavements in New Mexico." Journal of Transportation Engineering, ASCE, Volume 139, Issue 10.

Texas Department of Transportation (2012). "Traffic Recorder Instruction Manual" http://onlinemanuals.txdot.gov/txdotmanuals/tri/classifying_vehicles.htm

Thompson, M. (1996). "Mechanistic-Empirical Flexible Pavement Design: An Overview". Transportation Research Record, No. 1539, Transportation Research Board, Washington, D.C., pp. 1-5.

Timm, D., Robbins, M., Willis, J., Tran, N., and Taylor, A. (2012). "Evaluation of Mixture Performance and Structural Capacity of Pavements Utilizing Shell Thiopave®: Phase II: Construction, Laboratory Evaluation and Full-Scale Testing of Thiopave® Test Sections. Final Report." National Center for Asphalt Technology, Auburn, Alabama.

Timm, D. H., Bower, J. M., and Turochy, R. E. (2006). "Effect of Load Spectra on Mechanistic–Empirical Flexible Pavement Design." Transportation Research Record: Journal of the Transportation Research Board, No. 1947, Washington, D.C., pp. 146–154.

Timm, D. H. and Priest, A. L. (2005). "Wheel Wander at the NCAT Test Track." Report 05-02, National Center for Asphalt Technology, Auburn University, Alabama.

Timm, D. H., Priest, A.L., McEwen T.V. (2004). "Design and Instrumentation of the Structural Pavement Experiment at the NCAT Test Track." Report 04-01, National Center for Asphalt Technology, Auburn University, Alabama.

Tran, N., and Hall, K. (2007). "Development and Influence of Statewide Axle Load Spectra on Flexible Pavement Performance," Transportation Research Record: Journal of the Transportation Research Board, No. 2037, Washington, D.C., pp. 106–114.

Tran, N.H., and Hall, K.D. (2006). “An Examination of strain levels used in the dynamic modulus testing.” Journal of Association of Asphalt Paving Technologist, Vol. 75, pp. 321-343.

Walubita, L., Lee, S., Faruk, A. N., F., Hoeffner, J., Scullion, T., Abdallah, I., Nazarian, S. (2013). “Texas Flexible Pavements and Overlays: Calibration Plans for M-E models and Related Software.” Report No. FHWA/TX-13/0-6658-P4, Texas A&M Transportation Institute, College Station, Texas.

Zaman, M., Muraleetharan, K. K., Hossain, N., Solanki, P., and Breidy, M. (2009). “Field Performance Monitoring and Modeling of Instrumented Pavement on I-35 in McClain County.” Annual Report, The University of Oklahoma, Norman, Oklahoma.